Campanian-Maastrictian Ankylosaurs of West Texas

by

Bryanna Nicole West

Bachelor of Science, 2018

Texas Tech University

Lubbock, Tx

Submitted to the faculty of

College of Science and Engineering

Texas Christain University

In partial fulfillment of the requirements

for the degree of

Master of Science in Geology

May 2020

ACKNOWLEDGMENTS

I would like to thank my thesis advisor Dr. Busbey for taking me on as a graduate student and giving me the confidence to take on a project of this magnitude. I would also like to thank the rest of my advisory committee; Dr. Richard Denne who I got to know well by taking many of his courses. In addition, Dr. Tom Lehman who acted as an outside committee member and has been with me since day one to my very first geology class at Texas Tech. He has been a mentor to me for almost six years and I hope that I become a paleontologist that makes him and Dr. Busbey proud. I would also like to thank the various museum staff members who hosted me on my research trips; Nicole Ridgewell who had two ankylosaur skulls already waiting for me when I arrived at the University of New Mexico and Chris Mehling at the American Museum of Natural History who put up with my constant emails and who helped me retrieve specimens from drawers when my back gave out. And especially Dr. Chris Sagebiel and Dr. Matthew Colbert and the staff at the Vertebrate Paleontology Lab in Austin, Tx who scanned the osteoderm specimens for me. Finally, I would like to thank my family for their unwavering support. I would not have been able to attend TCU without my parents Bryan and Debi West. I would also like to dedicate this project to the remembrance of my grandmother Belia DeLaGarza who passed before I graduated from Texas Tech, but is with me in spirit.

Table of Contents

Acknowledgements ii
Table of Contents iii
List of Figures iv
Introduction 1
Stratigraphy 1
The Aguja Formation 2
The Javelina Formation 4
Osteological Terminology 5
Methods 6
Abbreviations 7
Ankylosaur Systematics and Taxonomy 7
Results
TMM 31078-1 9
TMM 45605-4 14
TVP 45866-2 18
Osteoderm #1 21
TMM 40484-46 24
TL-05-14 Sacrum 27
TL-05-14 Vertebra 29
TMM 43057-502 29
TMM 41836-1 31
TMM 42878-1 33
WPA-3 Quarry Specimens
Osteoderm #1 34
Osteoderm #2 35
Osteoderm #3 36
Osteoderm #4 37
Osteoderm #5 38
Osteoderm #6 39
Osteoderm #7 41
Ungual Phalanx #1 42
Metapodial #1 43
Vertebra #1 44
Vertebra #2 44
Radius #1 45
AMNH 3076 46
Review of Specimens from Mexico and New Mexico
Mexico 48
New Mexico 50
Phylogenetic Discussion 52
Conclusion 55
Appendix
Taxon List 57
Character Table 58
West Texas Specimens 63
Additional Tables 64
References 67
Vita
Abstract

List of Figures

Figure 1: Big Bend Stratigraphy 4
Figure 2: Description of TMM 31078-1 11
Figure 3: Histology of TMM 31078-1 13
Figure 4: Description of TMM 45605-4 15
Figure 5: Histology of TMM 45605-4 17
Figure 6: Description of TVP 45866-2 18
Figure 7: Histology of TVP 45866-2 20
Figure 8: Description of Osteoderm #1 21
Figure 9: Histology of Osteoderm #1 23
Figure 10: Description of TMM 40484-46 24
Figure 11: Histology of TMM 40484-46 26
Figure 12: Description of TL-05-14 Sacrum 28
Figure 13: Comparison of Ankylosaur Pelvi 28
Figure 13: Description of TL-05-14 Vertebra 29
Figure 14: Description of TMM 43057-502 30
Figure 15: Description of TMM 41836-1 32
Figure 16: Description of TMM 42878-1 33
Figure 17: Description of WPA-3 Osteoderm #1 34
Figure 18: Description of WPA-3 Osteoderm #2 35
Figure 19: Description of WPA-3 Osteoderm #3 36
Figure 20: Description of WPA-3 Osteoderm #4 37
Figure 21: Description of WPA-3 Osteoderm #5 38
Figure 22: Description of WPA-3 Osteoderm #6 40
Figure 23: Description of WPA-3Osteoderm #7 41
Figure 24: Description of WPA-3 Ungual Phalanx #1 42
Figure 25: Description of WPA-3 Metapodial #1 43
Figure 26: Description of WPA-3 Vertebra #1 and WPA-3 Vertebra #2 44
Figure 27: Description of WPA-3 Radius #1 45
Figure 28: Images of AMNH 3076 47
Figure 29: Illustrations of AMNH 3076 48
Figure 30: Comparison of Phylogenetic Trees 52

INTRODUCTION

This thesis focuses on the characterization and classification of ankylosaurs from Upper Cretaceous strata of West Texas. Fossil evidence of almost every major Late Cretaceous dinosaur clade has been collected from areas in and around Big Bend National Park in Texas, which contains floral and faunal assemblages similar to contemporaneous units in Utah and New Mexico. Ankylosaur specimens reported in the literature from the Big Bend region consist of a handful of teeth, osteoderms, a few long bones, and a skull discovered by Barnum Brown inside the park in 1940 (Carpenter and Breithaupt, 1986). There are more remains in collections and I have endeavored to find, list, and document all the material in the collections of UT Austin and the American Museum of Natural History. In addition, I have also compared ankylosaur specimens from Big Bend to those found in time correlative strata form the San Juan Basin in New Mexico which are held in collections at the University of New Mexico at Albuquerque.

In addition to standard osteological descriptions one goal of this project is to study the histology of some of the material. This study will allow me to: 1) compare to existing histological studies and, 2) test the results of Scheyer and Sander (2004) and Burns and Currie (2014) that purport to use osteoderm histology as a taxonomic tool. Ultimately the overall goal of this project is to provide a better understanding about southern ankylosaur diversity in the Western Interior of North America at the end of the Cretaceous.

STRATIGRAPHY

The stratigraphic units that are the primary focus of this study are the Aguja Formation and the Javelina Formation (Tornillo Group) of Big Bend National Park. Fossil assemblages from the two formations are allied to the “southern” Late Cretaceous faunas of New Mexico and Utah (Lehman, 1985 and Lehman et al., 2019). These units range from the Early Campanian to the Late Maastrichtian (a time

span of approximately 17.5 Ma); a period of time which records the final regression and closing of the Western Interior Seaway (WIS), the onset of the Laramide Orogeny, and the subsequent deposition of sediment in the Tornillo Basin. Lehman and Busbey (2007) hypothesized that the Cretaceous-Paleocene boundary was preserved locally within the lower Black Peaks Formation. Recently Leslie et al. (2013) revised the chronostratigraphic framework of the Dawson Creek locality of Big Bend and determined that the latest occurrence of dinosaur fossil in the Black Peaks is Lancian (Late Maastrichtian approx. 70-66 Ma) with the Cretaceous-Paleogene boundary placed near the base of the Black Peaks Formation. However, no ankylosaur fossils have been found within the Black Peaks Formation, suggesting that either ankylosaurs were not present at the end of the Maastrichtian or that environmental conditions were not conducive to preserving their remains.

Previous studies (Sankey 2001; Lehman 1985; Lehman et al. 2019) have suggested that dinosaur faunal assemblages from Big Bend were paleoecologically distinct from contemporaneous "northern" faunas during the Late Cretaceous of North America. Insofar as the ankylosaurs are concerned this theory might need to be altered with the possible discovery of southern *Euoplocephalus sp.* specimens in recent years. Stratigraphic terminology from Lehman et al., (2018; 2019) is used to describe these units as these are the most recent stratigraphic studies of this region.

The Aguja Formation

The Aguja Formation is an eastward thinning terrestrial unit that can be divided into two main subunits; two shale members known as the lower shale member and the upper shale member. These two subunits are separated by paralic marine deposits, denoted as the Pen Formation, which intertongues with the Aguja Formation (Lehman et al., 2019). The age of the terrestrial deposits of the Aguja Formation was determined using ammonite biostratigraphy from the interbedded Pen Formation and radiometric dating of pyroclastic deposits. The uppermost Pen Formation was dated using the ammonite *Scaphites hippocrepis III*, which establishes the lower limit of the Aguja Formation as 82 Ma (Waggoner, 2006;

Gradstein et al., 2012). *Baculites haresi* is found within the McKinney Springs member of the Pen Formation. This ammonite ranges as far as the *Baculites obtusus* zone, which has been dated using $^{40}Ar/^{39}Ar$ isotopes from an intercalated tuff bed, and designates the age of this marine deposit as 80 Ma (Obradovich, 1993). The upper age limit of the Aguja Formation was determined is between 77 Ma to 73 Ma, as determined by U/Pb dating of intercalated pyroclastic deposits (Breyer et al., 2007; Befus et al., 2008).

The lower shale member of the Aguja Formation consists of thick lignitic clay-rich shale and carbonaceous mudstone, varying in thickness from 40 m to 100 m. There are several prominent intervals of sandstone, concretions, and coal beds within the lower shale member. It should be noted that most outcrops of the of the lower shale member lie on private land, so access to study outcrops is limited (Lehman, 2019). The lower shale member was interpreted by Lehman (1985) to have been a coastal wetland environment such as a marsh or swamp. The sandstone intervals within this unit were associated with tidal creek or estuarine deposits associated with the coastal wetlands. Vertebrate fossils in the lower shale member are sparse with most specimens from this unit being fragmentary. Isolated osteoderms were identified as belonging to the Nodosauridae based on the lack of a highly excavated internal surface and a sparsely pitted external surface (Burns and Currie, 2014; Lehman 2019).

The upper shale member of the Aguja Formation consists of variegated mudstones and sandstones with conglomeratic lags of paleo-caliche nodules. The deposits are interpreted to be fluvial systems in a coastal or inland floodplain. This unit is believed to be the last of the pre-Laramide deposits in this region (Lehman 1985; 1991). The only known ankylosaur specimens from the upper shale member were found near the El Carricito township of Coahuila, Mexico. These specimens consist of thirteen osteoderms (ranging from keeled osteoderms to thoracic spines), fragments of two cervical vertebrae, a distal humerus, posterior illium, proximal scapula, one cervical rib, six fragments of thoracic ribs, and additional unknown appendicular elements (Rivera-Sylva et al., 2011).

The Javelina Formation

The Javelina Formation conformably overlies the Aguja Formation. The Javelina Formation represents the sediments deposited in the Tornillo Basin during the Laramide Orogeny. This unit ranges in thickness from 123 m to 183 m, and thickens to the east. The Javelina Formation contains well-indurated sandstone beds, with basal chert-pebble conglomerate lenses marking the lower contact with the Aguja Formation. This unit contains alternating beds of sandstone and mudstones, with thin beds of lacustrine fossiliferous limestone in the eastern areas of the basin. These thin limestone beds are evidence for a change from fluvial to lacustrine facies in the basin. In addition, these lacustrine facies seem to be restricted to the eastern exposures of the Javelina Formation. This could indicate that the rate of subsidence in the basin was greatest on its eastern side. This formation is the oldest unit within the Tornillo Group, which ranges in age from the mid- middle Maastrichtian to the earliest Eocene. The Javelina Formation itself ranges from the mid-middle to late Maastrictian. Most vertebrate fossils are found in the upper half of the Javelina Formation. (Lehman et al., 2018). Ankylosaur fossils have been recorded from the Javelina Formation; however, they are less abundant than other vertebrates (Lawson, 1976).

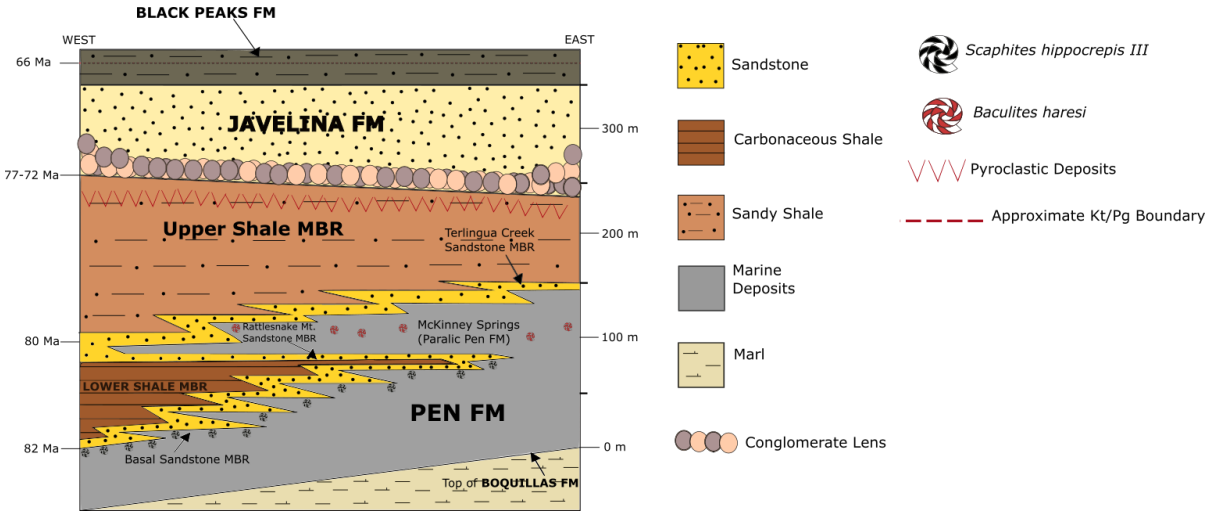

Figure 1. Stratigraphic cross-section of Late Cretaceous strata modified from Lehman et al., 2019 and Sankey, 2001.

Osteological Terminology

Due to the nature of this study it is important to outline certain terminology regarding the osteology and histology of the specimens herein. Osteological terminology (any terminology referring to skeletal elements such as their size, shape, and anatomical position on the organism) for the ankylosauria were taken from Coombs (1978), Carpenter and Currie, (1990), and Carpenter (2001). Whereas most of the osteological terms used here are standard for any study on large herbivorous dinosaurs, special consideration must be paid to the ankylosauria because of their extensive dermal armor. Before the work of Scheyer and Sander (2004) little effort was made to create a consistent osteological vernacular to describe ankylosaur osteoderms. Additionally, ambiguous synonyms such as 'plate', 'scute', and 'osteoscute' were used interchangeably until Vickayous and Sire (2009) discouraged the use of such terms. Therefore, this study uses the terminology of Scheyer and Sander (2004) which was later expanded upon by Burns and Currie (2014). The term osteoderm will be used to refer to any bony structure of the dermal skeleton which develops from the dermis of an organism. Median will refer to the position of the keel or apex relative to osteoderm itself, and medial, distal, and lateral will refer to the position of the osteoderm on the organism. Terms such as dorsal and ventral will be used to denote the plane of view on any image of illustration of a specimen. Terminology referring to bone texture follows (Hieronymus et al., 2009). Morphological shape of osteoderms will be described using the terminology of Ford (2000) and Blows (2001).

Standard histological terms (terminology referring to the internal structure and composition of bone) were taken from (Padian and Lamm, 2013). Again, no consistent terminology was in use until Scheyer and Sander (2004). The term 'basal' refers to the internal surface of the osteoderm where the bone was attached to the dermis itself. In contrast, the term 'external' refers to the surface that is connected to the more external layer of skin known as the epidermis, which might have even been partially exposed above this layer. Osteoderms are defined has having a single cortex or cortices (which

can be basal or external), which surrounds a core of varying composition. The cortices themselves are composed of a woven-fibered bone matrix made up of collagen fibers referred to in the literature as Interwoven Structure Fiber Bundles or ISFB for short (Burns and Currie, 2014).

METHODS

Specimens were prepared for microCT scanning by Drs. Chris Sagebiel and Matthew Colbert of the University of Texas at Austin. Each scan produced several hundred image slices of the specimens which were then converted to 16 bit tiff files. The files were downloaded into Dragonfly ORS, a 3-D imaging program that which can stitch together the sliced images and create digital models of each osteoderm. By using the active contouring tool on Dragonfly to identify different bone textures the bone analysis tool was used to segment out the cortical and trabecular bone. In some cases, where the core of the osteoderms where made up of Haversian bone, the segmentation of the core and cortices had to be done manually, as the program could not distinguish between cortical and Haversian bone. Once the segmentation was complete the histology of each specimen could be studied. In terms of an osteologic study the size, morphology, and external texture of each osteoderm was noted and compared to known specimens from the Late Cretaceous of North America. The osteologic study also included axial or appendicular elements from ankylosaurs found in Big Bend. Comparisons were made based on descriptions in the literature and on specimens studied at the Vertebrate Paleontology Lab of the University of Texas at Austin, the University of New Mexico, and the American Natural History Museum in New York. Osteoderm characteristics were added to the latest character matrix assembled by Arbour and Currie (2015) and analyzed using the phylogenetic software Mesquite 3.61 (Maddison, W. P. and D.R. Maddison, 2019). A phylogenetic tree using 50% majority consensus rule was created using this program and was then compared to the latest ankylosaur classification study conducted by Arbour and Currie (2015).

ABBREVIATIONS

TMM-Texas Memorial Museum, VPL- Vertebrate Paleontology Lab, TVP- Texas Vertebrate Paleontology, AMNH- American Natural History Museum, CPC- Colección Paleontológica de Coahuila, UABC FCM- Universidad Autónoma de Baja California Facultad de Ciencias Marinas, WSC- Western Science Center, ISFB- Interstitial Structure Fiber Bundles.

ANKYLOSAUR SYSTEMATICS AND TAXONOMY

Osborn (1923) defined the group Ankylosauria as a suborder sharing a common ancestry with the Stegosauria. Together they form the clade Thyreophora (Nopcsa, 1915), but the time of divergence between these two groups is yet to be determined. The first appearance of ankylosaurs is believed to have occurred during the Early to Middle Jurassic. The thyreophorans *Scelidosaurus* and *Scutellosaurus* are believed to be the earliest members of the suborder, with *Scelidosaurus* considered the most basal ankylosaur (Carpenter, 2012). This dinosaur had osteoderms similar to more derived ankylosaurs and showed evidence that the ilia of the pelvis had started to rotate to become more horizontal; unlike the condition in other ornithischians. The horizontal ilia would later come to be a synapomorphy for derived ankylosaurs (Carpenter, 2012).

Ankylosaurs were well established by the Late Jurassic; these early ankylosaurs were grouped into the sub-family Polocanthinae by Kirkland (1998). These ankylosaurs are distinguished by small ossicles covering the dorsal part of their skull, grooved neck and distal spines, and osteoderms with uniformly thick external and basal cortices enclosing a trabecular core (Scheyer and Sander, 2004; Burns and Currie, 2014) . However, the best well-known North American polocanthine, *Gargoyleosaurus*, (Morrison Formation- Late Cretaceous) has a pelvic condition similar to the more derived ankylosaurs from the Cretaceous (Carpenter et al., 2013). Due to a combination of both basal and derived characteristics it has been suggested to promote this group to its own family within the Ankylosauria

(Carpenter and Currie, 1990). By the Early Cretaceous, polocanthine diversity was ebbing, becoming extinct by the start of Barremian (129 Ma) and the ankylosaurs then diversified once again. These Cretaceous ankylosaurs were split into two families by Coombs (1978): the Nodosauridae and the Ankylosauridae. Interestingly enough the disappearance of the polocanthines and the emergence of nodosaurids occurred simultaneously with the establishment of angiosperms. However, there is no direct correlation between these events to suggest cause and effect (Carpenter, 2012).

The early evolutionary history of nodosaurids is unclear, as most taxa are only known from fragmentary remains. The genus E*dmontonia* from North America is an exception to this rule, as it is known throughout the continent from several skulls and partial skeletons preserved in the life positions. Nodosaurids exhibit a longer and narrower skull than other ankylosaurs and lack the tail clubs of derived ankylosaurids, instead they had specialized osteoderms that took the form of shoulder spikes that pointed upwards. Although the ilia are positioned more horizontally than in the basal ankylosaurs the pelvis, as a whole, is narrower than those of ankylosaurids (Carpenter, 2012). Scheyer and Sander (2004) study found that nodosaurids have osteoderms with a thick external cortex and thinner basal cortex (both cortices consist of three sets of ISFBs at 45° angles) and a trabecular core. Nodosaurids were so prolific that their range extended to North and South America, Europe, Asia, and Antarctica (Carpenter, 2012).

Ankylosaurids emerged as a group during the Early Cretaceous; the earliest ankylosaurids were assigned to the sub-family Shamosaurinae by Tumanova (1983). These ankylosaurids lacked the intricate cranial ornamentation and tail clubs of the more derived sub-family ankylosauinae, which were prolific in the Late Cretaceous. The most basal member of this group is *Cedarpelta;* the shamosaurines diversified during the Albian (113 Ma). It is hypothesized that ankylosaurids originated in North America during the Early Cretaceous and migrated to Asia where they further diversified into the sub-family Ankylosaurinae (Sereno, 1998). This sub-family is characterized by complex cranial ornamentation (including squamosal horns which projected over the eye orbit), boney tail clubs, fully horizontal ilia which is also rotated outwards from the body, and a boxy skull with a tapered muzzle (Carpenter, 2012).

Ankylosaurid osteoderms from both sub-families exhibit thin external and basal cortices with a core of dense Haversian bone. ISFB's are still found within the cortices, however they exhibit a random orientation (Scheyer and Sander, 2004). By the Cenomanian (100.5 Ma) the shamosaurines were extinct in North America and the ankylosaurines were reintroduced to North America. No ankylosaurines have been found in Europe or the Southern Hemisphere, suggesting that they had a more limited range then contemporary nodosaurids. The best known ankylosaurines from North America include *Ankylosaurus magniventris* and *Euoplocephalus tutus* which both survived until the K/P mass extinction (66 Ma) (Carpenter, 2012).

RESULTS

Each specimen was first studied by noting osteological characteristics such as bone morphology, texture, and external features such as vascular canals or foramina. For the selected osteoderms a histological study was also preformed using Dragonfly ORS. The histological study focused on the type of bone exhibited in each osteoderm, as well the amount of each type present in the specimen. This was determined by measuring the percent of total bone thickness that each type compromised. The presence of primary or secondary osteons were also recorded for each osteoderm, as any well as internal vascular canals present in the specimen. These features are markers of bone remodeling, which can be used to determine in the osteoderms came from adult or juvenile animals. Finally, osteological and histological characteristics were combined and compared to previously known taxa to determine the identity of the specimen.

TMM 31078-1 (Figures 2&3)

This specimen was discovered in an undermined locality in Brewster Co., Texas. This osteoderm is compressed dorsoventrally to give it a bladed appearance. The blade-like sides of the osteoderm terminate in an apex which projects posteriorly. The shape of the osteoderm falls under the Type B morphology (a circular osteoderm with an off-center apex) introduced by Ford (2000) and Blows

(2001). The base of the osteoderm is highly concave with most of the cortical surface eroded away leaving the core exposed on the ventral side of the osteoderm. This specimen is almost intact; however, it has been heavily fractured throughout, and has a piece missing from the base of the apex on the medial edge. No large foramina or vascular canals are present on the surface of the osteoderm. Additionally, no pitting or projecting rugosities are present on the external surface, giving the specimen a smooth external texture. These features could have been erased by the high amount of weathering present on the osteoderm surface.

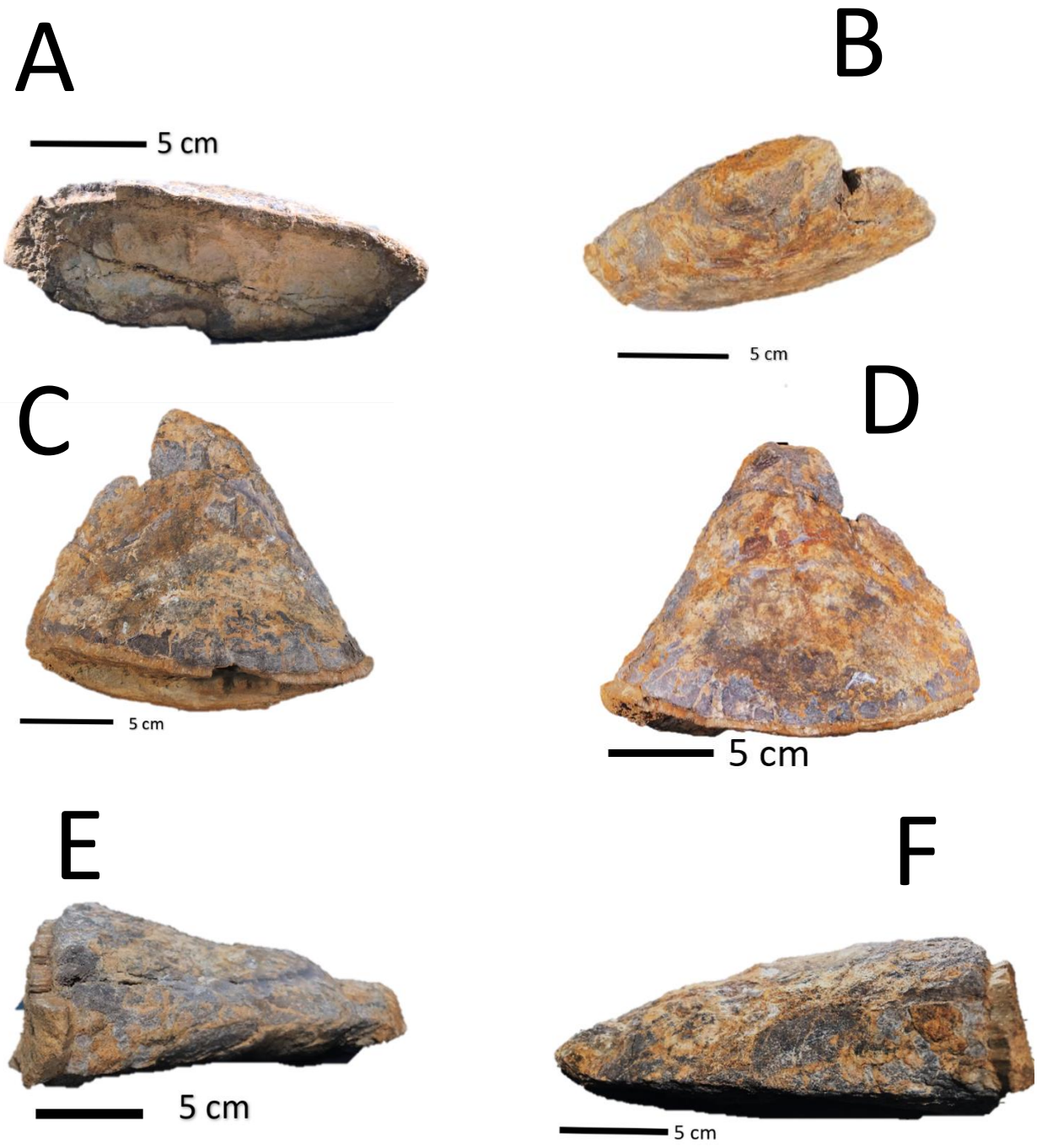

Figure 2. TMM 31078-1 is a large bladed osteoderm with a concave base and exposed core as seen in ventral view (A). From the dorsal view (B) it can be observed that the apex of the osteoderm projects posteriorly. In right lateral view (C) and left lateral view (D) the exterior surface of this specimen is highly weathered and rugose. Additionally, the core of the osteoderm is seen projecting out from the base of the osteoderm in anterior (E) and posterior (F) view.

The thickness of the cortices and the core were taking from a transverse section of the osteoderm from the left and right lateral sides through the apex. No measurements of the basal cortex were taken due to its absence in this specimen. The external cortex makes up 12.3±2% of the total osteoderm thickness. The external cortex is slightly thicker on the left lateral side and thins toward the apex. The external cortex is composed of cortical bone, which exhibit sparse ISFBs located close to the edge of the external cortex. The fibers appear to be orientated randomly in the cortex, which matches the cortical bone in most ankylosaurid osteoderms (Scheyer and Sander, 2004). The core makes up 87.7±2% of the total osteoderm thickness. Just as with the external cortex, the core is thickest at the base and thins toward the apex. The core of this osteoderm is made up of compact Haversian bone, with a well-defined border between the external cortex and the core itself. The dense Haversian tissue in the core has undergone extensive secondary remodeling, with secondary osteons cutting across and overlapping other each other. No primary tissue or structures remain after secondary remodeling (Padian and Lamm, 2013). The apex of the osteoderm preserves the primary vascular tissue, which take the form of faint trabeculae that escaped secondary remodeling. The absent basal cortex, concave base, and compact core made up of dense Haversian bone are all characteristics of derived members of the ankylosauridae. Specifically, these histologic features, combined with the bladed, Type B morphology, resemble distal osteoderms of the Ankylosaurinae; a group which includes taxa such as *Euoplocephalus sp, Ankylosaurus magniventris,* and *Ziapleta sanjaunensis* (Hayashi et al., 2010, Burns and Currie, 2014). The osteoderm closely resembles known specimens of distal thoracic osteoderms of *Euoplocephalus sp.* The size of the specimen and the secondary remodeling of the core suggest that the specimen came from an adult.

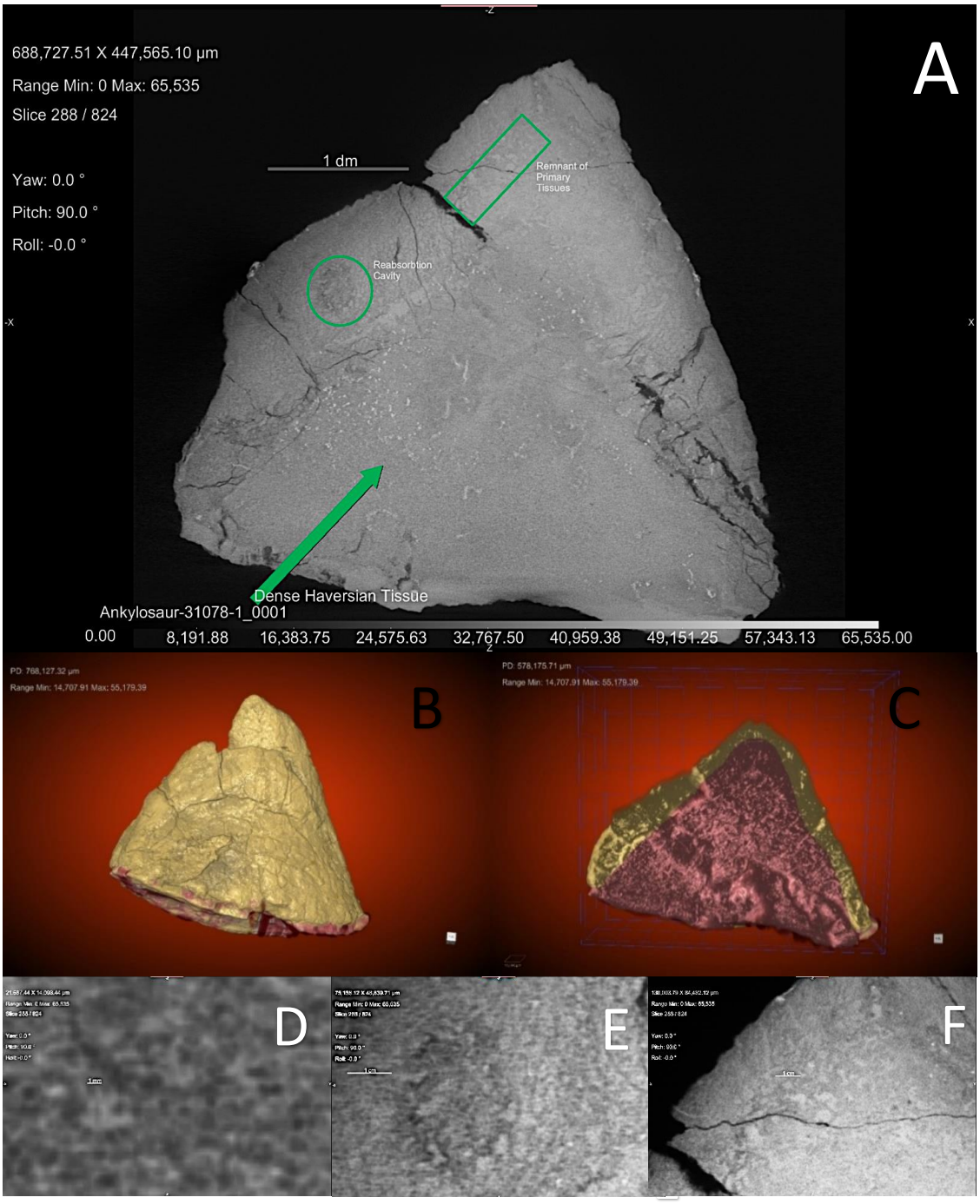

Figure 3. Transverse view showing dense Haversian bone, reabsorption cavities in the external cortex, and leftover primary vascular tissue in the apex of the osteoderm (A). The 3-D model shows what the osteoderm would look like in right lateral view (B). A 3-D image of the transverse view (C) shows the distribution of cortical bone (yellow) and the Haversian core (red). A close up of the Haversian tissue (D) shows the overlap of secondary osteons. In the external cortex reabsorption cavities are identified by the darkened, scalloped edges (E). Primary vascular tissue is preserved in the apex of the osteoderm (F), which had not yet undergone secondary remodeling.

TMM 45605-4 (Figures 4 & 5)

This osteoderm, found in the Aguja Formation, was incomplete and so highly fractured that the anterior edge and part of the right lateral side had to be reconstructed with putty and PaleoBond. From the dorsal view the specimen is elongate, and leaf shaped with a median keel which extends anteroposteriorly with a slight downward slope posteriorly. These features fall under Morphology Type A (pup-tent shaped osteoderm) of Ford (2000) and Blows (2001). The specimen exhibits no projecting rugosities and is sparsely pitted around the keel. On the right lateral side, the specimen has two large vascular foramina orientated obliquely to the osteoderm surface. This side also displays a large and well-developed neurovascular groove. The ventral view of the osteoderm shows a highly concave base; the left and right lateral sides are angled so that the base has a deep "V" shape.

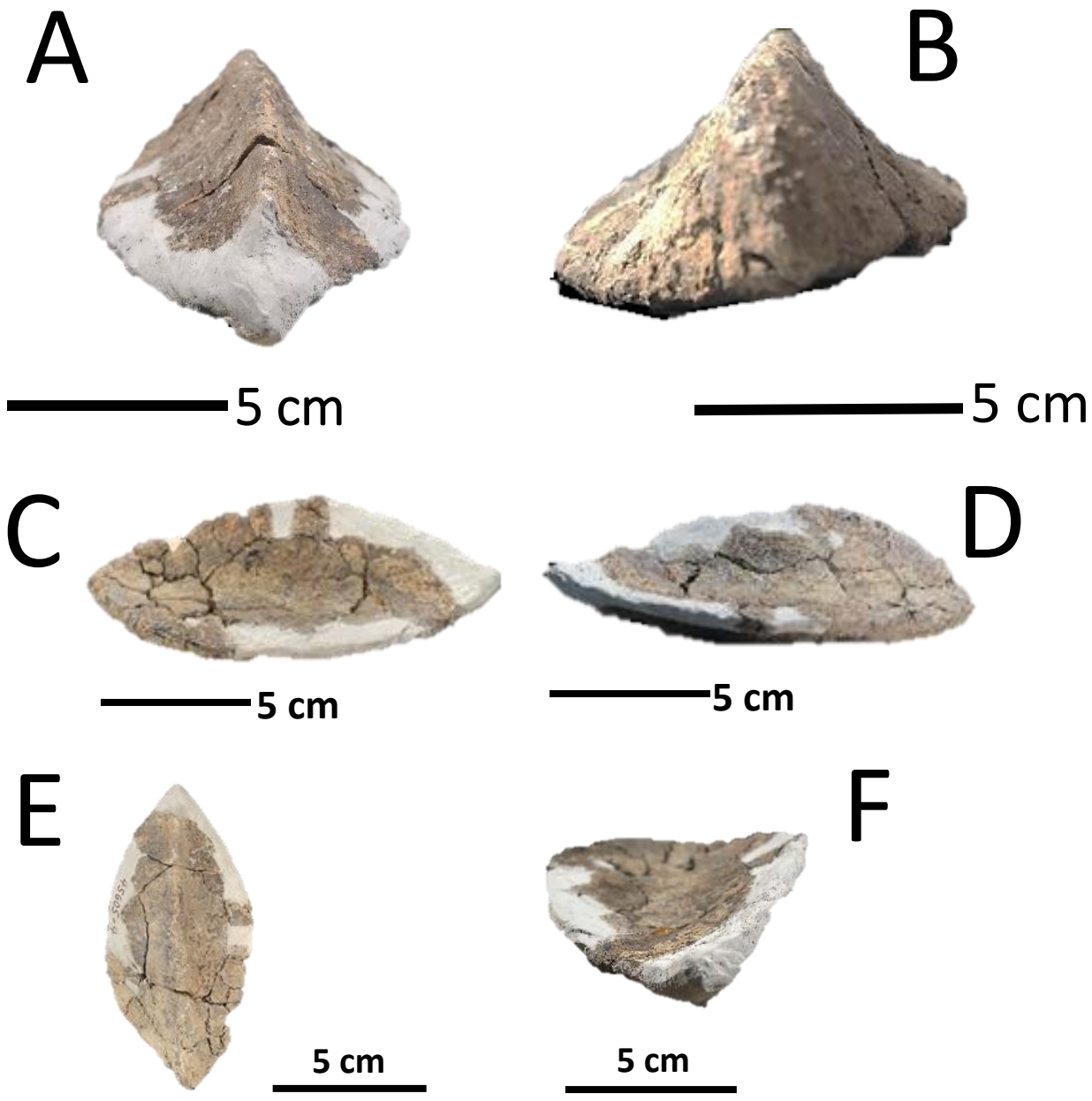

Figure 4. TMM 45605-4 elongated leaf shaped osteoderm with a length that is much longer than its width. From the anterior (A) and posterior (B) views a median keel can be seen running the anteroposterior length of the osteoderm. This view also shows the extensive reconstruction this specimen had to undergo. The right lateral (C) view and left lateral (D) view show the pup-tent morphology of the osteoderm with a slight posterior projection. The dorsal view (E) shows the symmetrical leaf shape of the osteoderm; this morphology is consistent with thoracic osteoderms. The ventral view is shown in part by image F (ventromedial axis), the basal side of the osteoderm is concave with the lateral sides making a deep "V" shape.

The external cortex is thin compared to the core of the osteoderm, however its thickness remains constant. The external cortex has a thickness of 8.7%, while the basal cortex is slightly thinner with a thickness of 6.1%. The cortices are composed of cortical bone but no ISFBs can be observed, possibly due to the mineralization of the specimen. The border between the cortices and core is not well defined, as there are many areas where cortical bone and the trabeculae of the cancellous core overlap. The core itself is 85.2% thick and is composed of a type of cancellous bone called trabecular bone. Trabecular bone is highly vascular, with large void spaces between trabeculae and often contains many vascular canals. These canals are reticular in shape and can be observed running the length of the osteoderm with several bifurcations. In transverse view a vascular canal can be observed with concentric circles of lamellar bone around it. The diameter of the vascular canal is approximately 0.25 cm; much larger than any other vascular canal found in the osteoderm. The concentric rings around the canal suggest that it was in the process of being remodeled into a primary osteon (Padian and Lamm, 2013). The 3-D segmentation also reveals that areas of the external and basal cortices are so eroded that the trabecular core is exposed. This feature would be very difficult to distinguish with the human eye given the pre-existing thinness of the cortices. The size and morphology of this osteoderm is typical of a medial cervical osteoderm, perhaps even part of a cervical half ring. Although the base of the osteoderm is highly concave, the thinness of the basal cortex, in relation to the thick trabecular core, is indicative of a nodosaurid (Scheyer and Sander, 2004). Due to the sparseness of neurovascular grooves on the surface this specimen is more likely to be related to *Edmontonia*, and *Panoplosaurus mirus* than *Glytodontopelta mimus.* The oval shape of the osteoderm and concentration of pitting around the keel distinguishes this specimen as *Panoplosaurus mirus* which exhibits long sub-oval to oval cervical osteoderms compared to the square or rectangular cervical osteoderms of *Edmontonia* (Carpenter and Currie, 1990*)*.

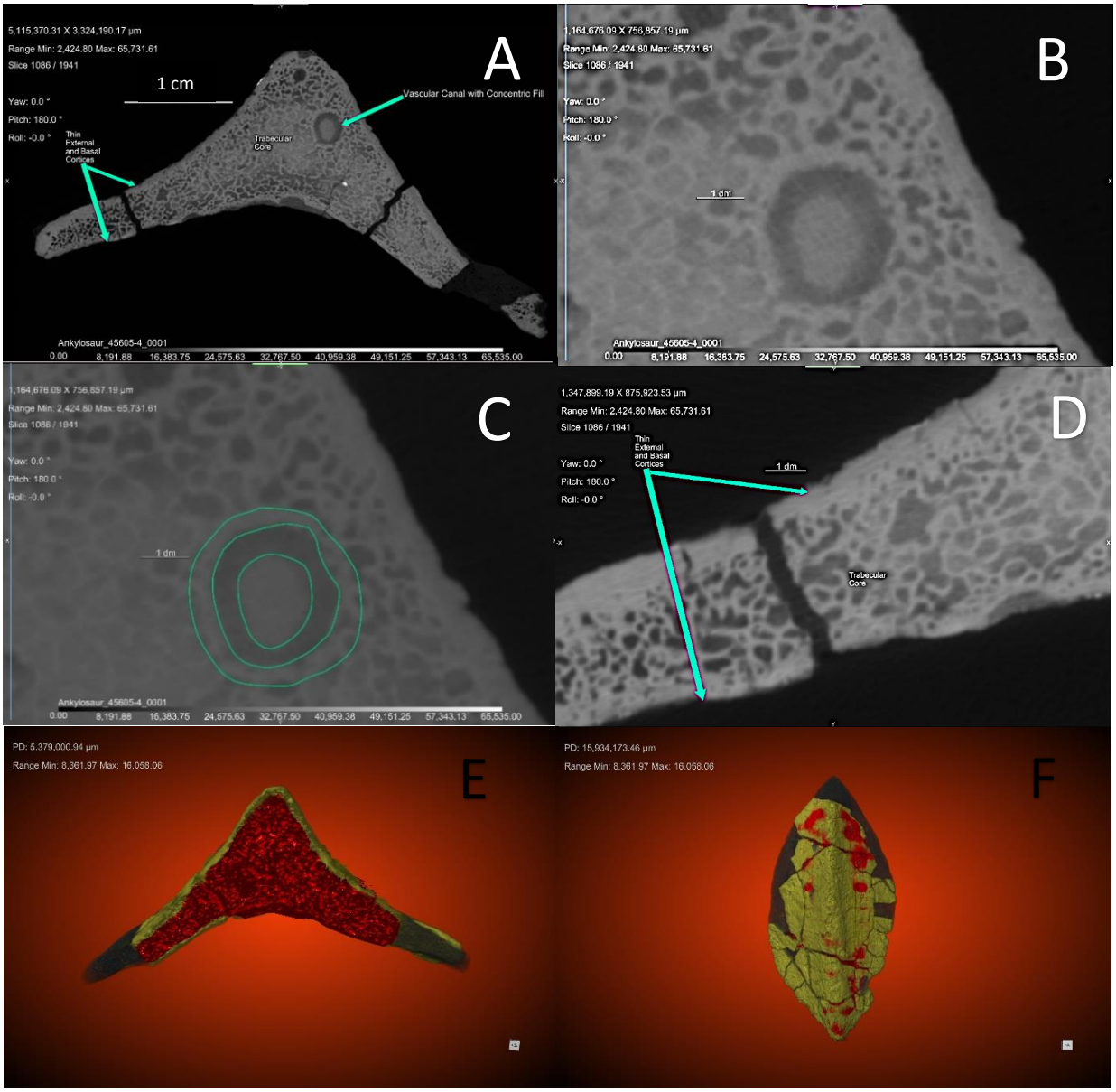

Figure 5. The transverse view of TMM 45605-4 show thin external and basal cortices compared to a thick trabecular core, with a prominent vascular canal on the right side of the slice (A). A close up of the vascular canal is seen in image B. In image C the concentric fill is seen to form concentric rings of lamellar bone around the canal. A close up of the cortices and core (D) show the relative thickness of these tissues in the specimen. A 3-D model of the transverse view reveals that part of the basal cortex is eroded (E). A dorsal view of the 3-D model also shows erosion of the external cortex (F).

TVP 45866-2 (Figures 6&7)

TVP 45866-2 (field number TL-05-01) was collected from a sandstone bed within the Aguja Formation by Dr. Lehman of Texas Tech University and Steve Wick in 2005. In 2019 Dr. Lehman confirmed that this specimen was an osteoderm belonging to a then unknown ankylosaur (Lehman pers. comm.). This osteoderm is sub-oval shaped (with slight erosion on the anterolateral edge) with a median keel. Given the almost circular base and keel structure this osteoderm falls under the Morphology A shape for ankylosaur osteoderms. The external surface of the osteoderm features extensive pitting with projecting rugosities along the keel and left lateral side. The dorsal side of this specimen exhibits four foramina and one prominent neurovascular groove, while the ventral side is smooth and almost completely flat. On the ventral side 3-D imaging shows that the basal cortex is extremely thin and has undergone extensive erosion to the point where the core of the osteoderm has been exposed. However, the erosion of the basal cortex reveals a large bifurcated vascular canal to be viewed in hand sample. Dorsal to the vascular canal the external cortex of the osteoderm projects laterally and is thickened at the base forming a small shelf. This region of the osteoderm would have been where the dermis and small muscles attached to the osteoderm to hold it in place.

Figure 6. The ventral side of TVP 45866-2 exhibits a smooth flat surface that is partially eroded (A). The dorsal side of the osteoderm has extensive pitting and projecting rugosities along the keel and left lateral side, as well as several foramina and one vascular canal (B).

The core of this osteoderm is made up of trabecular bone, which is 81% of the total osteoderm thickness. The trabecular core exhibits contrasting mineral fill, which made segmentation particularly difficult. The basal cortex is extremely thin and even missing in some areas, so no accurate thickness could be taken for this cortex. The external cortex is well preserved and accounts for 19% of the total osteoderm thickness. Reabsorption cavities are present in the external cortex indicating that the osteoderm underwent remodeling as the animal grew. A large primary osteon can be seen at the base of the keel in transverse view; the concentric lamellar bone around the osteon is well preserved. The first occurrence of ISFBs in this study is observed in the external cortex of TVP 45866-2. These fiber bundles are arranged 3-dimensionaly in the external cortex and intersect at 45° angles. This is indicative of the orientation of ISFBs in nodosaurid osteoderms (Scheyer and Sander, 2004). The morphology of the osteoderm is similar to that of the distal cervical osteoderms of *Edmontonia* (Carpenter and Currie, 1990). This along the histology of the specimen suggest that this specimen is from a nodosaurid.

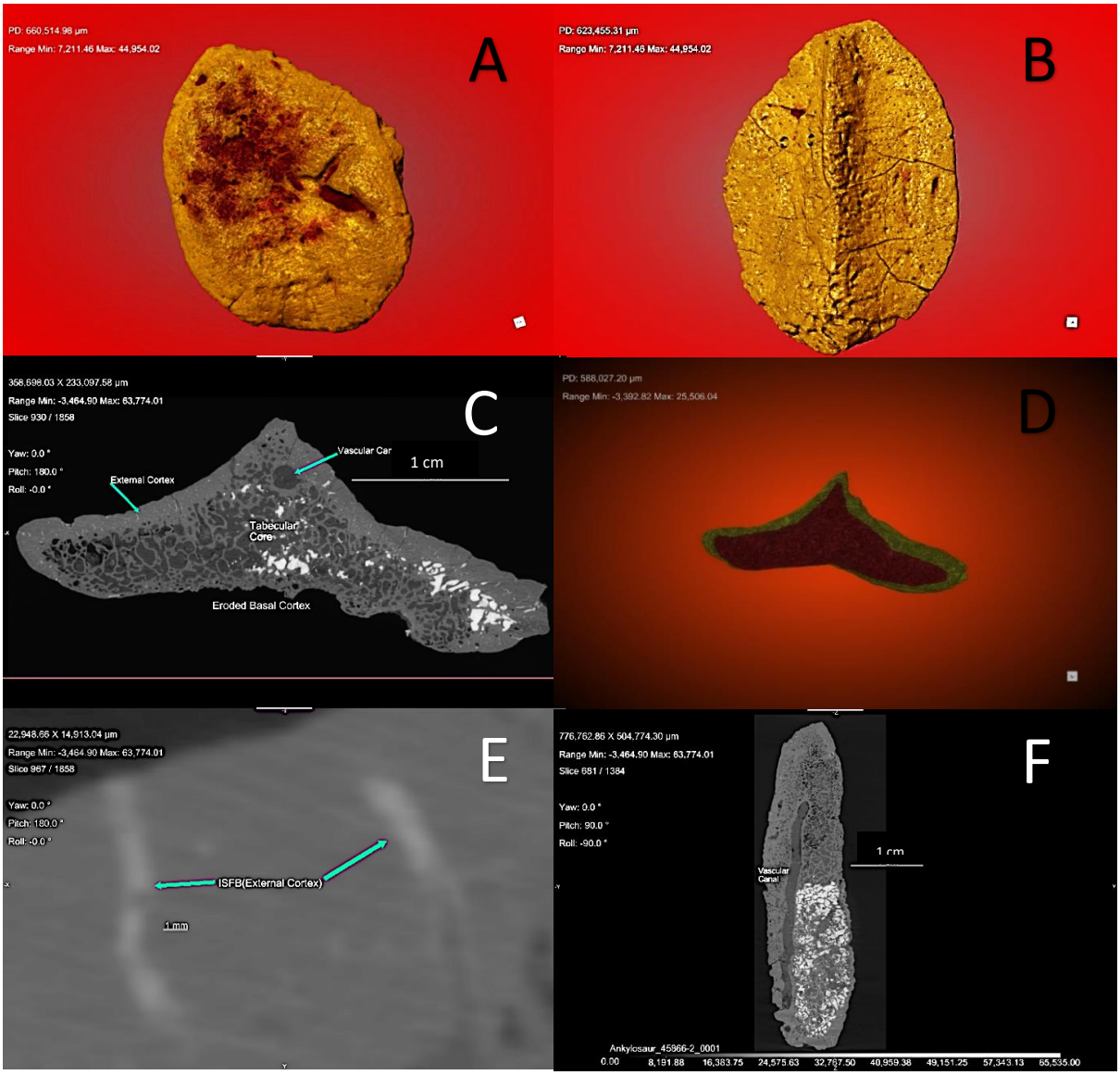

Figure 7. TVP 45866-2: Erosion of the basal cortex reveal bifurcating vascular canals in trabecular core (A). Dorsal view real four vascular foramina and one neurovascular groove (B). Pitting and projecting rugosities are also observable in dorsal view. The transverse view reveals the eroded basal cortex and thin external cortex (C). This image also shows a thick trabecular core with constating mineral fill and a vascular canal. A 3-D model of the transverse view exhibits the relative thickness of the core and cortices (D). The external cortex contains ISFBs orientated 3-dimensionally and intersect at 45° (E). A slice through the left lateral side reveals that the vascular had not undergone perforation (F).

Osteoderm #1 (Figs. 8 & 9)- see WPA-3 Specimens

This osteoderm is from the WPA-3 quarry; a fossil locality of the Aguja Formation in Big Bend National Park. The specimen was found in the basement with other ankylosaur specimens with the designation numbers WPA-3 and PL-3. These specimens were all found in the quarry and were therefore assumed to belong to the same individual. This was the initial specimen tested to determine whether paleohistology could be studied using Dragonfly ORS. This specimen falls under Morphology C with a median keel and an anterior and posterior ridge. The keel of the osteoderm is tall and curves to the right posteriorly, in addition there is a slight shelf on the posteroventral edge. This morphology suggests that this a right medial osteoderm of a cervical half ring. The base of the osteoderm appears to be flat but has been highly eroded to the point where the core has been exposed on the left ventral side. The external surface is slightly fractured, with sparse neurovascular grooves, and a pitted keel.

Figure 8. The dorsal view of an unknown TMM osteoderm with a high curved keel which projects to the right posteriorly. The left anterolateral edge and the base of the osteoderm is highly eroded.

The core of the osteoderm is made up of Haversian bone with a thickness of 64.4%. The basal cortex has a thickness of 15.6% while the external cortex has a thickness of 20%. There is evidence of secondary remodeling due to the presence of dense Haversian tissue. When zoomed in to 1mm scale in transverse view secondary osteons can be observed in the inner region of the primary osteon. This is

additional evidence of secondary remodeling. In dorsal view sparse Haversian canals can be observed along with blood vessels that have begun to pinch off. This is the start of the development of a primary osteon, which indicates that the osteoderm was actively undergoing remodeling. When secondary osteons are found within a primary osteon the structure is called an osteocyte (Padian and Lamm, 2013). Further evidence for this is the possible occurrence of remnant trabeculae at the border of the core and cortices. This specimen is one of only three where ISFBs can be viewed in the cortex (again due to possible difference in mineral fill) with two sets of fiber bundles orientated perpendicular to the osteoderm; no LAGS are observed in either of the cortices. The extensive remodeling and well-developed Haversian core suggest that this osteoderm came from an adult. These characteristics indicate that this specimen came from a derived ankylosaurid; those in the subgroup Ankylosaurinae. The osteology and histology of this osteoderm is similar to the cervical half-rings of known specimens of *Euoplocehpalus sp*.

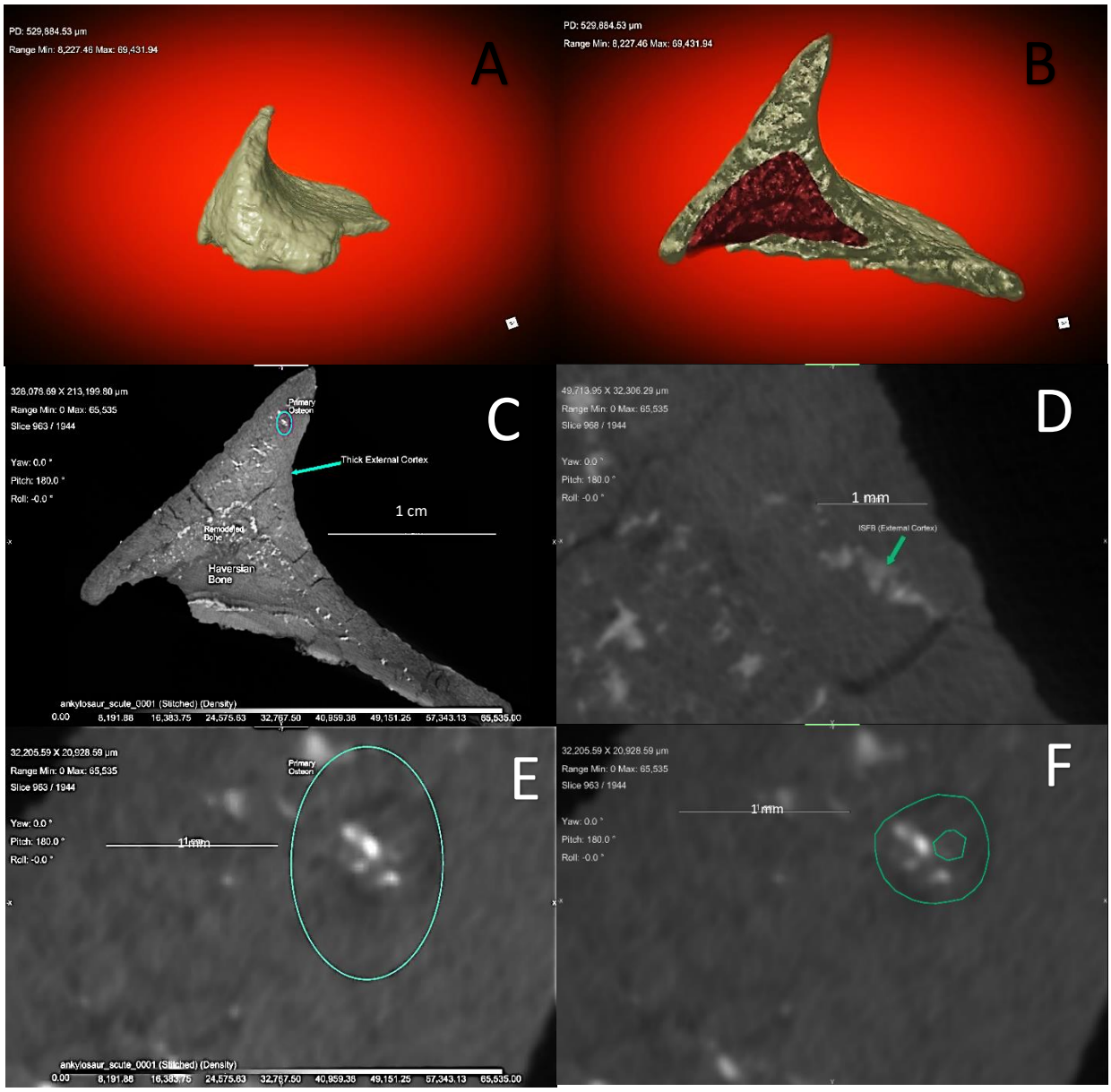

Figure 9. The 3-D model of the un-numbered TMM osteoderm in anterior view (A). The 3-D model of the transverse view show the thickened cortices compared to the small Haversian core (B). The transverse view shows a Haversian core with secondary remodeling of vascular tissue (C). This image also reveals a primary osteon in the keel of the osteoderm. A close-up view of the osteon is shown in image E, with the concentric lamellar fill outlined in image F. The external cortex exhibits ISFBs arranged in a random orientation (D).

TMM 40484-46 (Fig. 10)

This specimen is the only osteoderm not discovered in Big Bend National Park but was chosen to use as a comparison for the other osteoderms. This specimen was discovered in the Oldman Formation located near Steveville, Alberta, Canada and was identified as a left cervical osteoderm belonging to *Panoplosaurus mirus* (UT VPL Records). The osteoderm is sub-oval in shape, with the left anterolateral edge being eroded. The ventral side is flat while the dorsal side exhibits a low median keel; the shape of this specimen falls under Morphology A. The external texture of the specimen exhibits no projecting rugosities, however reticular vascular canals are present on the dorsal edge of the osteoderm with a large foramen on the left dorsal surface. Pitting on the surface is extensive on the external surface of the osteoderm. The cortical bone thickens on the left ventroposterior edge creating a shelf, which would have been where dermal muscles attached to the osteoderm. This is very similar to the osteology of TMM 45605-4, which has been identified in this study as *Panoplosaurus mirus* as well.

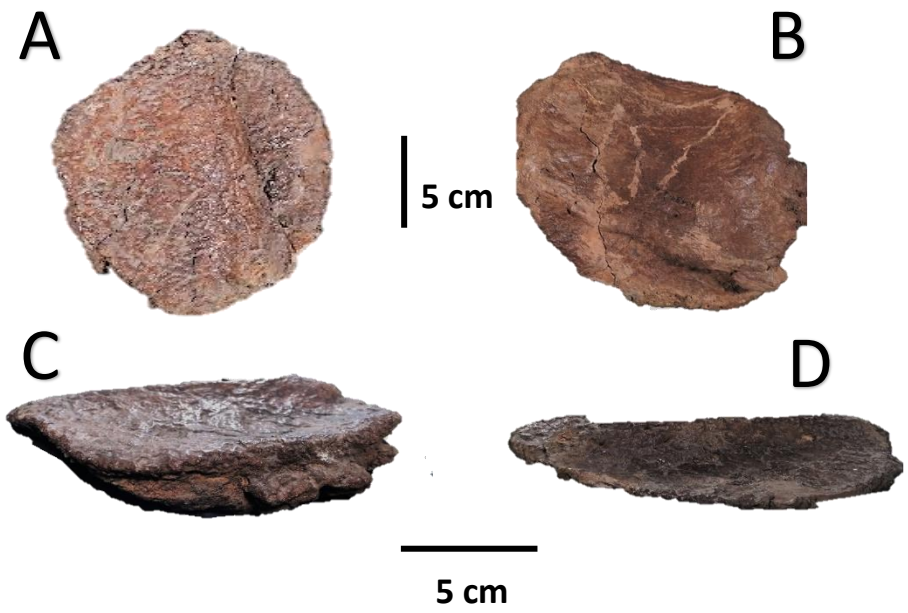

Figure 10. The dorsal view of TMM 40484-46 shows the sub-oval shape of the osteoderm, and one foramen on the external surface (A). The ventral view of the specimen exhibits a smooth flat base with a shelf on the left ventroposterior edge (B). The left lateral view reveals the thickening of the cortical bone to form the shelf, and extensive pitting on the external surface (C). The right lateral view exhibits the low median keel of the osteoderm (D).

The histology of this specimen is very complex and could not be segmented by the Dragonfly ORS program. Like most nodosaurids the basal and external cortices are thin compared to the core. The basal cortex makes up 32.3% of total osteoderm thickness, whereas the external cortex makes up 18.7% of the total thickness. The core itself consists mostly of trabecular bone, however, there is a region of Haversian bone in the center of the core which thickens towards the basal cortex. The overall thickness of the core is 49%. The border between the basal cortex and this region of Haversian bone is almost imperceivable as the Haversian tissue seems to grade into the cortical bone. The cortical bone of both cortices contains small reabsorption cavities. The specimen exhibits extensive pathways of vascular canals branching off laterally from one main feeder canal extending anteroposteriorly along the keel. Some of these blood vessels have begun to perforate (the first step in the process of osteon development), but no fully formed primary osteons are present. Lines of arrested growth were not found in the cortical bone; however, they may not be detectible in CT scans at this scale. These features indicate that the osteoderm was undergoing extensive secondary remodeling before the animal's death. The presence of trabecular and Haversian bone in the core, along with secondary remodeling of the osteoderm, indicate that the animal could have been a juvenile undergoing a period of growth. It is not uncommon for nodosaurid osteoderms to have Haversian bone in their cores (Scheyer and Sander 2004, Burns and Currie 2014). Most likely the presence of this bone tissue could be due to ontogenetic development, which would be consistent with the features observed in other specimens and previous studies.

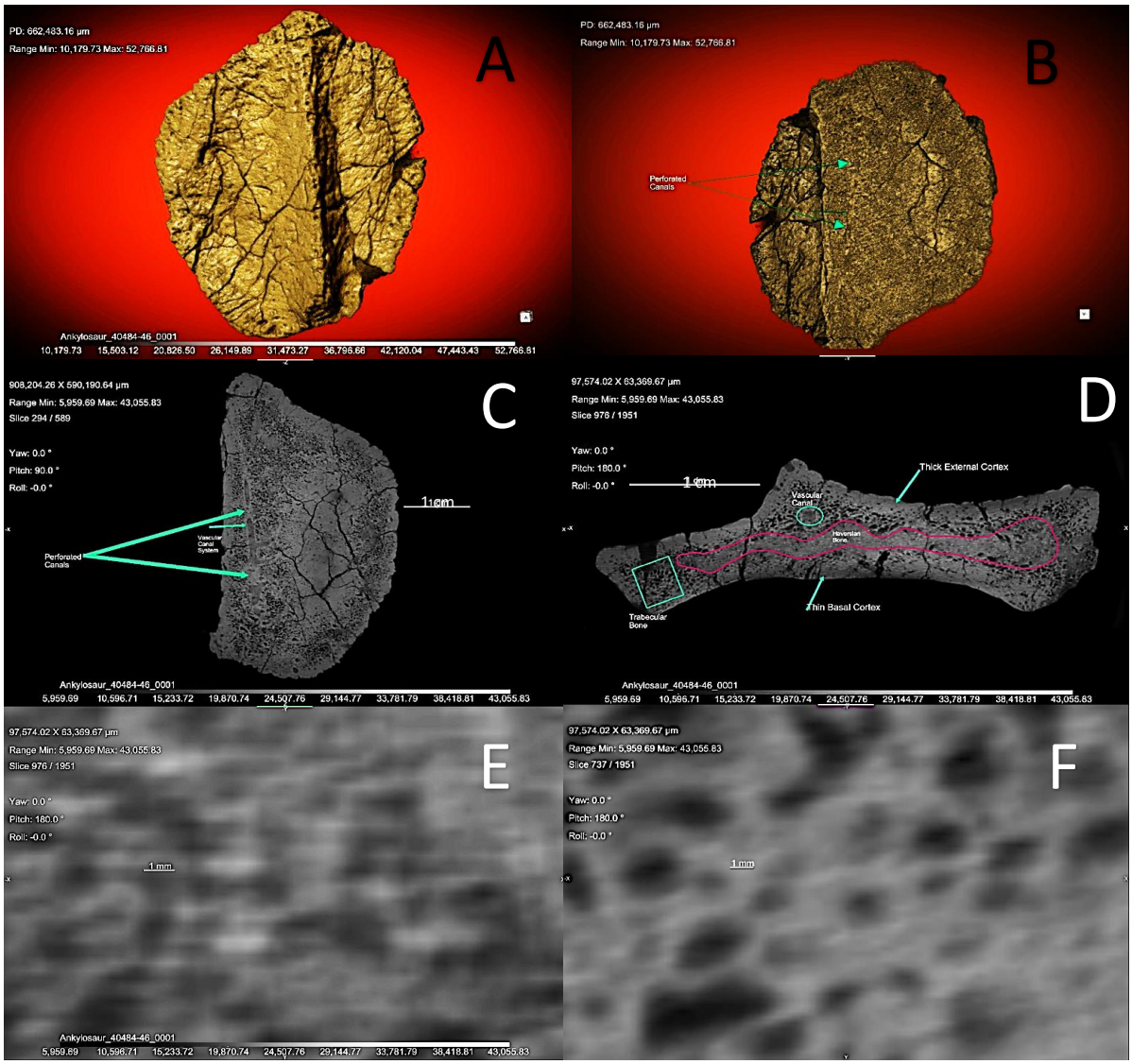

Figure 11. The 3-D model of dorsal view of the osteoderm enhances the external texture of the specimen, revealing a large foramen on the left dorsolateral side along with extensive pitting and neurovascular grooves (A). By clipping image an outline of vascular canal can be seen running anteroposteriorly along the keel (B). The same image can be seen in the dorsal view of a CT scan; perforation of the vascular vessels can also be observed (C). The transverse view of the CT scan reveals the complex histology of the osteoderm, along with the transverse view of the vascular canal (D). The close of the Haversian bone show overlapping secondary osteons, which indicate secondary remodeling in the specimen (E). At the same scale the texture of the trabecular bone can be used to compare primary bone tissue (vascular tissue) to secondary bone tissue (Haversian tissue) (F).

TL-05-14 Sacrum (Fig. 12)

This partial sacrum was found in the upper shale member of the Aguja Formation by Steve Wick and Dr. Lehman in 2005. The sacrum consists of a partial dorsal (pre-sacral) vertebra which is partially fused to the first sacral vertebra. The first and second sacral vertebrae have a pair of sacral ribs attached to them, however the shelf of the diapophyses, where the ribs attach is smooth resulting in some of the ribs having to be reattached to the sacrum using PaleoBond. Furthermore, there is no evidence that the distal edge of the sacral ribs had yet fused to the ilium. The neural arches of the sacral vertebrae are only a few centimeters high and are not fused together, which is a common condition in juvenile ankylosaurs of both families. The bones of the sacrum are either partially fused or not fused at all, another juvenile ankylosaur trait; as the animal grew the vertebrae and ribs would fuse to each other as the pelvis created a support system for a large heavy body (Coombs, 1978) The angle and width of the sacral ribs suggest that the ilia would have been in a horizontal position and would have been rotated slightly outward .This is a condition in derived ankylosaurids, and when compared to known ankylosaurinae the first sacral rib of the sacrum bears a remarkable resemblance to first sacral rib of *Euoplocephalus sp* (Carpenter 2012 and Carpenter et al., 2013). A specimen of this taxa, AMNH 5337, which has been studied extensively in previous literature and was studied in person at the AMNH in New York, is the closest match when compared to both derived and basal ankylosaurs.

Fig. 13 was taken from Carpenter et al. (2013) which compares pelvi from various ankylosaurs through time. This shows the evolution of the ankylosaur pelvis and the distinct pelvic characteristics of these six taxa. The *Euoplocephalus tutus* specimen is the same AMNH 5337 pelvis that is compared to TL-05-14. Note the differences between *Euoplocephalus* and *Edmontonia*. The *Edmontonia* specimen has two more pre-sacral ribs than *Euoplocephalus*, and the first sacral rib is fused to the acetabular process unlike the first sacral rib in *Euoplocephalus*. Futhermore, the ilia of *Edmontonia* have not undergone the degree of horizontal rotation observed in *Euoplocephalus*. It should be noted that in basal ankylosaurs and thyreophorans the ilia are vertically, as seen in *Strombergia* (basal

thyreophoran). The degree of horizontal rotation of the ilia undergone by later taxa is a substantial characteristic which delineates basal ankylosaurids and nodosaurids from members of the ankylosaurinae.

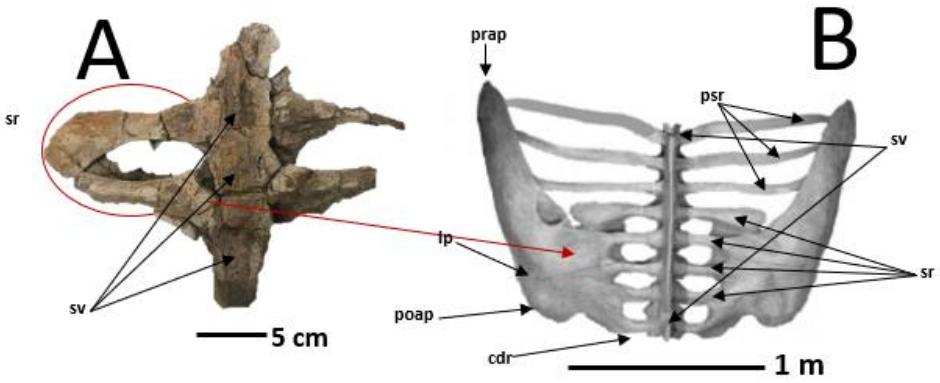

Figure 12. The TL-05-14 sacrum (A) compared to the complete AMNH 5337 (B) shows not only the size difference between the two, but the unfused elements of the TL-05-01 sacrum to the fused elements of AMNH 5337. The unfused sacral ribs and neural arches of TL-05-01 are the juvenile condition in ankylosaurs, while the fusion of such elements such as in AMNH 5337 are the typical adult condition. Abbrviations- sacral vertebra-sv, sr- sacral ribs, prap- preacetabular process, psr- pre-sacral ribs, lp- lateral process, poap- postacetabular process, cdr- caudal rib.

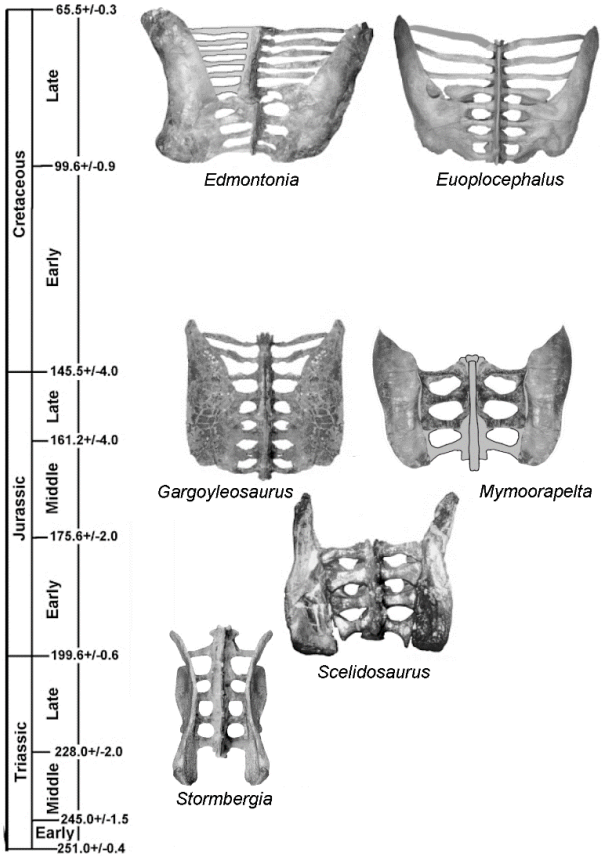

Figure 13. Image of thyreophoran pelvi taken from Carpenter et al.

TL-05-14 Vertebra (Fig. 14)

This specimen was found attached to the partial sacrum discovered by Steve Wick and Dr. Tom Lehman in 2005. This vertebra, as well as the sacrum, was found in the upper shale member of the Aguja Formation. This vertebra has similar width and height, and the spinous process is angled posteriorly. There is a partial transverse process remaining on the left side, whereas the on the right side the transverse process is missing entirely. Since the vertebra was attached to the sacrum in front of the first sacral rib this specimen can be identified as the third pre-sacral rib. There is a small thumb-shaped facet anterior to the left of the transverse process, and the neural arches appear to be only partially fused to the centrum, which is an ontogenetic feature of juvenile ankylosaurs (Coombs, 1978). Because this vertebra is part of the sacrum described above it can also be attributed to *Euoplocephalus sp.*

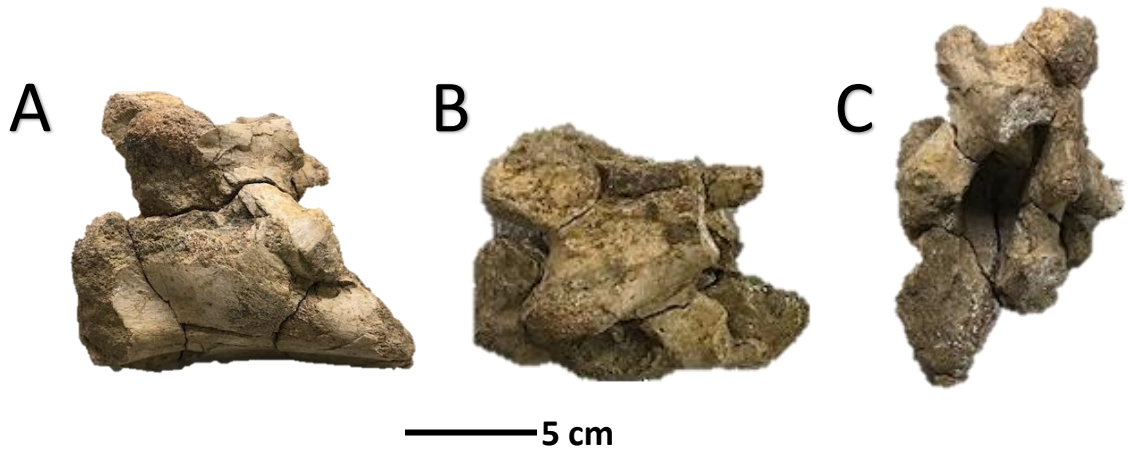

Figure 14. TL-05-14 in right lateral (A), dorsal (B), and anterior (C) views.

TMM 43057-502 (Fig. 15)

This specimen was collected from Terlingua Microsite #1 (Aguja Formation) by Tim Rowe and was identified by J.R. Wagner in 2006 as the sacral vertebra of a juvenile ankylosaur, as indicated by the

specimen note card. The specimen consists of only a partial centrum with no diapophyses, neural arch, or transverse processes. These could be missing due to these elements not being fused together in young ankylosaurs. However, after comparing the element to other known vertebrae the element is more consistent with a cervical or thoracic vertebra. The length and width of the centrum is not consistent with sacral vertebrae, which tend to be longer than they are wide. Unfortunately, no familial or taxa classification cannot be determined, although the size is consistent with the vertebra of a juvenile ankylosaur (Carpenter, 2012).

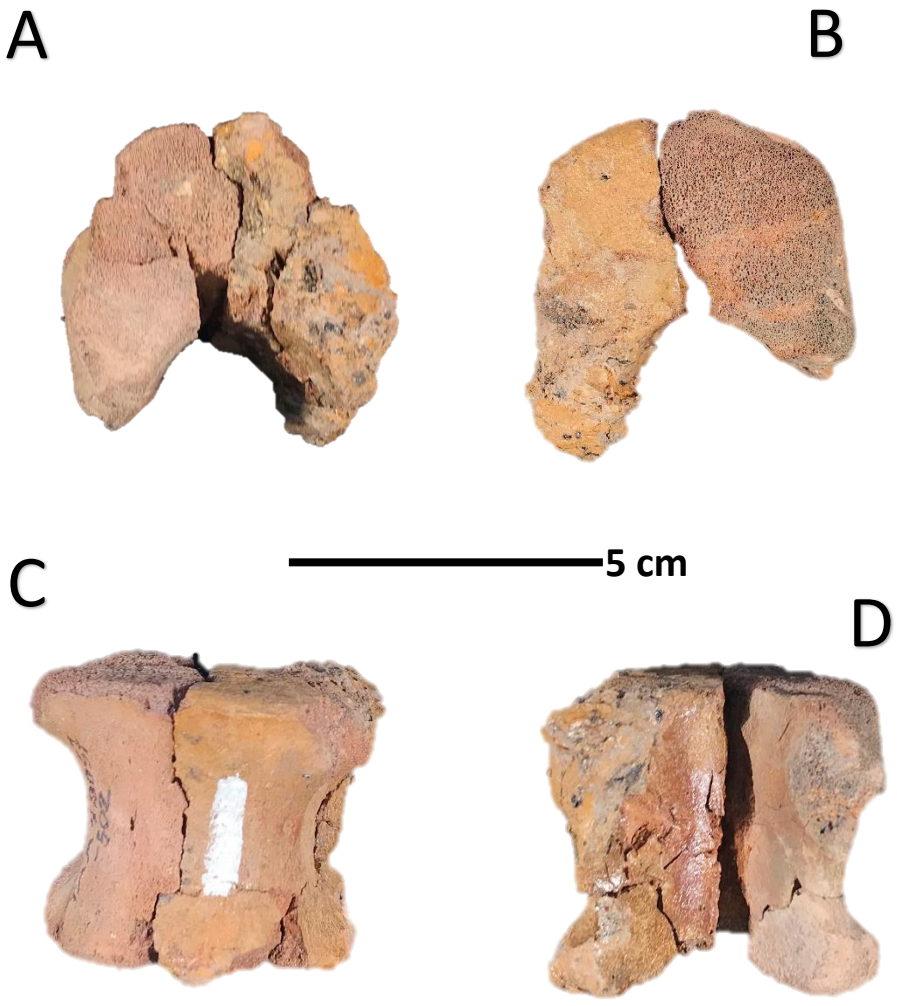

Figure 15. TMM 43057-502 in anterior (A), posterior (B), dorsal (C), and ventral (D) views.

TMM 41836-1 (Fig. 16)

This specimen is the right tibia of a nodosaurid collected from the Aguja Formation in 1976. Overall the tibia is in good condition with some missing pieces on the shaft being replaced by putty. The shape of this element is consistent with that of ankylosaurs of both families with the shaft twisted along its length so that the knee would be at a right angle with the foot. The cnemial crest (the point of insertion for the extensor muscles of the knee) on the proximal end of the tibia is slightly eroded. The astragalus is fused to the distal end of the tibia and is similarly damaged (Carpenter 2012). The assertion that the tibia is from a nodosaurid is disputable; nodosaurids have a longer tibia length compared to the femur whereas ankylosaurs have a tibia length that is less than two-thirds the length of the femur (Kirkland et al., 2013). Without the femur for comparison it cannot be assigned to the Nodosauridae.

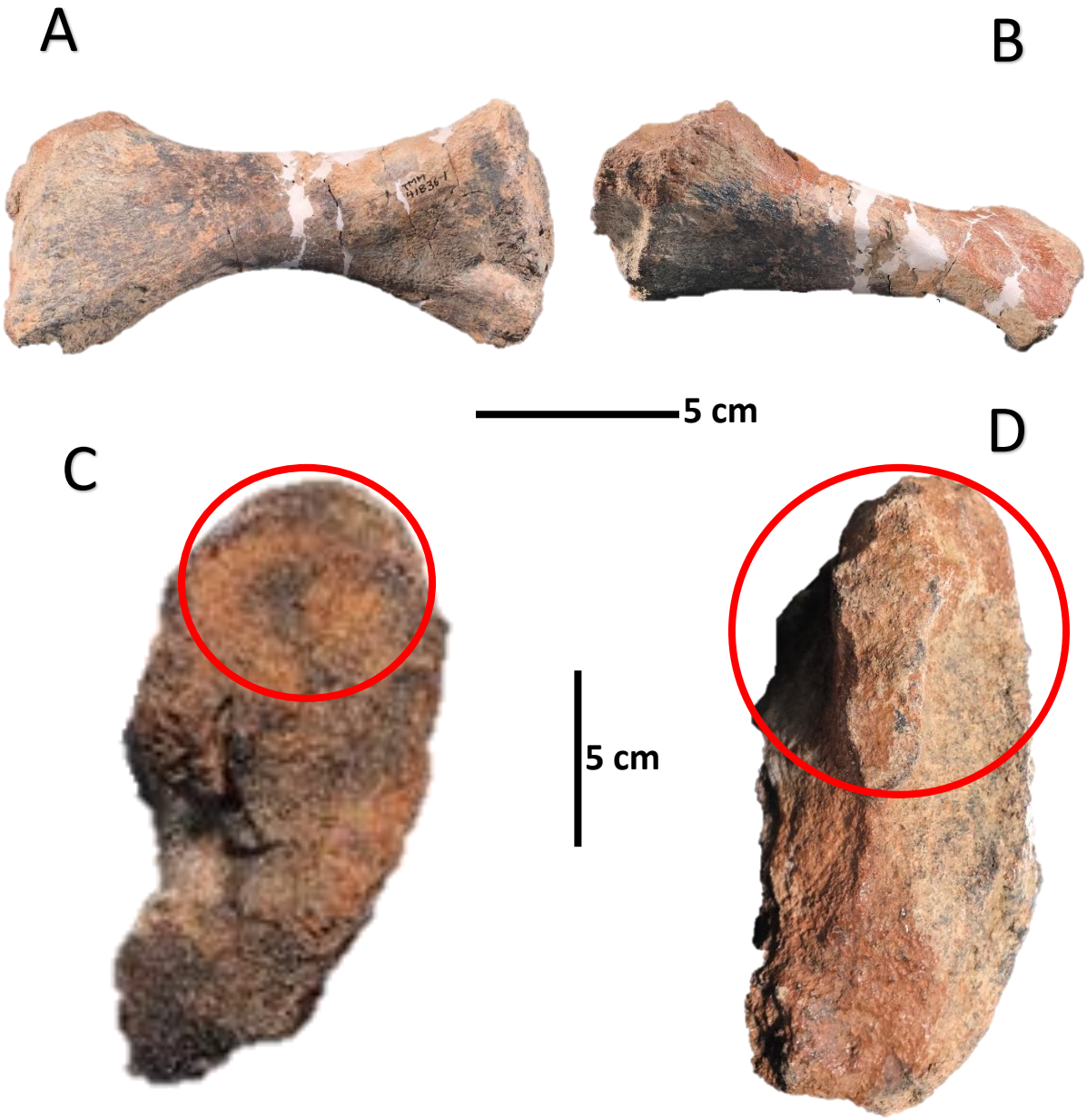

Figure 16. TMM 41836-1 in right lateral (A) and left lateral (B) views. The dorsal view (C) reveals what remains of the cnemial crest on the proximal end of the tibia. The ventral view (D) reveals what is left of the astragalus in ventral view.

TMM 42878-1 (Fig. 17)

This specimen is from the Peña Mt. area so is from the Aguja Formation. Previously identified as a distal limb bone of an undetermined ankylosaur, I determined that this specimen is the distal end of a femur of a juvenile ankylosaur. The ventral side reveals the medial and lateral condyles, which serve as the attachments for the tibia and fibula. The specimen in only 6 cm wide, indicating that this was a young ankylosaur. The anterior side of the shaft has been shorn revealing a glimpse of the trabeculae of the femoral shaft. Unfortunately, this is not enough evidence to assign this specimen to either family.

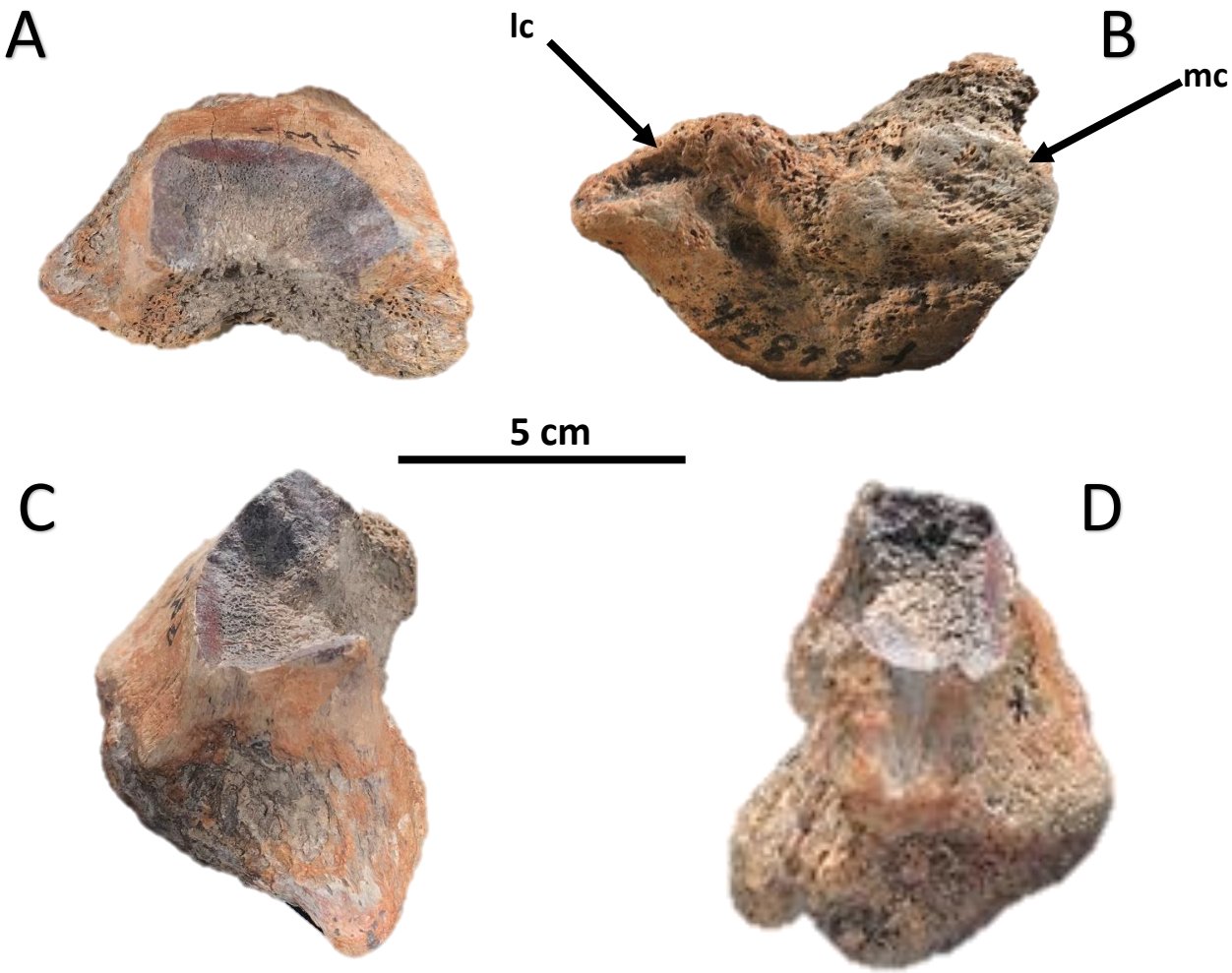

Figure 17. The distal end of TMM 42878-1 shown dorsal (A), ventral (B), left lateral (C), and right lateral (D) views. The ventral views exhibit the lateral (lc) and medial condyles (mc).

WPA-3 QUARRY SPECIMENS

The following specimens were found in the basement of the VPL. The specimens were identified with the designation PL-3 on an index card indicating that they were found in the Aguja Formation. Dr. Tom Lehman (pers. comm.) noted that these specimens were found in association with each other and are from the UTEP WPA-3 quarry in Big Bend. The following specimens are hereby designated by type of skeletal element and the order in which they were found.

Osteoderm #1 (Fig. 18)

As previously stated in the last section this specimen shares histological and osteological characteristics with the osteoderms of the cervical half-rings of *Euoplocephalus sp.*

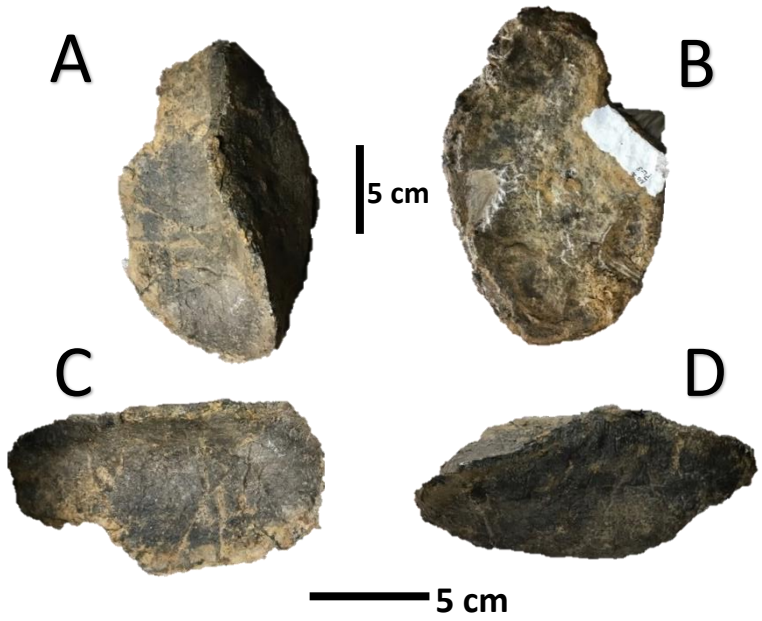

Figure 18. This WPA-3 osteoderm was found in the basement of the VPL along with other ankylosaur specimens from the Aguja Formation. The dorsal view (A) of an unknown TMM osteoderm with a high curved keel which projects to the right posteriorly. The left anterolateral edge and the base of the osteoderm is highly eroded. The shape of the osteoderm falls under Morphology A. In ventral view (B) the base of the osteoderm is relatively flat but is highly eroded. The left lateral (C) and right lateral (D) views show smooth external surface with sparse neurovascular grooves and pitting.

Osteoderm #2 (Fig. 19)

This osteoderm has a circular, slightly concave base with a tall median keel which projects posteriorly, giving it an almost conical appearance. The shape of this specimen falls under Morphology B. The base has been damaged during preparation, however the external texture of the specimen is still preserved. The external texture is smooth with sparse pitting and one bifucating neurovascular groove; a large fracture can be seen on the right lateral side. This morpholpogy of this specimen is similar to the median thoracic osteoderms of other Late Cretacous ankylosaurids such as *Ankylosaurus magniventris, Euoplocephalus sp,* and *Scolosaurus nopsca*. Considering that *Euoplocephalus sp* is the only known ankylosaurid confirmed in Big Bend it is possible that this osterderm belongs to this taxon. However, a histologic study in the future would be needed to confirm this.

Figure 19. Osteoderm #2 in dorsal (A), ventral (B), right lateral (C), and left lateral (D) views.

Osteoderm #3 (Fig. 20)

This specimen is similar to Osteoderm #2 with a tall median keel that projects posteriorly, however, the apex of the keel is broken. The base is more oval in shape than Osteoderm #2, but both specimens exhibit a slightly concave base. This is another osteoderm with a Type B morphology. The external surface of the specimen is smooth with sparse pitting; no neurovascular grooves where observed in this specimen. As with the previous specimen a histologic test would be needed to confirm whether this is indeed an ankylosaurid (perhaps even *Euoplocephalus sp)* osteoderm.

Figure 20. Osteoderm #3 in dorsal (A), ventral (B), left lateral (C), and right lateral (D) views.

Osteoderm #4 (Fig. 21)

This specimen is a small fragment of an osteoderm that appears to be the distal end of an osteoderm that has broken off. The external surface is highly eroded. Due to its size and fragmentary nature this element is nondiagnostic.

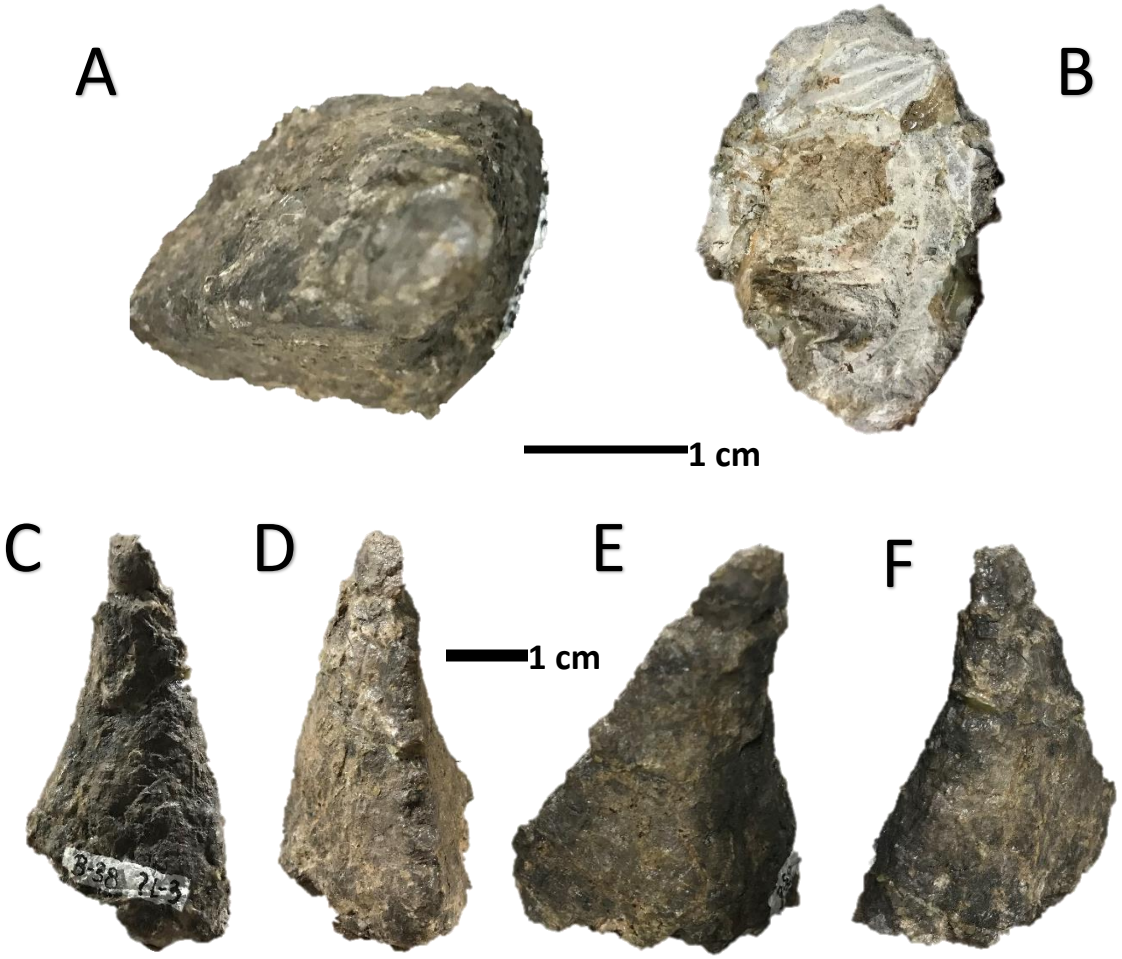

Figure 21. Osteoderm #4 in dorsal (A), ventral (B), anterior (C), posterior (D), left lateral (E), and right lateral (F) view.

Osteoderm #5 (Fig. 22)

This specimen has a Type B morphology similar to Osteoderms #2 and #3. The only outstanding difference is that Osteoderm #5 has a flat base. The external surface of this specimen is highly eroded, which has obscured any pitting or vascular canals that may be present. The apex of the osteoderm is missing as well. This osteoderm is similar to the caudal osteoderms of ankylosaurids as with the prevoius osteoderms future tests are needed to confirm this desgination.

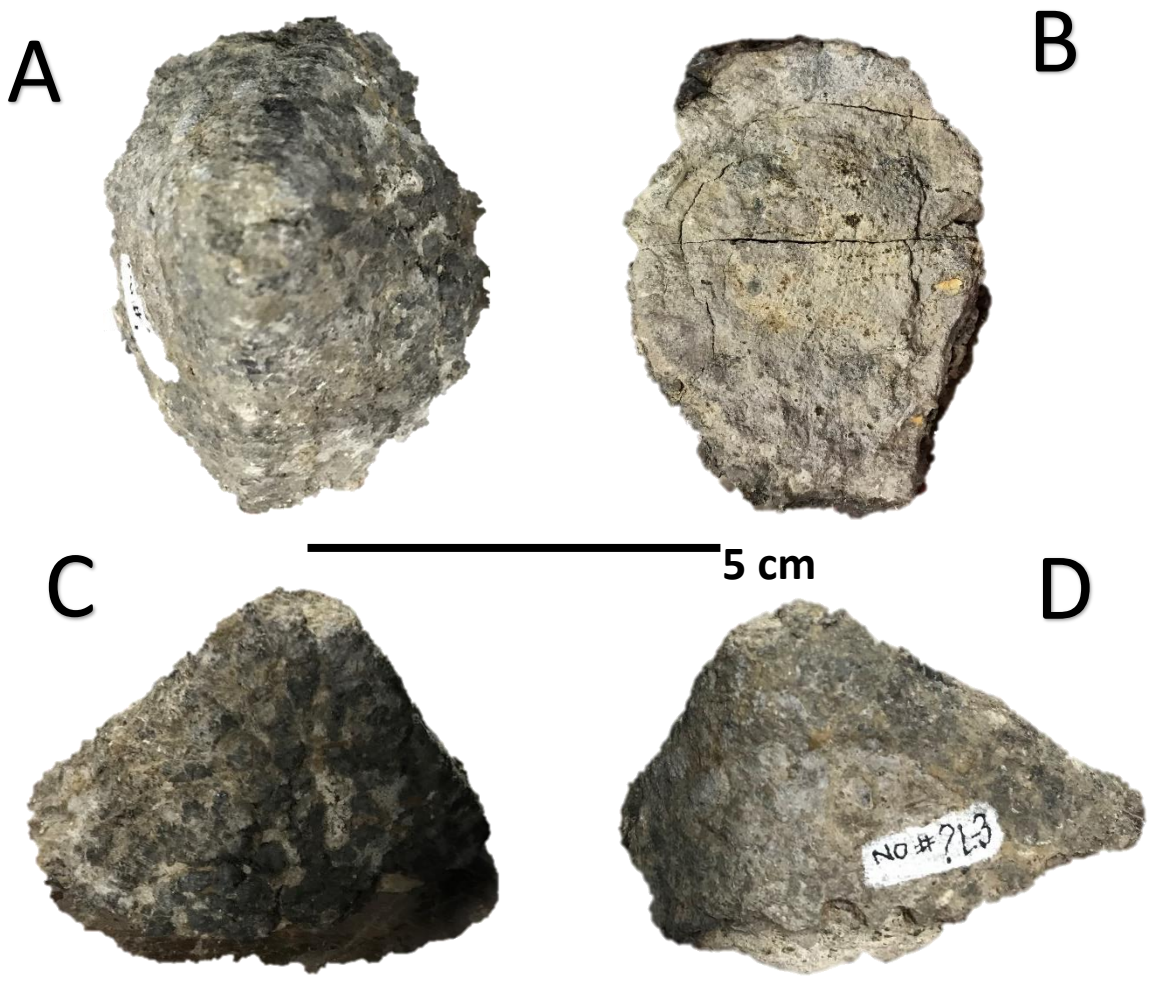

Figure 22. Osteoderm #5 in dorsal (A), ventral (B), left lateral (C), and right lateral (D) views.

Osteoderm #6 (Fig. 23)

This osteoderm is shaped similarily to most of the specimens mentioned above. The base is wider and flat but is circular in shape. The specimen has a median keel that projects posteriorly into a sharp apex. Once again this osteoderm has a Type B morphology. The only significant difference is a shelf along the posterior edge of the osteoderm. The shelf would have been imbedded in the dermis, and would have been held in place by dermal muscles. There is extensive tool damage to the base of the osteoderm, but the external texture is still preserved. The osteoerm surface exhibits projecting rugosities and extensive pitting; no neurovasculaer grooves were observered. The morphology of this osteoderm is similar to the lateral or distal thoracic osteoderms of ankylosaurids; the posterior projecting apex is very similar to *Ankylosaurus magniventris* and *Euoplocephalus sp*. Future histologic tests will be need to confirm this.

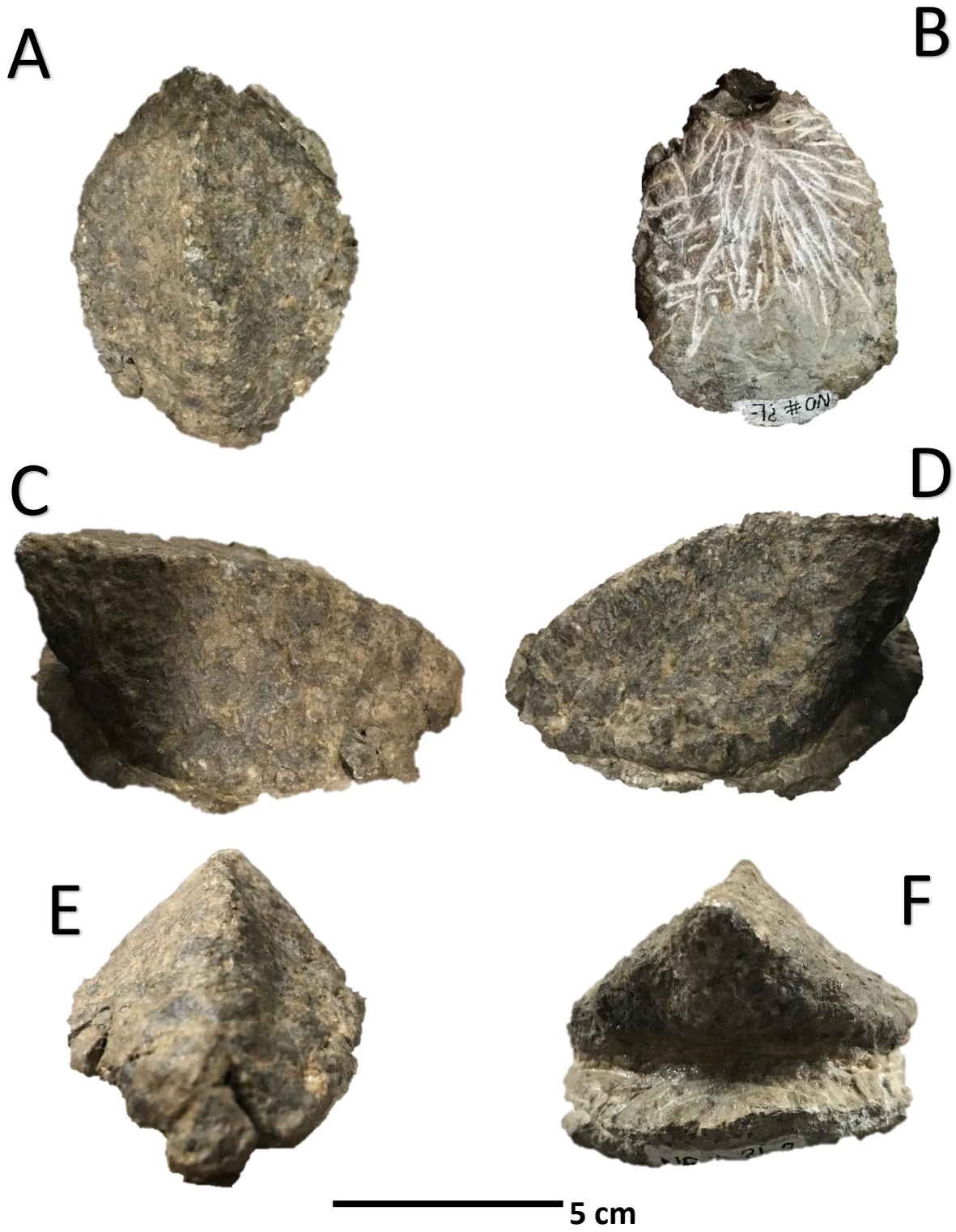

Figure 23. Osteoderm #6 in dorsal (A), ventral (B), right lateral (C), left lateral (D), anterior (E), and posterior (F) views.

Osteoderm #7 (Fig. 24)

This osteoderm is most similar to Osteoderm #1, with an oval shaped flat, base. This specimen exhibits the pup-tent shape of Morphology A. The keel is off-centered and projects posteriorly to the right. The external surface of the osteoderm is pitted extensively with sparse neurovascular grooves. Due to the close similarity it is possible that this osteoderm belonged to *Euoplocephalus sp* as well. This ostederm would be a prime candidate for microCT scanning to compare it to the histology of Osteoderm#1.

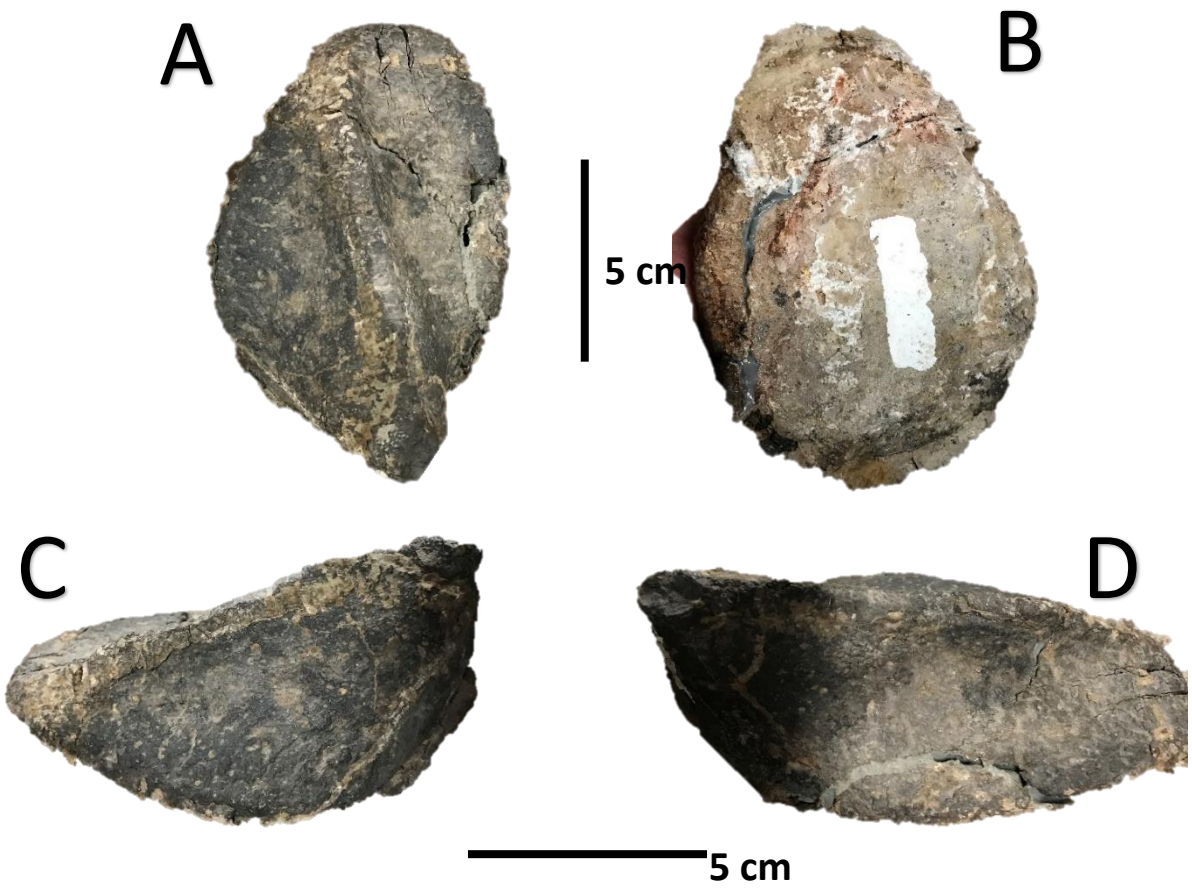

Figure 24. Osteoderm #7 in dorsal (A), ventral (B), left lateral (C), and right lateral (D) view.

Ungual Phalanx #1 (Fig. 25)

This specimen appears to be an ungual phalanx of an ankylosaur. At first glance this specimen could be mistaken for an osteoderm fragment however, the external surface has not been eroded and exhibits an overall smooth texture which is not common in most osteoderms. Typically, ankylosaurs from both families have five digits in the manus and four digits in the pes each with a triangular and bluntly pointed ungual phalanx or "toe claw" (McCrea at al., 2001). One exception to this rule is *Euoplocehalus sp.* which inly has three digits in the pes (Coombs and Maryasńska, 1990). Due to slight differences in size, shape, and number of digits of the manus and pes in ankylosaurs Coombs and Maryasńska (1990) considered these elements diagnostic for certain ankylosaur taxa, however because only this single ungual phalanx was found in the WPA-3 quarry it cannot be compared to other digit elements and is therefore undiagnostic.

Figure 25. The anterior view of ungual phalanx #1.

Metapodial #1 (Fig. 26)

This appendicular element was identified as an ankylosaur radius on an index card found with it in the VPL basement. However, this assignment may not be accurate; after comparing it to elemnts of the forelimbs and hind limbs described by Carpenter and Currie (1990), Mccrea et al. (2001) and Carpenter (2012) the specimen has more likely a metapodial element (a metacarpal or metatarsal). Due to the fact that this element was found with other ankylosaurid specimens it can be inferred to belong to this clade as well, however taxon classification is not possible from one isolated metapodial element.

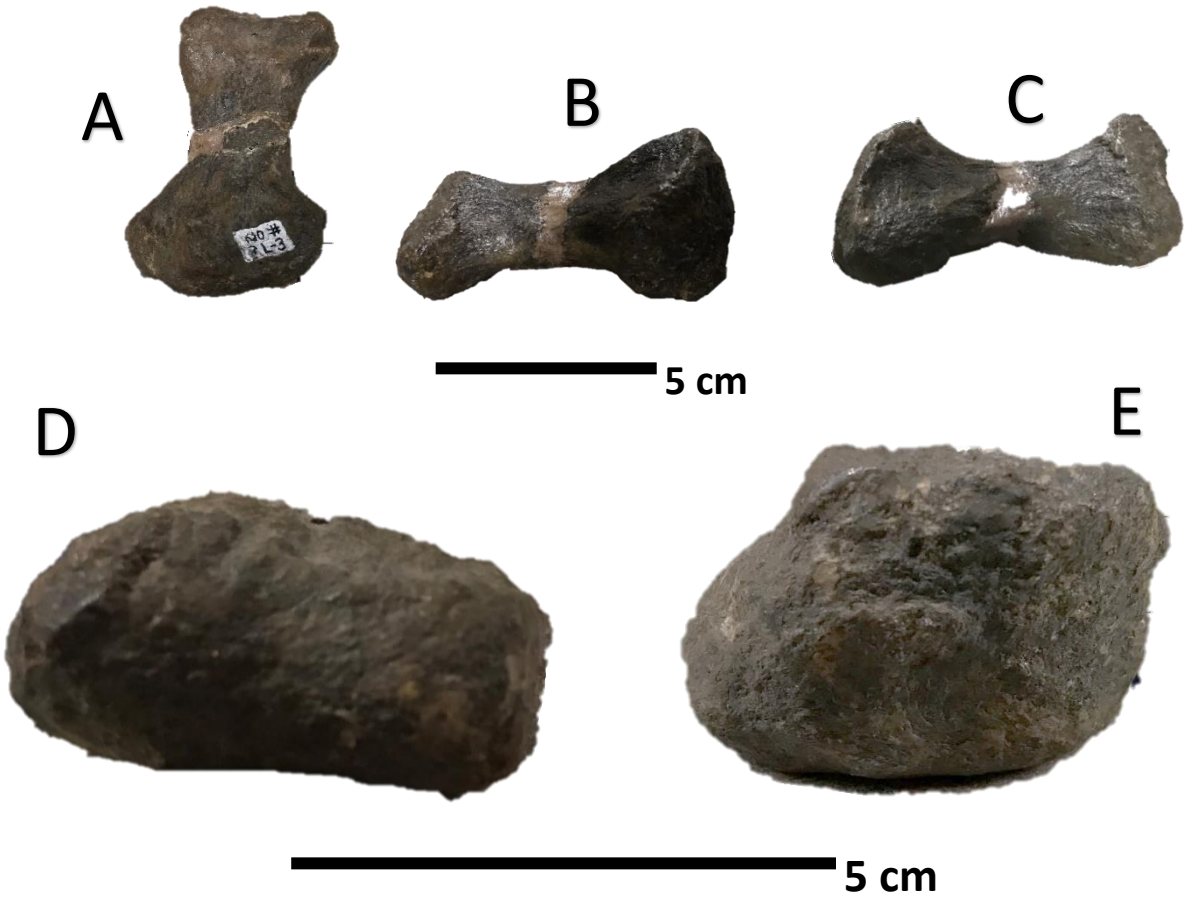

Figure 26. Metacarpal #1 in anterior (A), left lateral (B), right lateral (C), dorsal (D), and ventral (E) views.

Vertebra #1 and #2 (Fig. 27)

Vertebra #1 has a short spinous process with transverse processes (tp) that angle downward. The neural arches are completely fused to the centrum (c). This specimen has no diaphothesis (d) and together with the short spinous process indicates that this is a cervical vertebra. The fusion of the neural arches (na) to the centrum (c) indicate that this specimen came from a mature adult. The morphology of the specimen suggests it was close to the base of the skull, suggesting that it is a C1 or C2 vertebra. Vertebra #2 is a simialar size but has a different morphology. The spinous process (sp) is slightly longer than Vertebra #1, with almost horizontal transeverse processes (tp), and short diapohesys (d) are present in the specimen. Just as in the previous specimen the neural arches are fused to the centrum (c). The transverse process (tp) is not angled high enough to identify it as a dorsal vertebra. However, given the similar width and length of the centrum it is most likely a C7 or C8 cervical vertebra similar to the juvenile TL-05-14 specimen. The centra lack the hexagonal shape of a nodosaurid vertebra (Rivera-Sylva et al., 2011), therfore it belongs to a member of the Ankylosauridae. Unfortunately, there is not enough distintion between the cervical vertebrae of ankylosaurs to assign the specimens to any genera without other associated skeletal elements.

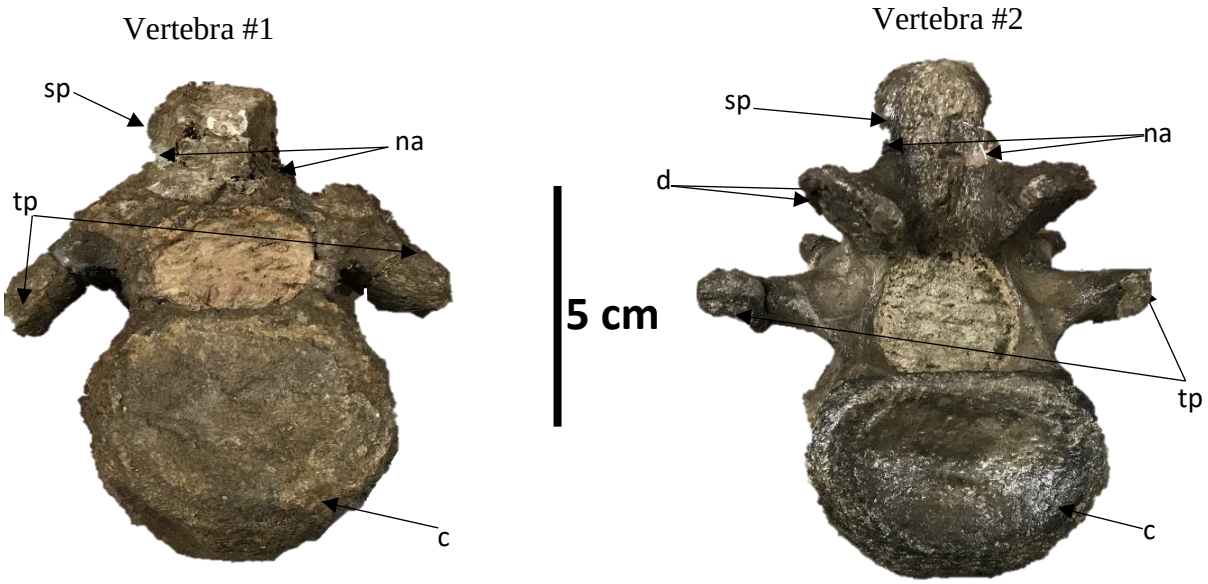

Figure 27. Vertebra #1 and Vertebra #2 in posterior view.

Radius #1 (Fig. 28)

As in most ankylosaurs the radius is shorter and more robust than the ulna (Carpenter, 2012). The shaft of the radius is straight as seen in anterior and posterior views. The proximal end of the radius is sub-oval in shape and is concave, this allows the radis to attach to the distal end of the humerus via the radial condyle of the humerus (Osi, 2005). The distal end of the radius is also sub-oval in shape, however the anterior surfcae is wide and flat in anterior view. In posterior view the distal end of the radius exhibits muscle scaring on the posterior surface. The shape of the radius in cross-section is an identifying feature between ankylosaurids and nodosaurids; Coombs (1978) described the proximal and distal ends of the radius in ankylosaurids to oval shaped in cross-section while nodosaurids are known to have a more circular shape in cross-section. Due to the sub-oval shape of the radius in proximal and distal view it can be determined that this element came from an ankylosaurid.

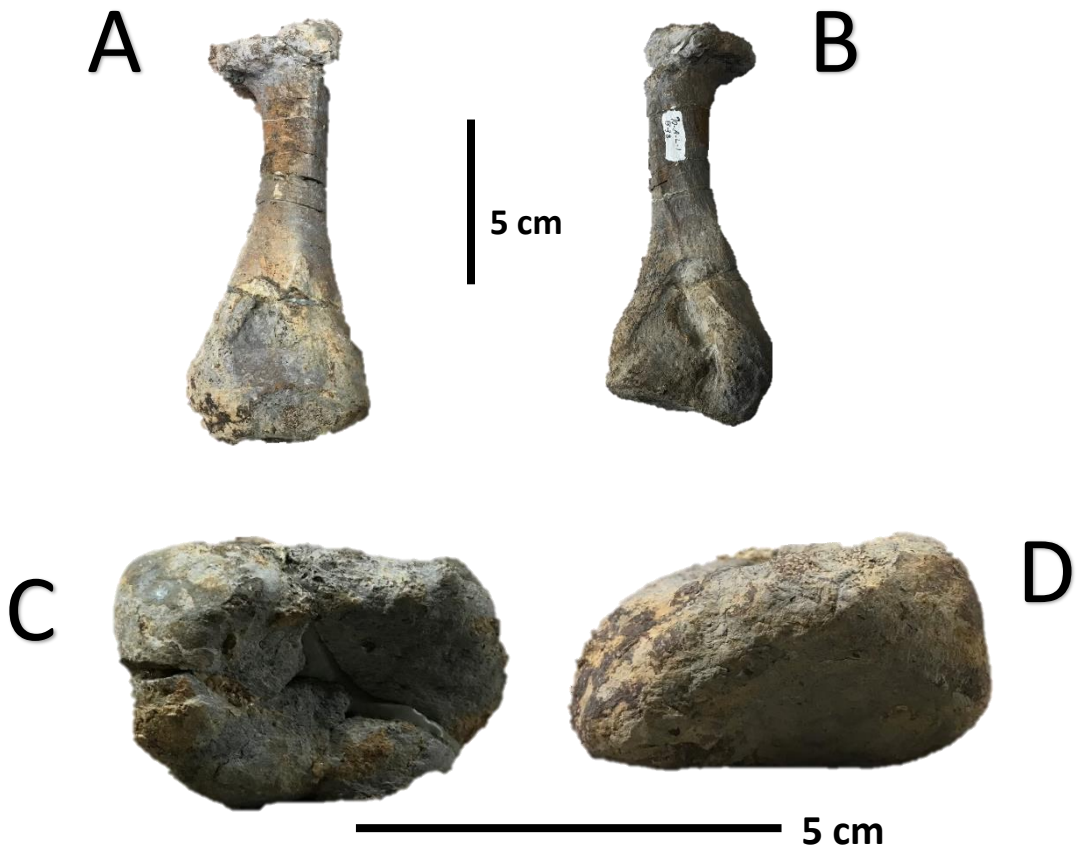

Figure 28. Radius #1 in anterior (A), posterior (B), proximal (C), and distal (D) views.

AMNH 3076

AMNH 3076 was the first ankylosaur specimen discovered in Big Bend National Park. Barnum Brown found the skull in 1940 in the Aguja Formation. The specimen was missing the lower jaw and was broken in half at the base of the snout. The skull was determined to belong to the genus *Edmontonia* due to the smooth texture of the cranial osteoderms and the lack delineation between them (Carpenter and Currie, 1990). In addition, whereas the skulls of *Panoplosaurus mirus* and *Edmontonia* sp are similar in size and shape, the muzzle is longer and narrower in *Edmontonia*. Because the skull is on display at the American Museum of Natural History it could not be removed for study. However, with the cooperation of the museum photos were taken of the specimen for use in this study. It should also be noted that Kenneth Carpenter and Philip Currie have described the specimen thoroughly in their joint publication *Ankylosaur systematics: Example using Panoplosaurus and Edmontonia (Ankylosauria: Nodosauridae).* In this article Carpenter published detailed sketches of the skull in three different views. The ventral view of the specimen exhibits alveoli on the maxillary (mx) bone where the teeth attached the skull. The nasal fossa can also be seen in this view on the pre-maxillary (pm) bone. These openings lead to complex nasal passages in the skull above the secondary palate. It is theorized that the complex nasal passages in ankylosaurs were used as a heat regulation system (Bourke et al., 2018). In fact, on the left side in ventral view the internal nares are exposed between the palatine (p) bone and the ectopterygoid bone (ec). The vomer (v) of *Edmontonia* appears as a thin ridge of bone between the two rows of alveoli. At the back of the skull the lateral temporal fenestra (lft) are set between the quadrate (qu) and quadratojugal (qj) bones. The two medial fenestrae at the back of the skull are the exoccipital fenestra (ex). The specimen exhibits one occipital condoyle (oc) at the base of the skull where the atlas vertebra would have connected. Lastly, lying between the fenestrae at the back of the skull and the palatine (p) bone are the suborbital fenestra (sof) (Carpenter and Currie, 1990).

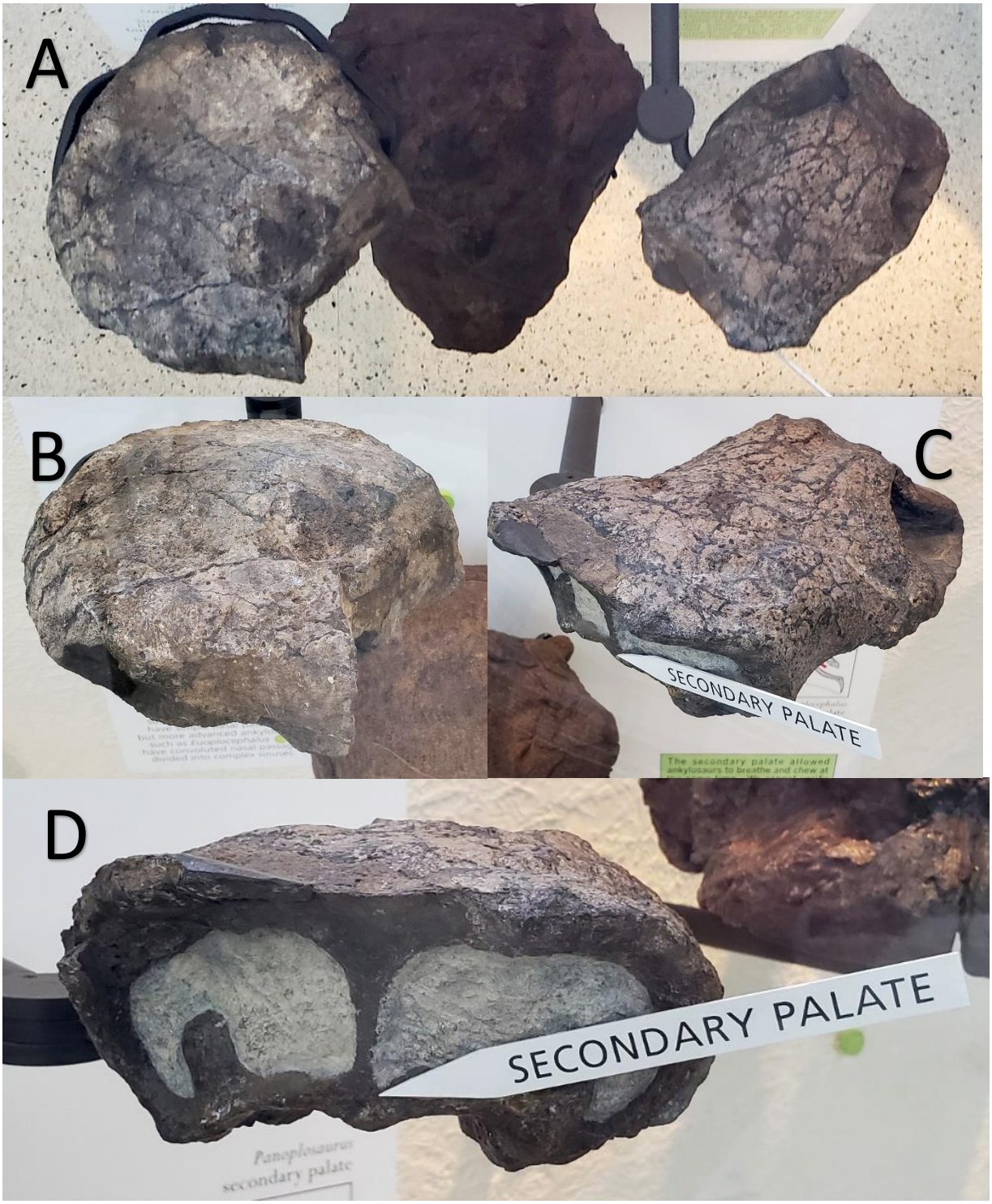

Figure 29. Images of AMNH 3076, as specimen of *Edmontonia sp.* in dorsal (A) view, the posterior half of the specimen (B), then anterior half of the specimen (C), an transverse view showing the secondary palate (D).

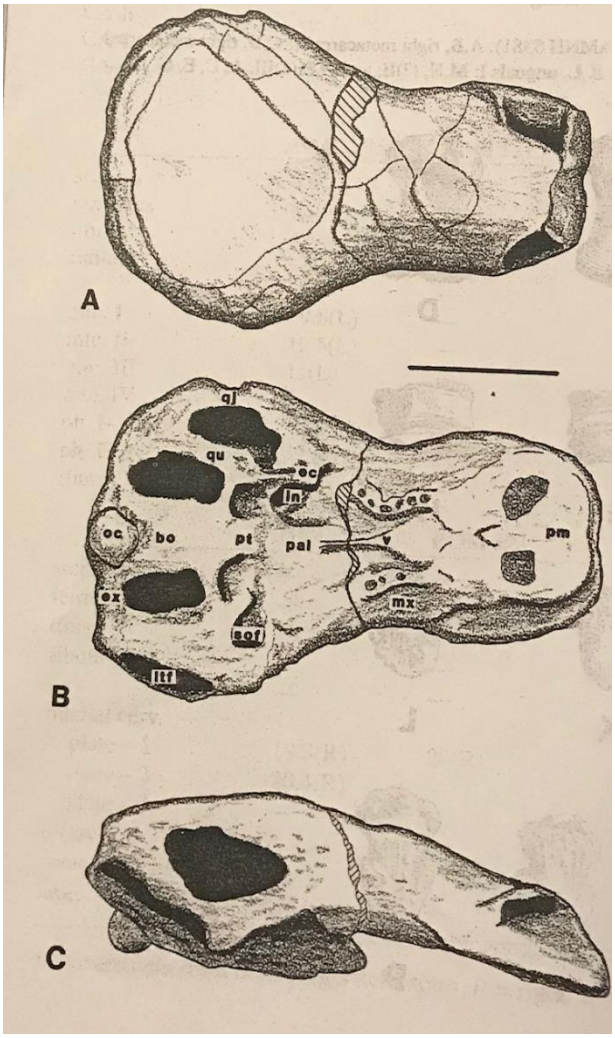

Figure 30. An illustration from Kenneth Carpenter (1990) of the AMNH 3076 skull in dorsal (A), ventral (B), and right lateral (C) views.

REVIEW OF SPECIMENS FROM MEXICO AND NEW MEXICO

The purpose of this section is to highlight other ankylosaur specimens from strata in Mexico and the Southwest that are time correlative to the Campanian and Maastrichtian units in Big Bend National Park.

Mexico

Rivera-Sylva (2011) described recent discoveries of Upper Cretaceous nodosaurids. In total, five fossil sites were studied; two sites across the Rio Grande from Big Bend in Coahulia, one site in

Southeast Coahulia, one site in Chihuahua, and one site in Baja, Mexico. Material from the fourth locality was found in the Pen Formation (Early Campanian). It is likely that the nodosaurid material was transported here, as the Pen Formation consists of a marine shale. Designated as CPC 272, the specimens discovered include the distal end of a right humerus, a right ulna, a dorsal and caudal vertebra, the distal end of a femur, one rib fragment, and one osteodermal spine. Due to the fragmentary nature of these elements no definitive identification could be made (Rivera-Sylva et al., 2011). The third locality yielded specimens from a sandy mudstone interval within the Aguja Formation. This site yielded two caudal vertebrae, on cervical rib, six rib fragments, an ilium fragment, fragments of long bones, the proximal end of a scapula, thirteen osteoderms, as well as 27 unidentified bone fragments. Designated as CPC 273 the osteoderms are the most diagnostic of all material. The first osteoderm is rectangular with a median keel, that terminates in a tall conical apex towards the posterior margin of the osteoderm (Rivera-Sylva et al., 2011). Two other osteoderms have a similar morphology but are broken down the middle. The fourth osteoderm is a conical anterolaterally directed cervical spine. There are three thoracic osteoderms that are circular with a low median keel; and another which was identified as a distal thoracic osteoderm. Lastly, there is a caudal osteoderm and one circular ossicle. (Rivera-Sylva et al., 2011). The external texture of the osteoderms resembles that of *Glyptodontopelta mimus*; a smooth surface with extensive pitting and vascular grooves that radiate from the keel (Burns, 2008). It is noted that the specimen has less pitting than most osteoderms attributed to this taxon, however this could be an individual variation of the character.

The fifth locality is located in Southeast Coahuila with one caudal vertebra collected from a sandstone layer within the Cerro del Pueblo Formation (considered to be Campanian and correlative with the upper shale member of the Aguja Formation and the lower half of the Javelina Formation). The vertebra, labeled as CPC 275, consists of a centrum without the neural arch, spine, and transverse processes. The centrum has a hexagonal shape in posterior, which is indicative of a nodosaurid. The centrum is also short anteroposteriorly with a pair of chevron facets on the posteroventral edge (Rivera-

Sylva et al., 2011). Unfortunately, the genus cannot be identified by one lone centrum. The first locality in Baja, Mexico yielded one tooth from a mudstone interval in the El Gallo Formation (Campanian). The tooth is small (5 mm in width) and lacks a root but is wide with a shelf-like cingulum. This is the typical condition of most nodosaurid teeth (Coombs, 1990). Fluting between marginal cusps are also observed on the tooth, which according to Coombs is also a major characteristic of nodosaurid teeth. The tooth, which is designated as UABC FCM 2625, has a six denticles on the labial side and three on the lingual side. (Rivera-Sylva et al., 2011). This tooth is similar to that of *Aletopelta coombsi* which was identified as an ankylosaurid by Ford and Kirkland (2001). However, Coombs and Demere (1996) originally described this ankylosaur as a nodosaurid. This is supported by tooth and osteoderm morphology observed by Kenneth Carpenter (Rivera-Sylva et al., 2011).

New Mexico

The San Juan Basin of New Mexico has yielded many species of ankylosaurs, some of which have only recently been discovered. Lucas et al. (1987) mentioned several fragments of ankylosaur remains, but the study never went into detail because the specimens were fragmentary. However, the discovery of *Alamosaurus sanjuanensis* allowed the correlation of Naashoibito member of the Kirtland Formation with the Javelina Formation in Big Bend.

Ford (2000) published a review of ankylosaur osteoderms from New Mexico. In this review three taxa from the Late Campanian through the Late Maastrictian were identified. The nodosaurid *Edmontonia* was identified by two medial cervical osteoderms attached at the midline. This specimen was found in the Kirtland Formation (Maastrictian). The osteoderms were unfused and had a median keel which ended in a short conical point (Ford, 2000). A pup-tent shaped osteoderm with an excavated base, believed to be from *Nodocephalosaurus kirtlandensis* was found in the De-na-zin member of the Kirtland Formation (Early Maastrictian) (Ford, 2000). Lastly, the holotype of *Glyptodontopelta mimus* was described in this

study from pelvic osteoderms. This specimen was found in the Naashiobito member of the Kirtland Shale (Maastrictian); this is also known as the Kirtland Formation (Ford, 2000).

In 2014 the holotype of *Ziapelta sanjuanensis* from the De-Na-Zen member of the Kirtland Formation was described from a complete skull, partial first and second cervical half-rings, and various post cranial osteoderms. In this study *Ziapelta* was determined to be related to the Ankylosaurinae. The holotype shares many similarities with Ankylosaurus, *Anodontosaurus lambei, Euoplocephalu*s *sp.*, and Scolosaurus *cutleri*, such as the flat, square-to-hexagonal based cranial caputegulae and a convex antorbital region of the skull roof (Arbour et al., 2014).

The latest ankylosaur to be discovered in the San Juan Basin is the nodosaurid *Invictarix zephyri*. From the Allison member of the Menefee Formation (Early Campanian) the holotype of this ankylosaur (WSC 16505) includes fragments of dorsal ribs, six osteoderms, and additional fragments of osteoderms. The specimen had unique osteoderm characteristics not seen in any other ankylosaur. The entire external surface is pitted with the largest of the pits occurring along the caudal margin and the caudal end of the keel (McDonald and Wolfe, 2018). These rugosities appear between the pits on the keel, which diminish toward the caudal margin. Toward the cranial margin the pitting is continuous, however the area between the pits is smooth. The transition from pitted with rugosities to pitted without rugosities is what differentiates *Invictarix zephyri* from other ankylosaurs (McDonald and Wolfe, 2018). It is this texture that McDonald and Wolfe cite as their reason to placing this ankylosaur in the Nodosauridae. However, they only compared it to the nodosaurid *Glyptodontopelta mimus* in terms of osteoderm texture. The holotype shares osteoderm morphology with *Anodontosaurus lambei* and *Aletopelta coombsi*, so it is possible that further study is required for this ankylosaur.

Tree A **Tree B**

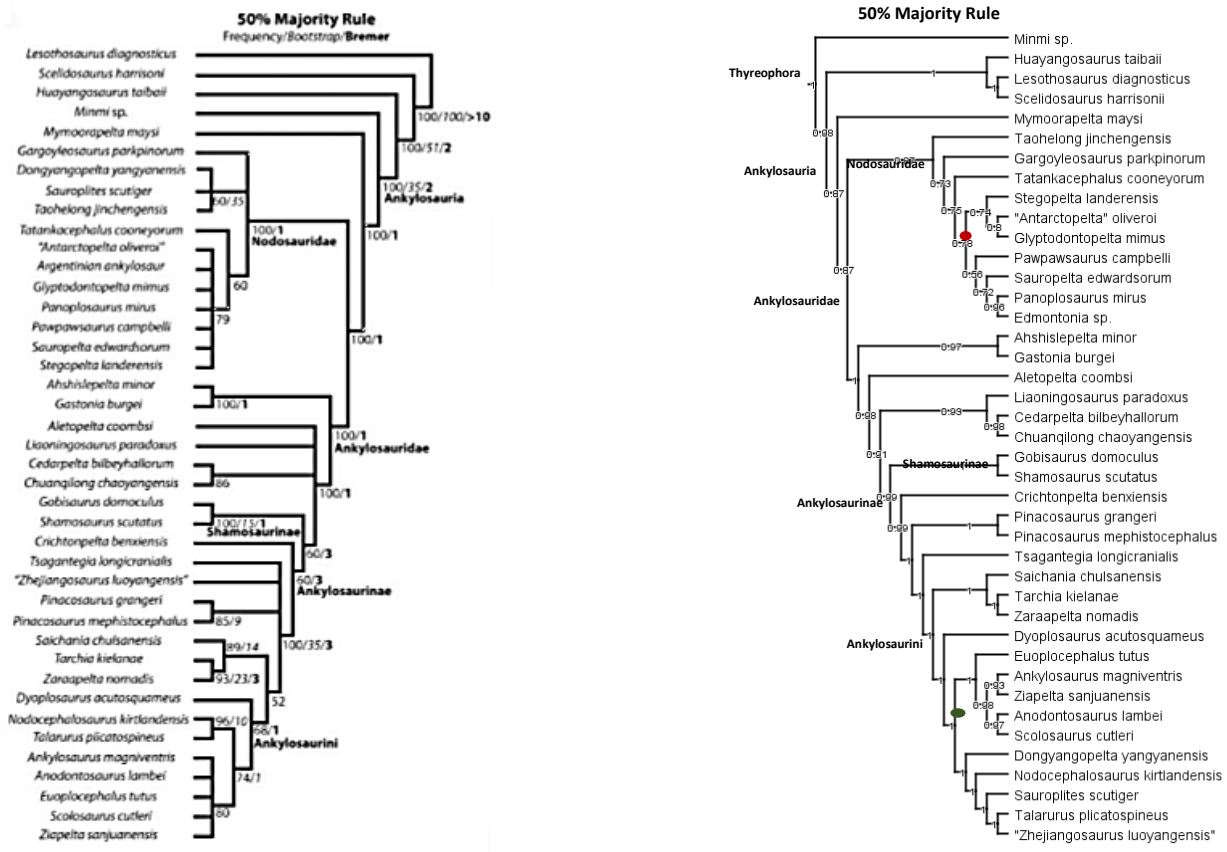

Figure 31. Tree A is the most the current phylogenetic tree for ankylosaurs created by Thompson et al. (2012) and updated by Arbour and Currie (2015). Tree B is the phylogenetic tree created by this study using 9 new characteristics based on osteoderm osteology and histology.

PHYLOGENETIC DISCUSSION

A phylogenetic analysis was performed using a heuristic majority rule consensus on 45 taxa and 186 characteristics using Mesquite 3.61 (Maddison, W. P. and D.R. Maddison, 2019) (Appendix 1). The basis for this analysis was the most current systematic study of ankylosaurs (Arbour and Currie, 2015). This study was also based on a previous study by Thompson et al., 2012; these two differ by the removal of taxa deemed junior synonyms and *nomen dubium* in the former.

During this current analysis 9 new characters based on osteoderm paleohistology and osteology from the 5 osteoderms studied using Dragonfly ORS were defined. These characteristics include the presence or absence of projecting rugosities and vascular foramina. For medial cervical plates, the characteristic of sub-oval versus rectangular or square shaped was added to the character matrix. Many histological characteristics were added including the maturity of primary osteons, the arrangement of ISFBs within the cortices, the presence or absence of secondary remodeling, the composition of the core being Haversian or trabecular bone, and cortical thickness. The character of smooth versus rugose cranial plates was added to the matrix as it is an identifying characteristic of *Panoplosaurus mirus (*Carpenter and Currie, 1990). No new additional characteristics from other skeletal elements were discovered during this study, thus none were added to the character matrix. In addition, this study added the genus *Edmontonia* to the taxa list from Arbour and Currie (2015) in which only a handful of nodosaurids were used for the study, among which *Edmontonia* was not included. There is fossil evidence for this genus in Big Bend, so for the purpose of this study it was added to the original taxa list. The taxa known only as "Argentinian ankylosaur" was removed from the phylogenetic tree this study produced due the specimen not being properly classified (Arbour and Currie speculated that some elements were mixed together with various marine reptiles). Lastly, some taxa such as *Zheijiangosaurus luoyangensis* and *Antarctopelta oliveroi* were not pruned from either tree despite being a junior synonym and a *nomen dubium* respectively due to their unusual geographic localities.

The phylogenetic tree produced with the new osteoderm characteristics (Tree B) is similar to the tree produced by Arbour and Currie (Tree A). However, there are some key differences such as *Minmi sp*. is now regarded as a basal thyreophoran instead of a primitive member of Ankylosauria. In the 2015 study this placement was occupied by *Mymoorapelta mysii. Sauroplites scutiger* and *Dongyangopelta yangyanensis* that were sister taxa under Nodosauridae but were determined to be derived ankylosaurids and were recovered as members of the Ankylosaurinae. Just as in Thompson et al. (2012) and Arbour and Currie (2015) the sub-family Polocanthinae was deemed to be invalid due to being

polyphyletic as evidenced in this study by *Gargoyleosaurus parkpinorum* and *Gastonia burgei* being recovered under the families Nodosauridae and Ankylosauridae respectively. Thompson (2012) determined that taxa that were previously considered polocanthids are now considered basal nodosaurids. This also suggests that the nodosaurids and ankylosaurids split from a common ancestor during the Early Cretaceous. The red node (Fig. 30) indicates where a split occurred within the Nodosauridae, splitting up many sister taxa, which does not occur in the Arbour and Currie (2015) tree. Additionally, the two Nodosaur taxa known from Big Bend, *Panoplosaurus mirus* and *Edmontonia*, are now grouped together as sister taxa. Just as in the 2015 study, the ankylosaurid sub-family Shamosaurinae is found to be valid, as the relationship between *Shamosaurus scutatus* and *Gobisaurus domoculus* as sister taxa is monophyletic. However, it should not be used to describe all early ankylosaurids since it does not contain the supposed basal member *Cedarpelta billbeyhallorum* and all other non-ankylosaurine ankylosaurids as documented by Carpenter (2012). Arbour and Currie (2015) used the clade Ankylosaurini to classify the most derived members of the Ankylosaurinae. This includes *Euoplocephalus sp.* (a Big Bend ankylosaurid) and its many sister taxa as seen in Tree (A); however in Tree (B) *Euoplocephalus sp.* is seen to be basal to other Ankylosaurini taxa. The green node (Fig. 30) indicates where splitting within the Ankylosaurini begins; suggesting that Ankylosaurini is an invalid paraphyletic clade. An observation of note, *Ziapelta sanjuanensis (*a southern assemblage ankylosaur*)* is found to be closer to *Ankylosaurus magniventris* (a northern assemblage ankylosaur) than previously thought. This further suggests that the separation of Late Cretaceous faunal assemblages within North America might need revision. The revision of the Arbour and Currie (2015) ankylosaur phylogenetic tree using osteoderm characteristics supports the hypothesis proposed by Scheyer and Sander (2004), and expanded upon by Hayashi et al. (2010), that osteoderms are important elements in determining relationship at generic and specific levels.

A note about Dragonfly ORS analysis: despite being an excellent histological tool the microCT scan technology is somewhat limited in the size range of features that can be clearly observed. Features smaller than 600 microns are difficult to determine at this scale by the program, even if the

contrast and resolution of the image slice are manipulated. As such, fabric types are easily identified, but individual osteocytes and even ISFB in cortical may not be seen in every specimen. This could also be because the fossils have undergone diagenesis and may combine the original hydroxyapatite with diagenetic apatite. The mineral fill or matrix of the specimen could also determine which features are observed. However, this is a novel approach to paleohistology and it is possible that the technology could be improved to better observe certain characteristics.

CONCLUSIONS

This study has determined that during the Campanian and Maastrichtian ages of the Late Cretaceous the area that is now Big Bend National Park, Tx was home to at least three species of ankylosaurs (Appendix I: West Texas Specimens table). Representing the nodosaurids were *Edmontonia* and *Panoplosaurus mirus*; two sister taxa which share a similar osteoderm histology but are differentiated by the external texture of their osteoderms. *Edmontonia* was first nodosaurid to be described from Big Bend, now with the presence of *Panoplosaurus mirus* our understanding of nodosaurid diversity in this region has changed. The ankylosaurid material has tentatively been referred to as *Euoplocephalus sp.* in this study, however there are two few ankylosaurid osteoderms in the histology review of this study to confirm the presence of this taxa in Big Bend based solely on osteoderms. The only definitive evidence of *Euoplocephalus sp. in* this region is the TL-14-05 partial sacrum. Compared to the pelvi of other ankylosaurs it most resembles that as *Euoplocephalus sp.* The remaining skeletal elements such as the WPA-3 specimens and the fragmentary axial and appendicular elements are non-diagnostic as to specific taxa, however they share characteristics of derived ankylosaurs such as members of the Ankylosaurinae sub-family which includes *Euoplocephalus sp.*, *Ankylosaurus magniventris*, *Scolosaurus cutleri*, and others. Dinosaur faunal assemblages from the Late Cretaceous were divided into “northern” and “southern” groups and were thought to be endemic to their geographical locations (Lehman,1985; 2019). However, with the presence of these three taxa in Big Bend (which also known from the northern assemblage), this assertion might need review.

The use of microCT scanning, in combination with Dragonfly ORS, has yielded positive results in this study. As a novel approach to paleohistoloy there is room for improvement as the technology is further developed, however it has proven to be an excellent alternative for more destructive methods. The findings of this study partially support the hypothesis of Scheyer and Sander (2004) that histologic and osteologic features of osteoderms can be used to determine relationship between taxa within the Ankylosauria. These finding are also conclusive with the results of Hayashi et al. (2014) and Burns and Currie (2014). Using characteristics observed in the osteoderms the relationship between the sub-families Polocanthinae and Shamosaurinae to the rest of the Ankylosauria need further study and revision. In addition, the relationships between members of the Ankylosaurini were determined to be more complex than previously thought, as this group contains many paraphyletic branches. Due to this the sub-group of Ankylosaurini may need revision in the future. In this study it has been shown that osteoderms from juvenile ankylosaurs have a more complex histology than previously reported in the study conducted by Scheyer and Sander (2004). This could account for the differences seen in the juvenile TMM 40484-46 osteoderm, which did not exhibit the typical characteristics of a nodosaurid osteoderm as outlined in the previous study. Osteoderms are still some of the least studied skeletal elements of any ankylosaur taxa, so continuing studies of this nature would continue to yield more information about ankylosaur systematics and classification.

APPENDIX

Taxon List

Taxon	Status (Burns & Currie 2015)
Lesothosaurus diagnosticus	Valid
Scelidosaurus harrisonii	Valid
Huayangosaurus taibaii	Valid
Ahshislepelta minor	Valid
Aletopelta coombsi	Valid
Ankylosaurus magniventris	Valid
Anodontosaurus lambei	Valid
"Antarctopelta" oliveroi	nomen dubium
Argentine ankylosaur	New taxon**
Bissektipelta archibaldi	Valid*
Cedarpelta bilbeyhallorum	Valid
Chuanqilong chaoyangensis	Valid
Crichtonpelta benxiensis	Valid- new combination of *Crichtonpelta benxiensis*
Dongyangopelta yangyanensis	Valid
Dyoplosaurus acutosquameus	Valid
Euoplocephalus tutus	Valid
Gargoyleosaurus parkpinorum	Valid
Gastonia burgei	Valid
Glyptodontopelta mimus	Valid
Gobisaurus domoculus	Valid
Liaoningosaurus paradoxus	Valid
Minmi paravertebra	nomen dubium*
Minmi sp.	Valid
Mymoorapelta maysi	Valid
Nodocephalosaurus kirtlandensis	Valid
Panoplosaurus mirus	Valid
Pawpawsaurus campbelli	Valid
Pinacosaurus grangeri	Valid
Pinacosaurus mephistocephalus	Valid
Saichania chulsanensis	Valid
Sauropelta edwardsorum	Valid
Sauroplites scutiger	Valid
Stegopelta landerensis	Valid
Scolosaurus cutleri	Valid
Shamosaurus scutatus	Valid

Talarurus plicatospineus	Valid
Taohelong jinchengensis	Valid
Tarchia kielanae	Valid
Tatankacephalus cooneyorum	Valid
"Tianchisaurus" nedegoapeferima	*nomen dubium**
Tsagantegia longicranialis	Valid
Zaraapelta nomadis	Valid
"Zhejiangosaurus luoyangensis"	Junior synonym for *Gobisaurus domoculus*
Ziapelta sanjuanensis	Valid
Edmontonia sp.	Not part of Burns & Currie 2015

*Removed by Burns and Currie.
**Removed during this study.

Character Table

Character Designation	Character
1	Composition of first cervical half ring with band: no cervical half ring with band (0), first cervical half ring has 4 to 6 primary osteoderms only (1), first cervical half ring has 4 to 6 primary osteoderms surrounded by small (<2 cm diameter) circular secondary osteoderms (2).
2	Antorbital fenestra: present (0) absent (1).
3	Lateral temporal fenestra, visible in lateral view: visible (0), not visible (1).
4	Supratemporal fenestra: open (0), closed (1).
5	Skull dimensions, including ornamentation: longer than wide (0), as wide, or wider than long (1).
6	Width of the posterior margin of the skull (including squamosal horns where applicable) relative to the maximum width across the orbits: greater or equal (0), less (1).
7	Antorbital region of the dorsal skull surface: flat (0), arched (1).
8	Deep longitudinal furrow on premaxilla: absent (0), present (1).
9	Ornamentation on premaxillary beak: absent (0), present (1).
10	Premaxillary sinus: absent (0), present (1)
11	Dimensions of premaxillary palate: longer than wide (0), wider than long (1).
12	Shape of the premaxillary palate: sub-triangular (0), sub-quadrate (1), sub-oval (2).
13	?V? or ?U?-shaped median indentation of the anterior margin of the premaxilla: absent (0), present (1).
14	Caudoventral extension of premaxillary tomium in lateral view: ends anteriorly to the maxillary teeth (0), obscures anteriormost maxillary teeth (1).
15	Bone bordering anterior margin of internal nares: premaxilla (0), maxilla (1).
16	External nares, defined as the outermost rim of the nasal vestibule, opening faces: laterally to anterolaterally (0) anteriorly (1) ventrolaterally (2).
17	External nares, visible in dorsal view: visible (0), hidden (1).
18	Modified: Paranasal apertures/fossae: no fossae or apertures present besides primary opening for nasal airway (0), paranasal apertures/fossae present (1).
19	Shape of respiratory passage: straight or arched (0), with anterior (rostral) and posterior (caudal) loops
20	New character: Vascular impressions on dorsal surface of posterior nasal passage (airway): absent (0) present (1).
21	Frontonasal and/or frontoparietal cranial ornamentation: absent (0) rugose, not differentiated into discrete polygons (caputegulae) (1), differentiated into discrete polygons (caputegulae) (2).

22	Number of caputegulae in frontonasal and prefrontal region: no caputegulae (0), 10 or fewer (1), 11 to 30 (2) more than 30 (3).
23	Majority of frontonasal and/or frontoparietal caputegulum relief: caputegulae absent (0), caputegulae concave or flat (1), caputegulae strongly bulbous (2).
24	Domed frontonasal caputegulae: domed caputegulae absent (0), rounded cones with circular bases (1) pyramidal with sharp edges (2).
25	Supranarial caputegulae, notch or embayment dorsal to nasal vestibule: no supranarial caputegulae (0), notch absent (1), notch present (2).
26	Number of internarial caputegulae: none (0), 1 (1), more than 1 (2).
27	Median nasal caputegulum (located posterior to the supranarial ornamentation, on the midline of the skull), which is at least twice as large as the other frontonasal caputegulae: absent (0), present (1).
28	Loreal caputegulum in lateral view: no caputegulum (0) 1 caputegulum (1), more than 1 caputegulum (2).
29	Shape of the maxillary tooth row: straight (0), medially convex (1).
30	Maxillary tooth row position: lateral margin of skull (0), inset (1).
31	Distance between posteriormost extent of maxillary tooth rows relative to the width of the premaxillary beak: wider (0), narrower (1).
32	Caudoventral secondary palate: absent (0), present (1)
33	Posterior palatal foramen: absent (0), present (1).
34	Gap between palate and braincase: open (0), closed by a dorsal projection of the pterygoid (1).
35	Lacrimal incisure (mediolateral constriction behind the nares/at the prefrontals, giving the skull an hourglass-shaped outline in dorsal view): absent (0) present (1).
36	Lacrimal caputegulum in lateral view: no caputegulum (0) 1 caputegulum (1), more than 1 caputegulum (2).
37	Prefrontal caputegulum: no caputegulum (0) flat (1), sharply pointed and pyramidal (2).
38	Scroll-like descending process of the frontal: absent (0) present (1)
39	Form of supraorbitals (including ornamentation): absent (0), boss-like, rounded laterally (1), sharp lateral rim, forming a ridge (2).
40	Supraorbitals, when viewed dorsally: no supraorbitals (0), combine to form continuous edge (1), have distinct apices (2).
41	Orbits, angle of orbital axis: <40º (0), >40º (1).
42	Ciliary osteoderm (eyelid ossification): absent (0) present (1)
43	Development of the postocular shelf: not developed (0), completely separating orbit from temporal space (1).
44	Proportions of jugal orbital ramus: depth greater than transverse breadth (0), transverse breadth greater than depth (1).
45	Depth of jugal ramus relative to orbit height: jugal height is less than 15% orbit height (0), jugal height is more than 15% orbit height (1)
46	Accessory postorbital ossification: absent (0), present (1)
47	Squamosal/postorbital horn: no horn (0) base has broad triangular cross-section and overall shape is pyramidal (1), base is oval in cross-section and overall shape is narrow, tapered cylinder (2).
48	Shape of jugal/quadratojugal horn in dorsal view: quadratojugal horn absent (0), horn U-shaped, with round distal edge (1), horn triangular, with pointed distal edge (2)
49	Jugal/quadratojugal horn: no horn (0) lacks distinct neck at base (1), has distinct neck at base (2).
50	Jugal or quadratojugal horn size relative to orbit size: no horn (0), length of base of jugal/quadratojugal horn equal to or less than the length of the orbit (1), length of base of jugal/quadratojugal horn is 110% or greater length of orbit (2).
51	Small (<2 cm diameter), circular caputegulae posterolateral to orbit (postocular caputegulae), along ventral edge of squamosal horn and/or along dorsal edge of quadratojugal horns: absent (0), present (1).
52	Form of the parietal surface: parietals flat to slightly convex (0), parietals concave, forming a trough-like surface posterior to the supraorbitals and anterior to the posterior edge of the skull (1).
53	A single large medial polygon of ornamentation in the parietal region: absent (0), present (1)
54	Number of discrete nuchal caputegulae: none (0), 2 (1), greater than 2(2)
55	Posterior projection of the nuchal shelf: does not obscure occiput in dorsal view (0), obscures occiput in dorsal view (1).
56	Shape of quadrate in lateral aspect: curved (anteriorly convex, posteriorly concave) (0), straight (1).
57	Inclination of quadrate in lateral aspect: near vertical (0), almost 45º anterolaterally (1).
58	Form of the anterior surface of the quadrate: transversely concave (0), not concave (1).

59	Ventral projection of the mandibular process of the quadrate in lateral view: projects beyond the quadratojugal ornamentation (0), hidden by quadratojugal ornamentation (1).
60	Form of quadrate mandibular extremity: symmetrical (0), medial condyle larger than lateral condyle (1).
61	Inclination of the articular surface of the quadrate condyle in posterior view: horizontal (0), ventromedially inclined at approximately 45° to horizontal (1)
62	Lateral ramus of the quadrate: present (0), absent (1).
63	Dorsoventral depth of the pterygoid process of the quadrate: deep (0), shallow (1).
64	Contact between paroccipital process and quadrate: sutural (0), fused (1).
65	Contact between pterygoids: pterygoids separate caudomedially, forming an interpterygoid vacuity (0), pterygoids joined medially forming a pterygoid shield (1).
66	Direction of the pterygoid flange: anterolateral (0), anterior/parasagittal (1).
67	Contact between basipterygoid processes and pterygoid: sutural (0), fused (1).
68	Position of ventral margin of the pterygovomerine keel relative to alveolar ridge: dorsal (0), level (1).
69	Dorsal extent of median vomer lamina: does not meet skull roof (0), meets skull roof (1).
70	Pterygoid foramen: absent (0), present (1).
71	Position of posterior margin of pterygoid body relative to the anterior margin of the quadrate condyle: anteriorly positioned (0), in transverse alignment (1).
72	Size of occiput: higher than wide (0), wider than high (1).
73	Direction of paroccipital process extension: caudolateral (0), lateral (1).
74	Bones forming the occipital condyle: basioccipital and exoccipital (0), basioccipital only (1).
75	Length of basisphenoid relative to the basioccipital: longer (0), shorter or equal (1).
76	Form of basisphenoidal tuberosities: medially separated rounded rugose stubs (0), continuous transverse rugose ridge (1).
77	Size of basipterygoid processes: twice as long as wide or over (0), less than twice as long as wide (1).
78	Form of the cranial nerve foramina IX-XII: separate foramina (0), single foramen shared with the jugular vein (1).
79	Position of mandible articulation relative to mandibular adductor fossa: posterior (0), posteromedial (1).
80	Mandibular fenestra: present (0), absent (1).
81	Depth of the dentary symphysial ramus relative to half the maximum depth of the mandibular ramus in lateral view: deeper (0), shallower (1).
82	Shape of dorsal margin of the dentary in lateral view: straight (0), sinuous (1).
83	Development of the coronoid process: not developed (0), distinct (1).
84	Position of glenoid for quadrate relative to mandibular axis: medially offset (0), in line (1).
85	Size and projection of the retroarticular process: small with no dorsal projection (0), well developed with a dorsal projection (1).
86	Size of predentary ventral process: distinct, prong shaped process (0), rudimentary eminence (1).
87	Length of mandibular caputegulum with respect to the length of the mandible: less than or equal to half the length (0), over three quarters the length (1).
88	Premaxillary teeth: present (0) absent (1).
89	Cingula on maxillary and/or dentary teeth: absent (0), present (1).
90	Maxillary and/or dentary tooth crown shape: pointed (0), rounded (1).
91	Maxillary and/or dentary tooth denticles: < 13 denticles (0), ?13 denticles (1) (Thompson et al. 2012: 65, in part; Arbour et al. 2014a: 53).
92	Number of dentary teeth: <25 (0), ?25 (1).
93	Type of articulation between the atlantal neural arch and intercentrum: open (0) fused in adult (1).
94	Type of contact between the atlantal neural arches: no median contact (0), median contact (1).
95	Contact between atlas and axis: articulated (0), fused (1).
96	Dimensions of cervical vertebrae centra: anteroposteriorly longer than transverse width (0), anteroposteriorly shorter than transverse width (1).

97	Ratio of maximum neural spine width to height in anterior cervicals: <0.25 (0), ?0.25 (1).
98	Ratio of anteroposterior dorsal centrum length to posterior centrum height: >1.1 (0), <1.1 (1).
99	Longitudinal keel on ventral surface of dorsal centra: present (0), absent (1).
100	Cross sectional shape of neural canal in posterior dorsals: circular (0) elliptical, with long axis running dorsoventrally (1)
101	Shape of the proximal cross-section of the dorsal ribs: triangular (0), ?L?- or ?T?-shaped (1).
102	Attachment of dorsal ribs to posterior dorsal vertebrae: articulated (0), fused (1).
103	Contact between posteriormost dorsal vertebrae: articulated (0), fused to form a presacral rod (1)
104	Longitudinal groove in ventral surface of the sacrum: absent (0), present (1).
105	Longitudinal ridge at approximate mid-height of centrum of mid and distal caudals: absent (0) present (1).
106	Ratio of maximum distal width to height of the neural spines of proximal caudals: ?0.2 (0), >0.2 (1).
107	Direction of the transverse processes of proximal caudals: craniolaterally projecting (0), caudolaterally projecting (1), laterally projecting (2)
108	Persistence of transverse processes down the length of the caudal series: not present beyond the mid-length of the series (0), present beyond the mid-length of the series (1).
109	Attachment of haemal arches to their respective centra: articulated (0), fused (1).
110	Extent of pre- and postzygapophyses over their adjacent centra in posterior vertebrae: extend over less than half the length of the adjacent centrum (0), extend over more than half the length of the adjacent centrum (1).
111	In tail club handle vertebrae, shape of each interlocking neural arch in dorsal view: distal caudal vertebrae do not form handle (0), V-shaped, angle of divergence about 22-26° (1), V-shaped, angle of divergence about 35-37° (2), U-shaped, angle of divergence greater than 60° (3).
112	Shape of the posterior haemal arches: rounded haemal spine in lateral view with no contact between haemal arches (0), inverted ?T?-shaped haemal spine in lateral view, with contact between the ends of adjacent spines (1).
113	Ossified tendons in distal region of tail: absent (0), present (1).
114	Dimensions of coracoid: longer than wide (0), wider than long or equal width and length (1).
115	Form of the anterior margin of the coracoid: convex (0), straight (1).
116	Cranioventral process of coracoid: absent (0), present (1).
117	Size of coracoid glenoid relative to scapula glenoid: sub-equal (0), half the size (1).
118	Contact between scapula and coracoid: articulated (0), fused (1).
119	Scapula glenoid orientation: ventrolateral (0), ventral (1).
120	Ventral process of scapula at the caudoventral margin of glenoid: absent (0), present (1)
121	Form of the scapula acromion process: not developed or ridge-like along the dorsal border of the scapula (0) flange-like and folded over towards the scapula glenoid (1) ridge terminating in a knob-like eminence (2).
122	Orientation of the acromion process of scapula: directed away from the glenoid (0), directed towards scapula glenoid (1).
123	Scapulocoracoid buttress: absent (0), present (1).
124	Distal end of scapula shaft: narrow (0), expanded (1).
125	Contact between sternal plates: separate (0), fused (1).
126	Length of the preacetabular process of ilium as a percentage of total ilium length: ? 50% (0), > 50 % (1)
127	Angle of lateral deflection of the preacetabular process of the ilium: 10º?20º (0), 45º (1).
128	Orientation of the preacetabular portion of the ilium: near vertical (0), near horizontal (1).
129	Form of the preacetabular portion of the ilium: straight process (0), pronounced ventral curvature (1).
130	Lateral edge of ilium in dorsal view: straight (0), sinuous (1).
131	Lateral exposure of the acetabulum: exposed (0) acetabulum partially obscured as it is partially encircled by the distal margin of the ilium (1).
132	Perforation of the acetabulum: present, open acetabulum (0), absent, closed acetabulum (1).
133	Postacetabular ilium length, relative to diameter of acetabulum: greater (0), smaller (1).
134	Pubis: present (0), indistinct from ilium/ischium (1)

135	Shape of ischium: straight (0), ventrally flexed at mid-length (1).
136	Shape of the dorsal margin of ischium: straight or concave (0), convex (1).
137	Separation of humeral head and deltopectoral crest in anterior view: continuous (0), separated by a distinct notch (1).
138	Separation of humeral head and medial tubercle in anterior view: continuous (0), separated by a distinct notch (1)
139	Ratio of deltopectoral crest length to humeral length: ?0.5 (0), >0.5 (1).
140	Orientation of deltopectoral crest projection: lateral (0), anterolateral (1).
141	Shape of the radial condyle of humerus round / proximal end of radius in end-on view: non-circular (0), circular (1).
142	Ratio of the length of metacarpal V to metacarpal III: ?0.5 (0), >0.5 (1).
143	Manual digit number: 5 (0), 4 (1), 3 (2).
144	Shape of manual and pedal ungual phalanges: narrow, claw-shaped (0) wide, hoof-shaped, U-shaped in dorsal view (1), wide, hoof-shaped, triangular in dorsal view (2)
145	Angle between long axis of femoral head and long axis of shaft: <100º (0), 100º to 120º (1), >120º (2).
146	Separation of femoral head from greater trochanter: continuous (0), separated by a distinct notch or change in slope (1).
147	Differentiation of the anterior trochanter of the femur: separated from femoral shaft by a deep groove laterally and dorsally (0), fused to femoral shaft (1).
148	Oblique ridge on lateral femoral shaft, distal to anterior trochanter: absent (0), present (1).
149	Form of the fourth trochanter: pendant (0), ridge-like (1).
150	Location of the fourth trochanter on the femoral shaft: proximal (0) distal, over half-way down the femoral shaft (1).
151	Maximum distal width of the tibia, compared to the maximum proximal width: narrower (0), wider (1).
152	Contact between tibia and astragalus: articulated (0), fused, with suture obliterated (1).
153	Number of pedal digits: 5 (0), 4 (1), 3 (2).
154	Phalangeal number in pedal digit IV: 5 (0), ?4 (1)
155	Postcranial osteoderm distribution: no postcranial osteoderms (0); postcranial osteoderms arranged in multiple transverse rows (1); postcranial osteoderms primarily present in two rows along midline (2).
156	Dimensions of largest osteoderm: no osteoderms (0) smaller than a dorsal centrum (1), equal to or larger than a dorsal centrum (2).
157	Basal surface of osteoderms: no osteoderms (0) flat or gently concave (1), deeply excavated (2), strongly convex (3).
158	External cortical histology of skeletally mature osteoderms: no osteoderms (0) lamellar bone (1), ISFB (2)
159	Haversian bone in osteoderms: no osteoderms (0) absent in core of skeletally mature osteoderms (1), may be present in in core of skeletally mature osteoderms (2).
160	Basal cortex of skeletally mature osteoderms: no osteoderms (0) present (1), absent or poorly developed (2).
161	Structrural fiber arrangement in osteoderms: no osteoderms (0) structural fibres absent (1), reaches orthoganal arrangment near osteoderm surfaces (2), diffuse throughout (3), highly ordered sets of orthoganally arranged fibers in the superficial cortex (4).
162	Gular osteoderms: absent (0), present (1).
163	Number of distinct cervical pectoral bands: none (0), one (1), two (2).
164	Form of cervical half rings: cervical half rings absent (0), composed of osteoderms that are either tightly adjacent to one another or coossified at the edges, forming arc over the cervical region (1), composed of osteoderms and underlying bony band segments, osteoderms may or may not cossify to the band, forming arc over the cervical region (2).
165	Distal spines on cervical half ring: absent (0), present, projecting dorsoposteriorly (1), present, projecting anteriorly (2).
166	Osteoderms on proximal limb segments: absent (0), present (1).
167	Millimeter-sized ossicles abundant in spaces between osteoderms in thoracic or caudal regions (excluding pelvic region), absent (0), present (1)
168	Deeply excavated, dorsoventrally flattened triangular osteoderms: absent (0), right or obtuse-angled triangles (1), right or obtuse-angled triangles that abruptly narrow distally into a spike ('splates' of Blows 2001) (2)
169	On deeply excavated triangular osteoderms, furrows perpendicular to basal edge: no deeply excavated triangular osteoderms (0), furrows absent (1), furrows present (2)
170	Lateralmost osteoderms in thoracic region: absent (0), ovoid or sub-ovoid with a longitudinal keel (1) triangular, dorsoventrally flattened elements (2), solid, conical spikes (3).

171	Thoracic osteoderms coossified to dorsal ribs: no osteoderms coossified to ribs (0), at least some osteoderms coossified to ribs (1)
172	Form of pelvic osteoderms: no osteoderms (0) unfused (1), coossified osteoderm rosettes (2), coossified evenly-sized polygons (3).
173	Caudal osteoderms: absent (0), present on dorsal or dorsolateral surfaces of tail only (1), completely surrounding tail (2).
174	Morphology of proximal, lateral caudal osteoderms: osteoderms absent (0), triangular with round/blunt apex (1) triangular with pointed apex (2).
175	Keel height of caudal osteoderms relative to thoracic osteoderms: osteoderms absent (0), keels equal in external-basal height (1), keels taller in caudal osteoderms (2).
176	Tail club knob shape: knob absent (0), major knob osteoderms semicircular in dorsal view (1), triangular in dorsal view (2).
177	Tail club knob proportions: knob absent (0), tail club knob length > width (1), length = width (2), width > length (3)
178	New character: External texture of osteoderm smooth (0), pitted with few or no projecting rugosities (1), pitted with many projecting rugosities (2)
179	New character: External surface of osteoderm has no or few vascular foramina (0), many vascular foramina (1)
180	New character: No primary osteons (0), primary osteons have begun to from (1), primary osteons are fully formed (2)
181	New character: ISFBs are arranged in 3-D arrangment at 45 degrees (0), ISFBs are arranged randomly (1)
182	New character: Osteoderm exhibits no secondary remodeling (0), osteoderm exhibits secondary remodeling (1)
183	New character: Mature osteoderm has Haversian core (0), mature osteoderm has trabecular core (1)
184	New character: Mature osteoderm has a uniform cortical thickness (0), mature ostedoerm has thin basal cortex and thick external cortex (1), mature osteoderms have thin cortices relative to core (2)
185	New character: Medial cervical plates are sub-oval or oval (0), medial cervical plates are square/rectangular (1)
186	New character: Cranial plates are smooth (0), cranial plates are rugose (1)

West Texas Specimens

Specimen	Classification	Formation	
TMM 31078-1	*Euoplocephalus sp.*	Aguja	(Brewster County)
TMM 45605-4	*Panoplosaurus mirus*	Aguja	
TVP 45866-2	*Edmontonia sp.*	Aguja	(Sandstone bed)
Osteoderm #1	*Euoplocephalus sp.*	Aguja	
TL-05-14 Sacrum	*Euoplocephalus sp.*	Aguja	(upper shale member)
TL-05-14 Vertebra	*Euoplocephalus sp.*	Aguja	(upper shale member)
TMM 43057-502	Undet. ankylosaur	Aguja	(Terlingua Microsite #1)
TMM 41836-1	Undet. ankylosaur	Aguja	
TMM 42878-1	Undet. ankylosaur	Javelina	
AMNH 3076	*Edmontonia sp.*	Aguja	
Osteoderm #2	Ankylosauridae	Aguja	
Osteoderm #3	Ankylosauridae	Aguja	
Osteoderm #4	Ankylosauridae	Aguja	
Osteoderm #5	Ankylosauridae	Aguja	
Osteoderm #6	Ankylosauridae	Aguja	
Osteoderm #7	Ankylosauridae	Aguja	
Ungual Phalanx #1	Ankylosauridae	Aguja	

Metapodial #1	Ankylosauridae	Aguja
Vertebra #1	Ankylosauridae	Aguja
Vertebra #2	Ankylosauridae	Aguja
Radius #1	Ankylosauridae	Aguja

Additional Tables

Taxon	Character
Lesothosaurus diagnosticus	Composition of first cervical half ring with band: no cervical half ring with band (0), first cervical half ring has 4 to 6 primary osteoderms only (1), first cervical half ring has 4 to 6 primary osteoderms surrounded by small (<2 cm diameter) circular secondary osteoderms (2).
Scelidosaurus harrisonii	Antorbital fenestra: present (0) absent (1).
Huayangosaurus taibaii	Lateral temporal fenestra, visible in lateral view: visible (0), not visible (1).
Ahshislepelta minor	Supratemporal fenestra: open (0), closed (1).
Aletopelta coombsi	Skull dimensions, including ornamentation: longer than wide (0), as wide, or wider than long (1).
Ankylosaurus magniventris	Width of the posterior margin of the skull (including squamosal horns where applicable) relative to the maximum width across the orbits: greater or equal (0), less (1).
Anodontosaurus lambei	Antorbital region of the dorsal skull surface: flat (0), arched (1).
Antarctopelta oliveroi	Deep longitudinal furrow on premaxilla: absent (0), present (1).
Argentine ankylosaur	Ornamentation on premaxillary beak: absent (0), present (1).
Bissektipelta archibaldi	Premaxillary sinus: absent (0), present (1)
Cedarpelta bilbeyhallorum	Dimensions of premaxillary palate: longer than wide (0), wider than long (1).
Chuanqilong chaoyangensis	Shape of the premaxillary palate: sub-triangular (0), sub-quadrate (1), sub-oval (2).
Crichtonpelta benxiensis	"VT or "UT-shaped median indentation of the anterior margin of the premaxilla: absent (0), present (1).
Dongyangopelta yangyanensis	Caudoventral extension of premaxillary tomium in lateral view: ends anteriorly to the maxillary teeth (0), obscures anteriormost maxillary teeth (1).
Dyoplosaurus acutosquameus	Bone bordering anterior margin of internal nares: premaxilla (0), maxilla (1).
Euoplocephalus tutus	External nares, defined as the outermost rim of the nasal vestibule, opening faces: laterally to anterolaterally (0) anteriorly (1) ventrolaterally (2).
Gargoyleosaurus parkpinorum	External nares, visible in dorsal view: visible (0), hidden (1).
Gastonia burgei	Modified: Paranasal apertures/fossae: no fossae or apertures present besides primary opening for nasal airway (0), paranasal apertures/fossae present (1).
Glyptodontopelta mimus	Shape of respiratory passage: straight or arched (0), with anterior (rostral) and posterior (caudal) loops
Gobisaurus domoculus	New character: Vascular impressions on dorsal surface of posterior nasal passage (airway): absent (0) present (1).
Liaoningosaurus paradoxus	Frontonasal and/or frontoparietal cranial ornamentation: absent (0) rugose, not differentiated into discrete polygons (caputegulae) (1), differentiated into discrete polygons (caputegulae) (2).
Minmi paravertebra	Number of caputegulae in frontonasal and prefrontal region: no caputegulae (0), 10 or fewer (1), 11 to 30 (2) more than 30 (3).
Minmi sp.	Majority of frontonasal and/or frontoparietal caputegulum relief: caputegulae absent (0), caputegulae concave or flat (1), caputegulae strongly bulbous (2).
Mymoorapelta maysi	Domed frontonasal caputegulae: domed caputegulae absent (0), rounded cones with circular bases (1) pyramidal with sharp edges (2).
Nodocephalosaurus kirtlandensis	Supranarial caputegulae, notch or embayment dorsal to nasal vestibule: no supranarial caputegulae (0), notch absent (1), notch present (2).
Panoplosaurus mirus	Number of internarial caputegulae: none (0), 1 (1), more than 1 (2).
Pawpawsaurus campbelli	Median nasal caputegulum (located posterior to the supranarial ornamentation, on the midline of the skull), which is at least twice as large as the other frontonasal caputegulae: absent (0), present (1).
Pinacosaurus grangeri	Loreal caputegulum in lateral view: no caputegulum (0) 1 caputegulum (1), more than 1 caputegulum (2).
Pinacosaurus mephistocephalus	Shape of the maxillary tooth row: straight (0), medially convex (1).
Saichania chulsanensis	Maxillary tooth row position: lateral margin of skull (0), inset (1).
Sauropelta edwardsorum	Distance between posteriormost extent of maxillary tooth rows relative to the width of the premaxillary beak: wider (0), narrower (1).
Sauroplites scutiger	Caudoventral secondary palate: absent (0), present (1)
Stegopelta landerensis	Posterior palatal foramen: absent (0), present (1).
Scolosaurus cutleri	Gap between palate and braincase: open (0), closed by a dorsal projection of the pterygoid (1).
Shamosaurus scutatus	Lacrimal incisure (mediolateral constriction behind the nares/at the prefrontals, giving the skull an hourglass-shaped outline in dorsal view): absent (0) present (1).
Talarurus plicatospineus	Lacrimal caputegulum in lateral view: no caputegulum (0) 1 caputegulum (1), more than 1 caputegulum (2).
Taohelong jinchengensis	Prefrontal caputegulum: no caputegulum (0) flat (1), sharply pointed and pyramidal (2).
Tarchia kielanae	Scroll-like descending process of the frontal: absent (0) present (1)
Tatankacephalus cooneyorum	Form of supraorbitals (including ornamentation): absent (0), boss-like, rounded laterally (1), sharp lateral rim, forming a ridge (2).
Tianchisaurus nedegoapeferima	Supraorbitals, when viewed dorsally: no supraorbitals (0), combine to form continuous edge (1), have distinct apices (2).
Tsagantegia longicranialis	Orbits, angle of orbital axis: <40ß (0), >40ß (1).
Zaraapelta nomadis	Ciliary osteoderm (eyelid ossification): absent (0) present (1)
Zhejiangosaurus luoyangensis	Development of the postocular shelf: not developed (0), completely separating orbit from temporal space (1).
Ziapelta sanjuanensis	Proportions of jugal orbital ramus: depth greater than transverse breadth (0), transverse breadth greater than depth (1).
Edmontonia sp.	Depth of jugal ramus relative to orbit height: jugal height is less than 15% orbit height (0), jugal height is more than 15% orbit height (1)
Taxon	Accessory postorbital ossification: absent (0), present (1)
Lesothosaurus diagnosticus	Squamosal/postorbital horn: no horn (0) base has broad triangular cross-section and overall shape is pyramidal (1), base is oval in cross-section and overall shape is narrow, tapered cylinder (2).
Scelidosaurus harrisonii	Shape of jugal/quadratojugal horn in dorsal view: quadratojugal horn absent (0), horn U-shaped, with round distal edge (1), horn triangular, with pointed distal edge (2)
Huayangosaurus taibaii	Jugal/quadratojugal horn: no horn (0) lacks distinct neck at base (1), has distinct neck at base (2).
Ahshislepelta minor	Jugal or quadratojugal horn size relative to orbit size: no horn (0), length of base of jugal/quadratojugal horn equal to or less than the length of the orbit (1), length of base of jugal/quadratojugal horn is 110% or greater length of orbit (2).
Aletopelta coombsi	Small (<2 cm diameter), circular caputegulae posterolateral to orbit (postocular caputegulae), along ventral edge of squamosal horn and/or along dorsal edge of quadratojugal horns: absent (0), present (1).
Ankylosaurus magniventris	Form of the parietal surface: parietals flat to slightly convex (0), parietals concave, forming a trough-like surface posterior to the supraorbitals and anterior to the posterior edge of the skull (1).
Anodontosaurus lambei	A single large medial polygon of ornamentation in the parietal region: absent (0), present (1)
Antarctopelta oliveroi	Number of discrete nuchal caputegulae: none (0), 2 (1), greater than 2(2)
Argentine ankylosaur	Posterior projection of the nuchal shelf: does not obscure occiput in dorsal view (0), obscures occiput in dorsal view (1).
Bissektipelta archibaldi	Shape of quadrate in lateral aspect: curved (anteriorly convex, posteriorly concave) (0), straight (1).
Cedarpelta bilbeyhallorum	Inclination of quadrate in lateral aspect: near vertical (0), almost 45ß anterolaterally (1).
Chuanqilong chaoyangensis	Form of the anterior surface of the quadrate: transversely concave (0), not concave (1).
Crichtonpelta benxiensis	Ventral projection of the mandibular process of the quadrate in lateral view: projects beyond the quadratojugal ornamentation (0), hidden by quadratojugal ornamentation (1).
Dongyangopelta yangyanensis	Form of quadrate mandibular extremity: symmetrical (0), medial condyle larger than lateral condyle (1).
Dyoplosaurus acutosquameus	Inclination of the articular surface of the quadrate condyle in posterior view: horizontal (0), ventromedially inclined at approximately 45ß to horizontal (1)
Euoplocephalus tutus	Lateral ramus of the quadrate: present (0), absent (1).
Gargoyleosaurus parkpinorum	Dorsoventral depth of the pterygoid process of the quadrate: deep (0), shallow (1).
Gastonia burgei	Contact between paroccipital process and quadrate: sutural (0), fused (1).
Glyptodontopelta mimus	Contact between pterygoids: pterygoids separate caudomedially, forming an interpterygoid vacuity (0), pterygoids joined medially forming a pterygoid shield (1).
Gobisaurus domoculus	Direction of the pterygoid flange: anterolateral (0), anterior/parasagittal (1).
Liaoningosaurus paradoxus	Contact between basipterygoid processes and pterygoid: sutural (0), fused (1).
Minmi paravertebra	Position of ventral margin of the pterygovomerine keel relative to alveolar ridge: dorsal (0), level (1).
Minmi sp.	Dorsal extent of median vomer lamina: does not meet skull roof (0), meets skull roof (1).
Mymoorapelta maysi	Pterygoid foramen: absent (0), present (1).
Nodocephalosaurus kirtlandensis	Position of posterior margin of pterygoid body relative to the anterior margin of the quadrate condyle: anteriorly positioned (0), in transverse alignment (1).
Panoplosaurus mirus	Size of occiput: higher than wide (0), wider than high (1).

Pawpawsaurus campbelli	Direction of paroccipital process extension: caudolateral (0), lateral (1).
Pinacosaurus grangeri	Bones forming the occipital condyle: basioccipital and exoccipital (0), basioccipital only (1).
Pinacosaurus mephistocephalus	Length of basisphenoid relative to the basioccipital: longer (0), shorter or equal (1).
Saichania chulsanensis	Form of basisphenoidal tuberosities: medially separated rounded rugose stubs (0), continuous transverse rugose ridge (1).
Sauropelta edwardsorum	Size of basipterygoid processes: twice as long as wide or over (0), less than twice as long as wide (1).
Sauroplites scutiger	Form of the cranial nerve foramina IX-XII: separate foramina (0), single foramen shared with the jugular vein (1).
Stegopelta landerensis	Position of mandible articulation relative to mandibular adductor fossa: posterior (0), posteromedial (1).
Scolosaurus cutleri	Mandibular fenestra: present (0), absent (1).
Shamosaurus scutatus	Depth of the dentary symphysial ramus relative to half the maximum depth of the mandibular ramus in lateral view: deeper (0), shallower (1).
Talarurus plicatospineus	Shape of dorsal margin of the dentary in lateral view: straight (0), sinuous (1).
Taohelong jinchengensis	Development of the coronoid process: not developed (0), distinct (1).
Tarchia kielanae	Position of glenoid for quadrate relative to mandibular axis: medially offset (0), in line (1).
Tatankacephalus cooneyorum	Size and projection of the retroarticular process: small with no dorsal projection (0), well developed with a dorsal projection (1).
Tianchisaurus nedegoapeferima	Size of predentary ventral process: distinct, prong shaped process (0), rudimentary eminence (1).
Tsagantegia longicranialis	Length of mandibular caputegulum with respect to the length of the mandible: less than or equal to half the length (0), over three quarters the length (1).
Zaraapelta nomadis	Premaxillary teeth: present (0) absent (1).
Zhejiangosaurus luoyangensis	Cingula on maxillary and/or dentary teeth: absent (0), present (1).
Ziapelta sanjuanensis	Maxillary and/or dentary tooth crown shape: pointed (0), rounded (1).
Edmontonia sp.	Maxillary and/or dentary tooth denticles: < 13 denticles (0), ?13 denticles (1) (Thompson et al. 2012: 65, in part; Arbour et al. 2014a: 33).
Taxon	Number of dentary teeth: <25 (0), ?25 (1).
Lesothosaurus diagnosticus	Type of articulation between the atlantal neural arch and intercentrum: open (0) fused in adult (1).
Scelidosaurus harrisonii	Type of contact between the atlantal neural arches: no median contact (0), median contact (1).
Huayangosaurus taibaii	Contact between atlas and axis: articulated (0), fused (1).
Ahshislepelta minor	Dimensions of cervical vertebrae centra: anteroposteriorly longer than transverse width (0), anteroposteriorly shorter than transverse width (1).
Aletopelta coombsi	Ratio of maximum neural spine width to height in anterior cervicals: <0.25 (0), ?0.25 (1).
Ankylosaurus magniventris	Ratio of anteroposterior dorsal centrum length to posterior centrum height: >1.1 (0), <1.1 (1).
Anodontosaurus lambei	Longitudinal keel on ventral surface of dorsal centra: present (0), absent (1).
Antarctopelta oliveroi	Cross sectional shape of neural canal in posterior dorsals: circular (0) elliptical, with long axis running dorsoventrally (1)
Argentine ankylosaur	Shape of the proximal cross-section of the dorsal ribs: triangular (0), ?L?- or ???-shaped (1).
Bissektipelta archibaldi	Attachment of dorsal ribs to posterior dorsal vertebrae: articulated (0), fused (1).
Cedarpelta bilbeyhallorum	Contact between posteriormost dorsal vertebrae: articulated (0), fused to form a presacral rod (1)
Chuanqilong chaoyangensis	Longitudinal groove in ventral surface of the sacrum: absent (0), present (1).
Crichtonpelta benxiensis	Longitudinal ridge at approximate mid-height of centrum of mid and distal caudals: absent (0) present (1).
Dongyangopelta yangyanensis	Ratio of maximum distal width to height of the neural spines of proximal caudals: ?0.2 (0), >0.2 (1).
Dyoplosaurus acutosquameus	Direction of the transverse processes of proximal caudals: craniolaterally projecting (0), caudolaterally projecting (1), laterally projecting (2)
Euoplocephalus tutus	Persistence of transverse processes down the length of the caudal series: not present beyond the mid-length of the series (0), present beyond the mid-length of the series (1).
Gargoyleosaurus parkpinorum	Attachment of haemal arches to their respective centra: articulated (0), fused (1).
Gastonia burgei	Extent of pre- and postzygapophyses over their adjacent centra in posterior vertebrae: extend over less than half the length of the adjacent centrum (0), extend over more than half the length of the adjacent centrum (1).
Glyptodontopelta mimus	In tail club handle vertebrae, shape of each interlocking neural arch in dorsal view: distal caudal vertebrae do not form handle (0), V-shaped, angle of divergence about 22-26° (1), V-shaped, angle of divergence about 35-37° (2), U-shaped, angle of divergence greater than 60° (3).
Gobisaurus domoculus	Shape of the posterior haemal arches: rounded haemal spine in lateral view with no contact between haemal arches (0), inverted ???-shaped haemal spine in lateral view, with contact between the ends of adjacent spines (1).
Liaoningosaurus paradoxus	Ossified tendons in distal region of tail: absent (0), present (1).
Minmi paravertebra	Dimensions of coracoid: longer than wide (0), wider than long or equal width and length (1).
Minmi sp.	Form of the anterior margin of the coracoid: convex (0), straight (1).
Mymoorapelta maysi	Craniaventral process of coracoid: absent (0), present (1).
Nodocephalosaurus kirtlandensis	Size of coracoid glenoid relative to scapula glenoid: sub-equal (0), half the size (1).
Panoplosaurus mirus	Contact between scapula and coracoid: articulated (0), fused (1).
Pawpawsaurus campbelli	Scapula glenoid orientation: ventrolateral (0), ventral (1).
Pinacosaurus grangeri	Ventral process of scapula at the caudoventral margin of glenoid: absent (0), present (1)
Pinacosaurus mephistocephalus	Form of the scapula acromion process: not developed or ridge-like along the dorsal border of the scapula (0) flange-like and folded over towards the scapula glenoid (1) ridge terminating in a knob-like eminence (2).
Saichania chulsanensis	Orientation of the acromion process of scapula: directed away from the glenoid (0), directed towards scapula glenoid (1).
Sauropelta edwardsorum	Scapulocoracoid buttress: absent (0), present (1).
Sauroplites scutiger	Distal end of scapula shaft: narrow (0), expanded (1).
Stegopelta landerensis	Contact between sternal plates: separate (0), fused (1).
Scolosaurus cutleri	Length of the preacetabular process of ilium as a percentage of total ilium length: ? 30% (0), > 30 % (1)
Shamosaurus scutatus	Angle of lateral deflection of the preacetabular process of the ilium: 10°?20° (0), 45° (1).
Talarurus plicatospineus	Orientation of the preacetabular portion of the ilium: near vertical (0), near horizontal (1).
Taohelong jinchengensis	Form of the preacetabular portion of the ilium: straight process (0), pronounced ventral curvature (1).
Tarchia kielanae	Lateral edge of ilium in dorsal view: straight (0), sinuous (1).
Tatankacephalus cooneyorum	Lateral exposure of the acetabulum: exposed (0) acetabulum partially obscured as it is partially encircled by the distal margin of the ilium (1).
Tianchisaurus nedegoapeferima	Perforation of the acetabulum: present, open acetabulum (0), absent, closed acetabulum (1).
Tsagantegia longicranialis	Postacetabular ilium length, relative to diameter of acetabulum: greater (0), smaller (1).
Zaraapelta nomadis	Pubis: present (0), indistinct from ilium/ischium (1)
Zhejiangosaurus luoyangensis	Shape of ischium: straight (0), ventrally flexed at mid-length (1).
Ziapelta sanjuanensis	Shape of the dorsal margin of ischium: straight or concave (0), convex (1).
Edmontonia sp.	Separation of humeral head and deltopectoral crest in anterior view: continuous (0), separated by a distinct notch (1).
Taxon	Separation of humeral head and medial tubercle in anterior view: continuous (0), separated by a distinct notch (1)
Lesothosaurus diagnosticus	Ratio of deltopectoral crest length to humeral length: ?0.5 (0), >0.5 (1).
Scelidosaurus harrisonii	Orientation of deltopectoral crest projection: lateral (0), anterolateral (1).
Huayangosaurus taibaii	Shape of the radial condyle of humerus round / proximal end of radius in end-on view: non-circular (0), circular (1).
Ahshislepelta minor	Ratio of the length of metacarpal V to metacarpal III: ?0.5 (0), >0.5 (1).
Aletopelta coombsi	Manual digit number: 3 (0), 4 (1), 3 (2).
Ankylosaurus magniventris	Shape of manual and pedal ungual phalanges: narrow, claw-shaped (0) wide, hoof-shaped, U-shaped in dorsal view (1), wide, hoof-shaped, triangular in dorsal view (2)
Anodontosaurus lambei	Angle between long axis of femoral head and long axis of shaft: <100° (0), 100° to 120° (1), >120° (2).
Antarctopelta oliveroi	Separation of femoral head from greater trochanter: continuous (0), separated by a distinct notch or change in slope (1).
Argentine ankylosaur	Differentiation of the anterior trochanter of the femur: separated from femoral shaft by a deep groove laterally and dorsally (0), fused to femoral shaft (1).
Bissektipelta archibaldi	Oblique ridge on lateral femoral shaft, distal to anterior trochanter: absent (0), present (1).
Cedarpelta bilbeyhallorum	Form of the fourth trochanter: pendant (0), ridge-like (1).
Chuanqilong chaoyangensis	Location of the fourth trochanter on the femoral shaft: proximal (0) distal, over half-way down the femoral shaft (1).
Crichtonpelta benxiensis	Maximum distal width of the tibia, compared to the maximum proximal width: narrower (0), wider (1).
Dongyangopelta yangyanensis	Contact between tibia and astragalus: articulated (0), fused, with suture obliterated (1).
Dyoplosaurus acutosquameus	Number of pedal digits: 5 (0), 4 (1), 3 (2).
Euoplocephalus tutus	Phalangeal number in pedal digit IV: 5 (0), ?4 (1)
Gargoyleosaurus parkpinorum	Postcranial osteoderm distribution: no postcranial osteoderms (0); postcranial osteoderms arranged in multiple transverse rows (1); postcranial osteoderms primarily present in two rows along midline (2).
Gastonia burgei	Dimensions of largest osteoderm: no osteoderms (0) smaller than a dorsal centrum (1), equal to or larger than a dorsal centrum (2).
Glyptodontopelta mimus	Basal surface of osteoderms: no osteoderms (0) flat or gently concave (1), deeply excavated (2), strongly convex (3).
Gobisaurus domoculus	External cortical histology of skeletally mature osteoderms: no osteoderms (0) lamellar bone (1), ISFB (2)
Liaoningosaurus paradoxus	Haversian bone in osteoderms: no osteoderms (0) absent in core of skeletally mature osteoderms (1), may be present in in core of skeletally mature osteoderms (2).
Minmi paravertebra	Basal cortex of skeletally mature osteoderms: no osteoderms (0) present (1), absent or poorly developed (2).
Minmi sp.	Structrural fiber arrangement in osteoderms: no osteoderms (0) structural fibres absent (1), reaches orthogonal arrangment near osteoderm surfaces (2), diffuse throughout (3), highly ordered sets of orthogonally arranged fibers in the superficial cortex (4).
Mymoorapelta maysi	Guiar osteoderms: absent (0), present (1).
Nodocephalosaurus kirtlandensis	Number of distinct cervical pectoral bands: none (0), one (1), two (2).
Panoplosaurus mirus	Form of cervical half rings: cervical half rings absent (0), composed of osteoderms that are either tightly adjacent to one another or coossified at the edges, forming arc over the cervical region (1), composed of osteoderms and underlying bony band segments, osteoderms may or may not ossify to the band, forming arc over the cervical region (2)
Pawpawsaurus campbelli	Distal spines on cervical half ring: absent (0), present, projecting dorsoposteriorly (1), present, projecting anteriorly (2).
Pinacosaurus grangeri	Osteoderms on proximal limb segments: absent (0), present (1).

Pinacosaurus mephistocephalus	Millimeter-sized ossicles abundant in spaces between osteoderms in thoracic or caudal regions (excluding pelvic region), absent (0), present (1)
Saichania chulsanensis	Deeply excavated, dorsoventrally flattened triangular osteoderms: absent (0), right or obtuse-angled triangles (1), right or obtuse-angled triangles that abruptly narrow distally into a spike ('splates' of Blows 2001) (2)
Sauropelta edwardsorum	On deeply excavated triangular osteoderms, furrows perpendicular to basal edge: no deeply excavated triangular osteoderms (0), furrows absent (1), furrows present (2)
Sauroplites scutiger	Lateralmost osteoderms in thoracic region: absent (0), ovoid or sub-ovoid with a longitudinal keel (1) triangular, dorsoventrally flattened elements (2), solid, conical spikes (3).
Stegopelta landerensis	Thoracic osteoderms coossified to dorsal ribs: no osteoderms coossified to ribs (0), at least some osteoderms coossified to ribs (1)
Scolosaurus cutleri	Form of pelvic osteoderms: no osteoderms (0) unfused (1), coossified osteoderm rosettes (2), coossified evenly-sized polygons (3).
Shamosaurus scutatus	Caudal osteoderms: absent (0), present on dorsal or dorsolateral surfaces of tail only (1), completely surrounding tail (2).
Talarurus plicatospineus	Morphology of proximal, lateral caudal osteoderms: osteoderms absent (0), triangular with round/blunt apex (1) triangular with pointed apex (2).
Taohelong jinchengensis	Keel height of caudal osteoderms relative to thoracic osteoderms: osteoderms absent (0), keels equal in external-basal height (1), keels taller in caudal osteoderms (2).
Tarchia kielanae	Tail club knob shape: knob absent (0), major knob osteoderms semicircular in dorsal view (1), triangular in dorsal view (2).
Tatankacephalus cooneyorum	Tail club knob proportions: knob absent (0), tail club knob length > width (1), length = width (2), width > length (3)
Tianchisaurus nedegoapeferima	New character: External texture of osteoderm smooth (0), pitted with few or no projecting rugosities (1), pitted with many projecting rugosities (2)
Tsagantegia longicranialis	New character: External surface of osteoderm has no or few vascular foramina (0), many vascular foramina (1)
Zaraapelta nomadis	New character: No primary osteons (0), primary osteons have begun to from (1), primary osteons are fully formed (2)
Zhejiangosaurus luoyangensis	New character: ISFBs are arranged in 3-D arrangment at 45 degrees (0), ISFBs are arranged randomly (1)
Ziapelta sanjuanensis	New character: Osteoderm exhibits no secondary remodeling (0), osteoderm exhibits secondary remodeling (1)
Edmontonia sp.	New character: Mature osteoderm has Haversian core (0), mature osteoderm has trabecular core (1)
Taxon	New character: Mature osteoderm has a uniform cortical thickness (0), mature osteoderm has thin basal cortex and thick external cortex (1), mature osteoderms have thin cortices relative to core (2)
Lesothosaurus diagnosticus	New character: Medial cervical plates are sub-oval or ovai (0), medial cervical plates are square/rectangular (1)
Scelidosaurus harrisonii	New character: Cranial plates are smooth (0), cranial plates are rugose (1)

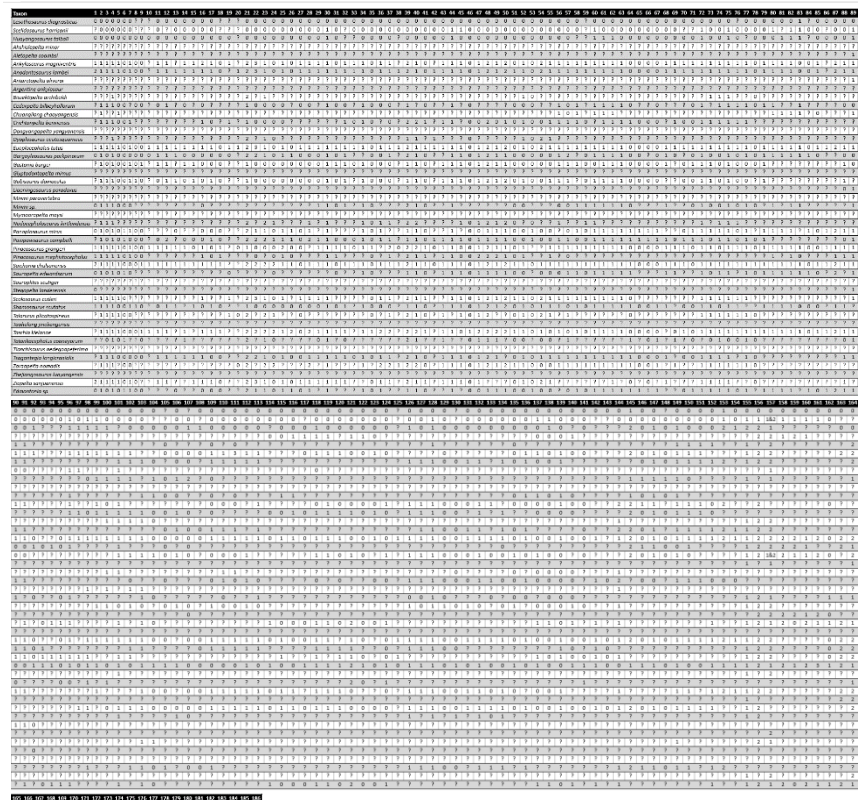

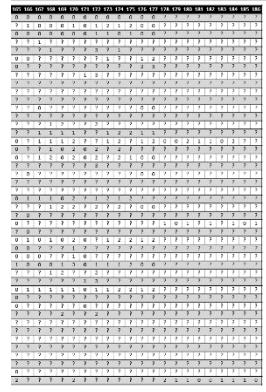

REFERENCES

Arbour VM, Burns ME, Sullivan RM, Lucas SG, Cantrell AK, et al. (2014) A New Ankylosaurid Dinosaur from the Upper Cretaceous (Kirtlandian) of New Mexico with Implications for Ankylosaurid Diversity in the Upper Cretaceous of Western North America. PLOS ONE 9(9): e108804. https://doi.org/10.1371/journal.pone.0108804

Arbour V.M., & Philip J. Currie (2015) Systematics, phylogeny and palaeobiogeography of the ankylosaurid dinosaurs, Journal of Systematic Palaeontology, 14:5, 385-444, DOI: 10.1080/14772019.2015.1059985

Befus et al. (2008) Befus, K.S., Hanson, R.E., Lehman, T.M., Griffin, W.R. (2008) Cretaceous basaltic phreatomagmatic volcanism in West Texas: Maar complex at Peña Mountain, Big Bend National Park. Journal of Volcanology and Geothermal Research 173, 245.

Bourke JM, Porter WR, Witmer LM (2018) Convoluted nasal passages function as efficient heat exchange in ankylosaurs (Dinosauria: Ornithischia: Thyreophora). PLoS ONE 13(12): e0207381

Blows, W.T. (2001) Dermal armor of the polacanthine ankylosaurs. In: K.Carpenter (ed.),*The Armored Dinosaurs*, 363–385.Indiana University Press, Bloomington

Breyer, John & Busbey, Arthur & Hanson, Richard & Befus, Kenneth & Griffin, W. & Hargrove, Ulysses S & Bergman, Steven. (2007) Evidence for Late Cretaceous Volcanism in Trans-Pecos Texas. The Journal of Geology. 115. 243-251. 10.1086/510640.

Burns, M. E., & Currie, P. J. (2014) External and internal structure of ankylosaur (Dinosauria, Ornithischia) osteoderms and their systematic relevance. Journal of Vertebrate Paleontology, 34(4), 835-851.

Carpenter, K. and Currie P.J., (1990) Ankylosaur systematics: Example using *Panoplosaurus* and *Edmontonia* (Ankylosauria: Nodosauridae). In Carpenter K., Currie P. J. (Eds.), *Dinosaur Systematics: Perspectives and Approaches, pp.282-298*. Cambridge Univ. Press, New York, NY.

Carpenter, K., and Breithaupt, B. (1986) Latest Cretaceous occurrences of nodosaurid ankylosaurs (Dinosauria: Ornithischia) in western North America and the gradual extinction of the dinosaurs. Journal of Vertebrate Paleontology 6:251-257

Carpenter, K. (2001) Phylogenetic analysis of the Ankylosauria. Pp. 455–484 in K. Carpenter (ed.) The Armored Dinosaurs. Indiana University Press, Bloomington.

Carpenter K. (2012) Ankylosaurs. In: Brett-Surman MK, Holtz TR, Farlow JO, editors. The complete dinosaur. 2nd ed. Bloomington: Indiana University Press; p. 505–252.

Carpenter K, DiCroce T, Kinner B, Simon R (2013) Pelvis of *Gargoyleosaurus* (Dinosauria: Ankylosauria) and the Origin and Evolution of the Ankylosaur Pelvis. PLoS ONE 8(11): e79887

Coombs, W. P. (1978) The families of ornithischian dinosaur order Ankylosauria. Palaeontology, 21, Part 1, 143-170.

Coombs, W. P. and Maryanska, T. (1990) *The Dinosauria Ankylosauria*, 1st edition, Edited by: Weishampel, D. B., Dodson, P. and Osmólska, H. 456–483. Berkeley: University of California Press

Coombs, W. (1990). Teeth and taxonomy in ankylosaurs. In K. Carpenter & P. Currie (Eds.), Dinosaur Systematics: Approaches and Perspectives (pp. 269-280). Cambridge: Cambridge University Press.

Coombs, W.P., Demeré,T.A., (1996) A Late Cretaceous nodosaurid ankylosaur (Dinosauria: Ornithischia) from marine sediments of Coastal California: Journal of Paleontology, 70, 311-326.

Ford, Tracy. (2000) Ford, T. L., 2000, A review of ankylosaur osteoderms from New Mexico and a preliminary review of ankylosaur armor: In: *Dinosaurs of New Mexico*, edited by Lucas S. G., and Heckert A. B., New Mexico Museum of Natural History and Science Bulletin n. 17, p. 157-176.. New Mexico Museum of Natural history Bulletin. 17. 157-176.

Ford, T., Kirkland, J.I., (2001) Carlsbad ankylosaur (Ornithischia, Ankylosauria): An ankylosaurid and not a nodosaurid, in Carpenter, K. (ed.), *The Armored Dinosaurs*: Bloomington, Indiana University Press, 239-260.

Gradstein, F.M., Ogg, J.G., Schmitz, M.D., Ogg, G.M., (2012) The Geologic Time Scale. Elseviar, Amsterdam, p. 1144

Hayashi, S., Carpenter, K., Scheyer, T. M., Watabe, M., & Suzuki, D. (2010) Function and evolution of ankylosaur dermal armor. Acta Palaeontologica Polonica, 55(2), 213-228.

Hieronymus, T.L., Witmer, L.M., Tanke, D.H. and Currie, P.J. (2009) The Facial Integument of Centrosaurine Ceratopsids: Morphological and Histological Correlates of Novel Skin Structures. Anat Rec, 292: 1370-1396. doi:10.1002/ar.20985

Kirkland, J.I. (1998) A polocanthine ankylosaur (Ornithischia: Dinosauria) from the Early Cretaceous (Barremian) of Eastern Utah. In S.G. Lucas, J.I. Kirkland, and J.W. Estep (eds.), *Lower and Middle Cretaceous Terrestrial Ecosystems. New Mexico Museum of Natural History and Sciences Bulletin* 14: 271-281.

Lawson, D.A., (1976) Tyrannosaurus and Torosaurus, Maastrictian dinosaurs from Trans-Pecos Texas: Journal of Paleontology, v. 50, p. 158-164.

Lehman, T.M. (1985) Stratigraphy, sedimentology, and paleontology of Upper Cretaceous (Campanian-Maastrictian) sedimentary rocks in Trans-Pecos, Texas. Unpublished PhD. Dissertation, University of Texas at Austin, Austin. 299p.

Lehman, T.M., (1991) Sedimentation and tectonism in the Laramide Tornillo Basin of West Texas: Sedimentary Geology, v. 75, p 9-28.

Lehman, T. M., & Wheeler, E. A. (2001) A fossil dicotyledonous woodland/forest from the Upper Cretaceous of Big Bend National Park, Texas. *Palaios, 16*(1), 102-108. doi:2.0.CO;2

Lehman, T. M., and Busbey, A. B., (2007) Big Bend Field Trip Guidebook: Society of Vertebrate Paleontology, 69 p.

Lehman, T. M., Wick, S. L., Beatty, H. L., Straight, W. H., & Wagner, J. R. (2018) Stratigraphy and depositional history of the tornillo group (upper cretaceous-eocene) of west texas. *Geosphere (Boulder, CO), 14*(5), 2206-2244.

Lehman, Thomas & Wick, Steven & Brink, Alyson & Shiller, Thomas. (2019) Stratigraphy and vertebrate fauna of the lower shale member of the Aguja Formation (lower Campanian) in West Texas. Cretaceous Research. 99. 10.1016/j.cretres.2019.02.028.

Leslie, Caitlin & Peppe, Daniel & Williamson, Thomas & Heizler, Matthew & Jackson, Mike & Atchley, Stacy & Nordt, Lee & Standhardt, Barbara. (2018) Revised age constraints for Late Cretaceous to early

Paleocene terrestrial strata from the Dawson Creek section, Big Bend National Park, West Texas. GSA Bulletin. 130. 1143-1163. 10.1130/B31785.1.

Lucas, S. G., Mateer, N. J., Hunt, A. P., & O'Neill, F. M. (1987) Dinosaurs, the age of the Fruitland and Kirtland formations, and the Cretaceous-Tertiary boundary in the San Juan Basin, New Mexico. Special Paper - Geological Society of America, 209, 35-50.

Maddison, W. P. and Maddison, D.R.2019) Mesquite: a modular system for evolutionary analysis. Version 3.61 http://www.mesquiteproject.org

McDonald, A. T., & Wolfe, D. G. (2018) A new nodosaurid ankylosaur (Dinosauria; Thyreophora) from the upper Cretaceous Menefee Formation of New Mexico. PeerJ, Article 5435, 29.

McCrea, R. T., Lockley, M. G., and Meyer, C. A. (2001) Globaldistribution of purported ankylosaur track occurrences. In Carpenter, K. (ed.). *The Armored Dinosaurs*. Indiana Uni-versity Press, Bloomington, IN, 413–454

McDonald AT, Wolfe DG. (2018) A new nodosaurid ankylosaur (Dinosauria: Thyreophora) from the Upper Cretaceous Menefee Formation of New Mexico. *PeerJ* 6:e5435 https://doi.org/10.7717/peerj.5435

Nopcsa (1915) Nopcsa F. Die Dinosaurier der siebenbürgischen Landesteile Ungarns. Mitteilungen aus dem Jahrbuche der Königlich-Ungarischen Geologischen Reichsanstalt. 1915;23:1–26.

Padian, K., & Lamm, E. (Eds.). (2013) *Bone Histology of Fossil Tetrapods: Advancing Methods, Analysis, and Interpretation*. University of California Press.

Obradovich, J.D., (1993) A Cretaceous Time Scale. Geological Association of Canada, Special Paper 48, pp. 201-227.

Osborn, H.F. (1923) Two Lower Cretaceous dinosaurs of Mongolia. Am. Mus. Novit. 95, 1-10.

Attila Ősi. (2005) *Hungarosaurus tormai*, a New Ankylosaur (Dinosauria) from the Upper Cretaceous of Hungary. *Journal of Vertebrate Paleontology, 25*(2), 370-383. Retrieved April 16, 2020, from www.jstor.org/stable/4524451

Rivera-Sylva, H., Carpenter, K., & Aranda-Manteca, F. (2011) Late Cretaceous Nodosaurids (Ankylosauria, Ornithischia) from Mexico. Revista Mexicana De Ciencias Geologicas, 28(3), 371-378.

Sankey, J. T. (2001) Late Campanian southern dinosaurs, Aguja Formation, Big Bend, Texas. Journal of Paleontology, 75(1), 208-215.

Scheyer, T. M., & Sander, P. M. (2004) History of ankylosaur osteoderms; implications for systematics and f Standhardt, B. R.*Vertebrate paleontology of the Cretaceous/Tertiary transition of Big Bend National Park, Texas* Available from GeoRef. (51088978; 1987-041929).

Sereno, P. C. (1998) A rationale for phylogenetic definitions, with application to the higher-level taxonomy of Dinosauria. Neues Jahrbuch für Geologie und Pal€aontologie, Abhandlungen, 210, 41-83.

Thompson, R. S., Parish, J. C., Maidment, S. C. R. & Barrett, P. M. (2012) Phylogeny of the ankylosaurian dinosaurs (Ornithischia: Thyreophora). Journal of Systematic Palaeontology, 10, 301312.

Tumanova T.A., (1983) "Pervyy ankilozavr iz nizhnego mela Mongolii", In: L.P. Tatarinov, R. Barsbold, E. Vorobyeva, B. Luvsandanzan, B.A. Trofimov, Yu. A. Reshetov, & M.A. Shishkin (eds.), *Iskopayemyye reptilii mongolii*. Trudy Sovmestnaya Sovetsko-Mongol'skaya Paleontologicheskaya Ekspeditsiya **24**: 110-118

Vickaryous, M. K., & Sire, J. Y. (2009) The integumentary skeleton of tetrapods: origin, evolution, and development. *Journal of anatomy*, *214*(4), 441–464. https://doi.org/10.1111/j.1469-7580.2008.01043.x

Waggoner, K. J. 2006. Sutural form and shell morphology of Placenticeras, and systematic descriptions of Late Cretaceous ammonites from the Big Bend region, Texas. Unpublished Ph.D. Dissertation, Texas Tech University, Lubbock, Texas. 398 pp

VITA

The youngest of three children Bryanna West was born and raised in Dallas, Tx. In 2014 she graduated from Coppell High School as an Academic All American after participating in Women's Varsity Wrestling and Athletic Training. She earned her Bachelor of Science in Geosciences from Texas Tech University in August of 2018.

Just a week after graduating from Texas Tech she started as a graduate student at Texas Christian University to study vertebrate paleontology under the tutelage of Dr. Arthur Busbey. Currently she is seeking employment as a fossil preparator and plans to return to school to obtain a PhD. in Vertebrate Paleontology in the near future. Until then she plans to tend to her family's ranch in Oklahoma with her three dogs, Bonnie, Clyde, and Sundance.

ABSTRACT

Big Bend National Park is known for its unique Late Cretaceous fauna, such as *Alamosaurus sanjuanensis* and *Quetzalcoatlus northropi*. Most major groups of dinosaurs are represented in the Late Cretaceous strata, which ranges from the Early Campanian through the Late Maastrichtian (approximately 17.6 Ma). However, one group of herbivorous dinosaurs, the armored ankylosaurs, have never been described in detail from this area. Fossil remains of these dinosaurs are sparse and fragmentary; the only skeletal elements found in abundance are the dermal plates, known as osteoderms, that these animals utilized for defense and display. Previous studies such as Scheyer and Sander (2004), Hayashi et al. (2010), and Burns and Currie (2014) have attempted to classify ankylosaurs by families, genera, and even species by using thin sections to examine the paleohistology of osteoderms. Using new microCT scanning techniques this study has attempted to classify the ankylosaur specimens found in Big Bend so that the fossil record for this area during the Campanian and Maastrichtian.